Prediction of Water Activity in Cured Meat using Microwave Spectroscopy

Magomed Muradov

A thesis submitted in partial fulfilment of the requirements of Liverpool John Moores University for the degree of Doctor of Philosophy

January 2017

Dedicated to my beloved parents

Ramzan and Aizan

Acknowledgments

I wish to express my gratitude to my director of study, Dr Alex Mason for his invaluable support and guidance during my research. Deepest gratitude is also due to the members of the supervisory group Prof Andrew Shaw and Prof A. Al-Shamma'a. I am grateful to Dr Jeff Cullen for his abundant knowledge and assistance.

Also, I would like to thank the entire RFM group and members of the Built Environment and Sustainable Technologies (BEST) Research Institute, specifically Dr Mamadou Diallo for his support with the electronic side of my project, Dr Badr Abdullah, Dr Eduardo Cordova-Lopez and Dr Muhammad Ateeq for providing transportation whenever it was required and also, I would like to thank Dr Olga Korostynska for her guidance and support during the write-up of my thesis and papers.

Special thanks to my friend and colleague Patryk Kot who has been on the same journey with me by achieving Bachelors of Science, Masters of Science and Doctor of Philosophy since 2009. I also would like to thank Keyur Joshi and Salifu Osman for sharing their knowledge and experience with me.

Furthermore, I would like to thank the Chechen Government and Chechen Ministry of Education and Science for their financial support during my studies.

I wish to express my love, respect and gratitude to my beloved parents for their endless love, support and patience through the duration of my studies. My thanks are also due to my whole family, three sisters and to my only brother.

Abstract

This work addresses the use of microwave techniques to determine quality parameters in cured meat. The first approach is online monitoring of weight loss in the meat curing process, which is a significant measurement for the meat industry because the weight loss is used as a method of tracking the curing process. Currently, weight loss is measured by using ordinary weighing scales, which is a time-consuming and impractical technique. Thus, a novel method is required to simplify the process by implementing an online monitoring technique.

In this work, a set of microwave sensors were modelled using High Frequency Structure Simulation Software and then constructed and tested. Weight loss of the sample and change in the S_{11}-parameter illustrated a strong linear relationship ($R^2 > 0.98$). The prediction model then was developed using the Partial Least Squares method, which exhibited a good capability of microwave sensors to predict weight loss, with $R^2_{p\ (prediction)} = 0.99$ and root mean square error of prediction (RMSEP) = 0.41.

The second approach is to determine water activity (a_w) in cured meat, which is the parameter that describes available water for microorganisms and influences different chemical reactions in the product. For the cured meat industry, a_w is the only moisture related measurement that is an accepted Hazard Analysis and Critical Control Point plan. This is important for safety reasons, but also for energy optimisation since curing requires controlled continuous temperature and humidity.

Currently, a_w is being measured by the meat industry using commercially available instruments, which have limitations, namely being destructive, expensive and time-consuming. Few attempts to develop non-destructive methods to predict a_w have used X-ray systems (namely Computed Tomography), Near Infrared (NIR) and Hyperspectral Imaging (HSI). Although the techniques provided promising results, they are expensive, impractical and not commercially available for the meat industry.

The results from the microwave sensors demonstrated a linear relationship ($R^2 = 0.75$, $R^2 = 0.86$ and $R^2 = 0.91$) between the S_{11} and a_w at 2.4 GHz, 5 GHz and 7 GHz, respectively. The prediction model exhibited a good capability of the sensors to predict a_w ($R^2_p = 0.91$ and RMSEP = 0.0173)

Table of Contents

Acknowledgments ii

Abstract iii

List of Figures ix

List of Tables xviii

List of Acronyms xix

Chapter 1 Introduction 1

1.1. Aim and Objectives 5

1.2. Statement of Novelty 6

1.3. Overview of the Thesis 6

Chapter 2 Literature Review 8

2.1. Water Activity 8

2.2. Meat Curing 10

2.3. Commercially Available Water Activity Meters 13

2.3.1. Chilled Mirror Dew Point 14

2.3.2. Resistive Electrolytic Hygrometer 18

2.3.3. Capacitive Electrolytic Hygrometer 21

2.4. Water Activity Measurement in the Research Domain 22

2.4.1. Computed Tomography 23

2.4.2. Near Infrared 26

2.4.3. Hyperspectral Imaging 27

2.4.4. LJMU Microwave cavity sensor 29

2.5. Summary 31

Chapter 3 Introduction to Electromagnetic Waves and Design Considerations of Microwave Sensor 33

3.1. Electromagnetic radiation 33

3.2. Microwave Sensor Systems 34

3.3. Design Considerations for a Microwave Sensor 36

3.3.1. Electromagnetic Sensors 37

3.3.2. Patch sensor design 43

3.3.3. Feed techniques 47

3.3.4. Substrate 50

3.4. Summary 54

Chapter 4 Research Methodology 55

4.1. Design process 55

4.2. Design and Simulations 58

4.3. Sample preparation. 58

4.4. Continuous Monitoring of Drying Process 61

4.5. Discrete Monitoring for Prediction of Water Activity in Cured Meat 64

4.6. Data Processing and Prediction Models 65

4.7. Summary 67

Chapter 5 Sensor Design, Implementation and Validation....68

5.1. Sensor Design....68

5.2. Sensor Simulation Results....71

5.3. Sensor Implementation....77

5.3.1. EAGLE Models of the Sensors....77

5.3.2. Printing of the Sensors using CNC Routing Machine....79

5.3.3. Simulation and Experimental Measurements of the Sensors in Air. 81

5.4. Validation of the Theoretical Model....84

5.4.1. HFSS Simulation....84

5.4.2. Experimental Setup....86

5.4.3. Real-world Experimental Results....88

5.5. Summary....91

Chapter 6 Continuous Monitoring of Drying Process....92

6.1. Sensor Version 1....92

6.1.1. Real-world Experimental Results....92

6.1.2. Discussion....96

6.2. Sensor Version 2....97

6.2.1. Real-world Experimental Results....97

6.2.2. Discussion....100

6.3. Sensor Version 3....101

6.3.1. Real-world Experimental Results 101

6.3.2. Discussion 105

6.4. Summary 105

6.4.1. Summary of the Results 105

6.4.2. Issues with Continuous Monitoring 106

Chapter 7 Discrete Monitoring for Prediction of Water Activity in Cured Meat 109

7.1. Sensor Version 3 109

7.1.1. Real-world Experimental Results 109

7.1.2. Discussion 112

7.2. Hand-held Prototype and Industrial Testing 113

7.2.1. Real-world Experimental Results 115

7.2.2. Results based on Animalia data 118

7.2.3. Discussion 120

7.3. Sensors version 3.1 and version 3.2 121

7.3.1. Real-world Experimental Results 121

7.3.2. Discussion 125

7.4. Summary 125

Chapter 8 Conclusion and Future Work 127

8.1. Conclusion 127

8.2. Future Work 131

Reference.....133

Appendix A.....146

Appendix B.....153

List of Figures

Figure 1.1. (a) Traditional ham curing process in Spain and (b) an example of a finished dry-cured ham product. 2

Figure 2.1. Meat curing process at Prolongo; (a) hams buried underneath a pile of salt, (b) salt equalisation, (c) washing process and (d) curing process. 12

Figure 2.2. Cured meat products from Prolongo (2016); (a) "Jamon Curado Duroc" (cured ham), (b) "Salchichon Tunel Pimienta" (Tunnel Peppered Salami), (c) "Chorizo Lomo Tunel Pinienta" (Tunnel Peppered Chorizo) and (d) "Salami Extra". 13

Figure 2.3. AquaLab Pre Water Activity Meter (Labcell Ltd, 2016b).....15

Figure 2.4. AquaLab Series 4TE (Decagon Devices, 2017) 16

Figure 2.5. Rotronic HydroLab C1 (Rotronic Instruments Ltd, 2016). 17

Figure 2.6. Rotronic HYGROPALM - HP23-A (Rotronic, 2012).....18

Figure 2.7. Novasina LabMaster-a_w (Cole-Parmer, 2016a). 20

Figure 2.8. Novasina LabStart-a_w (Novasina, 2016).....21

Figure 2.9. AquaLab Pawkit (Labcell Ltd, 2016a). 22

Figure 2.10. Scan of dry-cured ham using computed tomography (Font, Fulladosa and Garcia-Gil, 2013). 24

Figure 2.11. The location of the slice was at 10 cm from the aitchbone in the distal direction, at the widest part of the ham. A CT image (tomogram) showing a cross-sectional slice of a dry-cured ham at the end of the resting period. (Santos-Garcés *et al.*, 2010).....25

Figure 2.12. Remote measurement probe: Spectral acquisition setup on the gracilis muscle (Collell *et al.*, 2011). 27

Figure 2.13. Schematic diagrams of main components of the hyperspectral imaging system (Liu *et al.*, 2013).....28

Figure 2.14. Microwave cavity sensor (Mason *et al.*, 2016).....30

Figure 2.15. The correlation between the amplitude at 4.93 GHz and the water (Bjarnadottir *et al.*, 2014). 30

Figure 2.16. Flow chart of a_w measurement by commercially available devices. 31

Figure 3.1. Electromagnetic Radiation Spectrum (Lawson, 2005). 34

Figure 3.2. Microwave resonance curves. With increasing water content, the microwave resonance frequency decreases, while the frequency bandwidth increases. Resonance curves in air (solid line). Resonance curve in wet material (dash line) (Buschmüller *et al.*, 2008). 35

Figure 3.3. Block diagram of microwave sensor system. 36

Figure 3.4. The half-wave dipole. (left) Current distribution. (right) Radiation pattern (Stutzman and Thiele, 2013). 38

Figure 3.5. A traditional monopole antenna (Stutzman and Thiele, 2013). 38

Figure 3.6. Loop sensor [Adopted from (Mess-Elektronik, 2016)]. 39

Figure 3.7. Helical sensor (Balanis, 2005) 40

Figure 3.8. Microstrip patch sensor (Nitikanikks, 2017). 41

Figure 3.9. Phased array sensor (Ehyaie, 2011). 41

Figure 3.10. Aperture antenna (Balanis, 2005). 42

Figure 3.11. Structure of a rectangular patch sensor (Balanis, 2005). 43

Figure 3.12. Common forms of patch layer (Balanis, 2005).....43

Figure 3.13. Fringing field (Balanis, 2005). 45

Figure 3.14. Microstrip line feed (Balanis, 2005). 48

Figure 3.15. Coaxial feeding method (Balanis, 2005). 49

Figure 3.16. Coaxial probe with capacitive feed method (Balanis, 2008). 49

Figure 3.17. The aperture-coupled patch (Balanis, 2005). 50

Figure 3.18. HFSS model of rectangular edge-fed patch sensor. 52

Figure 3.19. Return loss vs. frequency from the five substrates. 52

Figure 4.1. Flow diagram of a methodology. 56

Figure 4.2. Cured meat products from *Roma's* (Romas, 2016). 57

Figure 4.3. Design of experiment for the dry-cured ham model analysed in this study. 59

Figure 4.4. (a) Sliced meat samples, (b) salted meat sample (c) vacuum sealed sample and (d) meat samples inside temperature and humidity monitored refrigeration system. 60

Figure 4.5. Incubation system. 60

Figure 4.6. Dry-curing lambs' legs in Prolongo, Spain. 61

Figure 4.7. Block diagram of the incubation system. 63

Figure 4.8. Experimental setup for monitoring of the meat drying process with (a) scales for monitoring weight loss, drip catchers/fans to move excess moisture away from sensor ((a) and (b) version 1, (c) version 2 and (d) version 3) and (b) humidity/temperature sensing to monitor drying condition inside incubation system. 63

Figure 4.9. (a) Meat samples placed inside an incubation system at 12-14°C and 72-74 % RH for curing process, (b) experimental setup for measurement of S_{11} parameter using sensor and (c) AquaLab a_w meter used for correlation purposes. 64

Figure 4.10. LabVIEW program for R-squared determination. 65

Figure 4.11. Adding PLSR library to the search path of MATLAB. 67

Figure 5.1. Top view of sensors (a) version 1, (b) version 2 and (c) version 3. 69

Figure 5.2. Top and bottom view of HFSS models of sensors (a) version 3.1 and (b) version 3.2. 69

Figure 5.3. Return loss of sensors (a) version 3.1 and (b) version 3.2 with CSRR and without CSRR cells. 70

Figure 5.4. Theoretical models of sensors (a) version 1, (b) version 2, (c) version 3, (d) version 3.1 and (e) version 3.2. 71

Figure 5.5. HFSS simulation results for sensors version 1. 72

Figure 5.6. HFSS simulation results for sensors version 2. 73

Figure 5.7. HFSS simulation results for sensors version 3. 73

Figure 5.8. HFSS simulation results for sensors version 3.1. 74

Figure 5.9. HFSS simulation results for sensors version 3.2. 74

Figure 5.10. Results from HFSS simulation of meat curing process imitation using sensor version 1; correlation between relative permittivity and (a) resonance frequency shift, with $R^2 = 0.87$ and (b) S_{11} change at 1.7 GHz, $R^2 = 0.99$. 75

Figure 5.11. Results from HFSS simulation of meat curing process imitation using sensor version 2; correlation between relative permittivity and (a) resonance frequency shift, with $R^2 = 0.99$ and (b) S_{11} change at 2.2 GHz, with $R^2 = 0.99$. 75

Figure 5.12. Results from HFSS simulation of meat curing process imitation using sensor version 3; correlation between relative permittivity and (a) resonance frequency shift, with $R^2 = 0.99$ and (b) S_{11} change at 2.4GHz, with $R^2 = 0.95$. 76

Figure 5.13. Results from HFSS simulation of meat curing process imitation using sensor version 3.1; correlation between relative permittivity and (a) resonance frequency shift, with $R^2 = 0.94$ and (b) S_{11} change at 3.67GHz, with $R^2 = 0.98$. 76

Figure 5.14. Results from HFSS simulation of meat curing process imitation using sensor version 3.2; correlation between relative permittivity and (a) resonance frequency shift, with $R^2 = 0.99$ and (b) S_{11} change at 2.5GHz, with $R^2 = 0.96$. 76

Figure 5.15. PCB layouts of sensors (a) version 1, (b) version 2 and (c) version 3 in EAGLE software. 77

Figure 5.16. PCB layouts of sensors (a) version 3.1 ((*left*) top and (*right*) bottom) and (b) version 3.2 ((*left*) top and (*right*) bottom) in EAGLE software. 78

Figure 5.17. CNC Routing machine connected to a PC. 79

Figure 5.18. Top view of the sensors (a) version 1, (b) version 2 and (c) version 3 fabricated with the CNC Routing machine. 80

Figure 5.19. (a) Top and (b) bottom views of the Sensor version 3.1. 81

Figure 5.20. (a) Top and (b) bottom views of the Sensor version 3.2. 81

Figure 5.21. Demonstrating the modelled and measured return loss of sensor version 1...82

Figure 5.22. Demonstrating the modelled and measured return loss of sensor version 2...82

Figure 5.23. Demonstrating the modelled and measured return loss of sensor version 3...83

Figure 5.24. Demonstrating the modelled and measured return loss of sensor version 3.1. 83

Figure 5.25. Demonstrating the modelled and measured return loss of sensor version 3.2. 84

Figure 5.26. HFSS simulation that imitates a meat drying process (e represents an epsilon, i.e. relative permittivity). 85

Figure 5.27. Results from HFSS simulation of meat drying process imitation; correlation between relative permittivity and resonance frequency shift, with $R^2 = 0.99$. 85

Figure 5.28. Block diagram of the experimental setup. 87

Figure 5.29. (a) Experimental setup inside the refrigerator, showing the water run-off system, digital scales, meat sample, sensor and fan system used to promote rapid drying and reduce water residue; (b) the relay system for controlling fan via LabVIEW. 87

Figure 5.30. (a) Vector Network Analyser and (b) LabVIEW interface utilised for continuous automated measurements over the experimental period of 28 days. 88

Figure 5.31. Readings from the electromagnetic wave sensor; measurements were taken once per hour in the frequency range 1-6 GHz; for clarity data from 1-2.5 GHz is presented, with measurements from 5 hour intervals over a 4 day period. 89

Figure 5.32. Linear correlation between weight loss and (a) frequency shift and (b) amplitude shift at 2 GHz 90

Figure 6.1. Readings from the electromagnetic wave sensor; measurements were taken once per hour in the frequency range 1-6 GHz, but for clarity data measurements from 5 hour intervals and from 1-2.5 GHz are presented. 93

Figure 6.2. Correlation of weight loss and (a) resonance frequency, with $R^2 = 0.85$ and (b) R^2 between weight loss and S_{11} change across the full frequency spectrum (sensor version 1). 94

Figure 6.3. Linear fit between weight loss and S_{11} change at 4.5 GHz, with $R^2 = 0.99$. 95

Figure 6.4. Measured and predicted weight loss from sensor version 1. 96

Figure 6.5. Deformed shape of the meat samples due to curing process. This figure presents (a) a meat sample under the test and (b) a meat sample at the end of the curing process....97

Figure 6.6. Readings from the electromagnetic wave sensor; measurements were taken once per hour in the 1-6 GHz frequency range.....98

Figure 6.7. Correlation of weight loss and resonance frequency, with $R^2 = 0.79$. 98

Figure 6.8. Linear correlation between weight loss and S_{11} change across the full frequency spectrum (sensor version 2). 99

Figure 6.9. Correlation of weight loss and S_{11} at 5 GHz, with $R^2 = 0.99$. 99

Figure 6.10. Measured and predicted weight loss from sensor version 2 using PLSR prediction model.....100

Figure 6.11. Readings from the electromagnetic wave sensor; measurements were taken (a) once per hour in the frequency range 1-6 GHz and (b) but for clarity data measurements from 5 hour intervals and from 2-3 GHz are presented. 102

Figure 6.12. Correlation of weight loss and resonance frequency, with $R^2 = 0.94$.....103

Figure 6.13. Linear correlation between weight loss and S_{11} change across the full frequency spectrum (sensor version 3). 103

Figure 6.14. Correlation of weight loss and S_{11} at 5.5 GHz, with $R^2 = 0.97$. 104

Figure 6.15. Measured and predicted weight loss from sensor version 3 using PLSR prediction model.....104

Figure 6.16. (a) Tinning 2 GHz rectangular patch sensors and (b) oxidized corners of the sensor and "weights" at end of the experiment. 107

Figure 6.17. (a) Conformal polypropylene based spray coated sensor version 3 and (b) oxidized meat sample at end of the experiment. 107

Figure 6.18. Uncured spots (red circles) on meat samples that were caused by the presence of a sensor. 108

Figure 7.1. Readings from the electromagnetic wave sensor; measurements were taken from 83 cured meat samples over a period of 7 months in the frequency range 1-13 GHz. 110

Figure 7.2. Correlation of a_w and resonance frequency, with $R^2 = 0.72$. 111

Figure 7.3. Linear correlation between water activity and S_{11} change across the full frequency spectrum (sensor version 3). 111

Figure 7.4. Correlation of a_w and S_{11} change at 7 GHz, with $R^2 = 0.81$. 112

Figure 7.5. Design of the Hand-Held Prototype.....113

Figure 7.6. (a) Experimental setup with head of a hand-held prototype (b) hand-held prototype. 114

Figure 7.7. Experimental work conducted in Norwegian pilot plant owned by Animalia, using hand-held prototype to measure dry cured lamb test products.....114

Figure 7.8. Readings from the hand-held prototype; measurements were taken from 83 cured meat samples over a period of 7 months in the frequency range 1-13 GHz. 115

Figure 7.9. Correlation of water activity and (a) resonance frequency, with $R^2 = 0.75$ and (b) S_{11} at 2.37 GHz, with $R^2 = 0.75$. 116

Figure 7.10. Linear correlation between water activity and S_{11} change across the full frequency spectrum (hand-held prototype). 116

Figure 7.11. Correlation of a_w and (a) S_{11} at 5 GHz, with $R^2 = 0.86$ and (b) S_{11} at 7 GHz, with $R^2 = 0.91$. 117

Figure 7.12. Measured and predicted a_w data (LJMU data only) from hand-held prototype using PLSR prediction model (see Appendix B for more details on this prediction model). 118

Figure 7.13. Animalia data fitted into LJMU data cluster. 119

Figure 7.14. Measured and predicted a_w data (LJMU and Animalia data) from hand-held prototype using PLSR prediction model. 119

Figure 7.15. Measuring a meat sample with prototyped sensor.....120

Figure 7.16. Readings from the sensor version 3.1; measurements were taken on 37 dry-cured meat samples. 121

Figure 7.17. Readings from the sensor version 3.2; measurements were taken on 37 dry-cured meat samples. 122

Figure 7.18. Correlation of a_w and resonance frequency, with $R^2 = 0.77$ and with $R^2 = 0.80$ from the results obtained using (a) version 3.1 and (b) version 3.2, respectively. 123

Figure 7.19. Linear correlation between water activity and S_{11} change across the full frequency spectrum from the sensors (a) version 3.1 and (b) version 3.2. 123

Figure 7.20. Correlation of a_w and (a) S_{11} at 3.8 GHz, with $R^2 = 0.80$ for sensor version 3.1 and (b) S_{11} at 3.6 GHz, with $R^2 = 0.80$ for sensor version 3.2. 123

Figure 7.21. Measured and predicted a_w data from sensors (a) version 3.1 and (b) version 3.2 using PLSR prediction model. 124

List of Tables

Table 2.1. Water activity and growth of microorganisms in food (Decagon Devices, 2012). 9

Table 2.2. Water Activity meters from key manufacturers. 14

Table 2.3. Comparison of research based methods for a_w prediction. 23

Table 2.4. Prediction models for a_w using different sets of samples. 25

Table 2.5. Prediction models for a_w determination of dry-cured ham samples. 27

Table 2.6. Performance of PLSR (full and simplified), PCR and MLR models for salt and a_w parameters. 29

Table 3.1. Characteristics of common substrates. 53

Table 7.1. Comparison of prediction models between hand-held prototype, sensor version 3.1 and sensor version 3.2. 126

List of Acronyms

a_w	Water Activity
BEST	Built Environment and Sustainable Technologies
BF	Biceps femoris muscle
CAT	Computerized Axial Tomography
CSRR	Complementary Split Ring Resonator
CT	Computed tomography
EM	Electromagnetic
ERH	Equilibrated Relative Humidity
EU	European Union
EUFIC	European Food Information Council
FDA	Food and Drug Administration
FT	Fourier Transform
HACCP	Hazard Analysis and Critical Control Point
HFSS	High Frequency Structural Simulation
HSI	Hyperspectral Imaging
ISM	Industrial Scientific and Medical radio band
LHCP	Left Hand Circular Polarized
LJMU	Liverpool John Moores University
LOD/IR	Infrared Light Exposure
MLR	Multiple Linear Regression
MRT	Microwave Resonance Technology
NIR	Near Infrared Spectroscopy
PC	Personal Computer
PCR	Principal Component Regression

PLSR	Partial Least Squares Regression
RH	Relative Humidity
RHCP	Right Hand Circular Polarized
RMSEP	Root Mean Square Error of Prediction
ROIs	Regions of Interest
RPD	Residual Predictive Deviation
SM	Semimembranosus muscle
ST	Semitendinosus muscle
tan	The Loss Tangent
VNA	Vector Network Analyser
WHC	Water Holding Capacity
WHO	World Health Organisation

Chapter 1 Introduction

Products of certified high quality are increasingly sought by both consumers and manufacturers (Verbeke, 2011). Products in the meat industry are no exception to this rule (Verbeke *et al.* 2006; Verbeke *et al.* 2010), although it is a challenging task since the product exhibits considerable variability as a result of the natural raw material (Damez and Clerjon, 2013). Therefore, a rapid measurement system for ensuring quality of the products would be beneficial for the meat industry.

Meat curing is the process by which food products are preserved and flavoured, typically through the addition of salts, nitrates, nitrites or sugars and perhaps in combination with other cooking or smoking processes. For the cured meat industry, water activity (a_w) is the only moisture related measurement that is an accepted Hazard Analysis and Critical Control Point (HACCP) plan (US Public Health Service, 2013). It is particularly important in intermediate, shelf-stable food products.

Despite curing being used as early as 1300 BC in China, there are few techniques for monitoring the curing process with producers typically relying upon "rule of thumb" methods or crude measurements such as product weight or solidity. While fresh meat products have benefitted from the advent of sensor systems, with near-infrared (NIR) and X-ray based techniques being the most prevalent for applications such as meat composition monitoring (Prediktor, 2016), sorting (Tomra, 2016) and foreign object detection (i.e. detection of metal, plastic and bone shards) (Nielsen *et al.*, 2013), these technologies have made little impact on the monitoring of cured meat production. Thus there is heavy reliance upon the experience of key workers within the industry which leads to problems of consistency if the instincts or opinions of those workers vary (Swiss Meat, 2014).

These days, fresh meat can be purchased in local stores and supermarkets owing to use of mechanical refrigeration systems (Rentfrow, Chaplin and Suman, 2012). However, across much of Europe, cured meat products (see Figure 1.1) have retained a place in the consumer market.

Regional speciality dry-cured meat products, such as the premium, heritage dry-cured hams produced by Prolongo[1], have been in Europe for centuries, and are engrained in European culture – it is well known for example as a key ingredient of the Mediterranean diet. Spain is the main producer of dry-cured ham products, followed by Italy, France, Germany, Poland and Greece. Consumption figures (yearly per capita) build a broader picture of the importance of dry-cured meats: Spain (4.4 kg), Italy (2.4 kg), France (0.9 kg), Belgium (0.6 kg) and Germany (0.4 kg), and there is a growing market in the UK for premium product domestically-produced charcuterie (Resano *et al.*, 2011).

In Norway, dry-cured ham consumption is 0.46 kg per capita and traditional dry-cured lamb (*fenalår*) is estimated at 0.12 kg per capita – while this is lower than ham products in other European countries. There is growing interest in traditional products and in how they can be used in supporting and developing local, tourist and even export markets, and thereby maintaining and creating local businesses in remote areas in the West-Nordic regions. In 2012, a federation of nine manufacturers of *fenalår* received the geographically protected designation "*Fenalår* from Norway", and in 2015 deals were made with both France and Switzerland to begin exports under this brand (Berglund, 2015).

(a) (b)

Figure 1.1. (a) Traditional ham curing process in Spain and (b) an example of a finished dry-cured ham product.

[1] Prolongo (Spanish Meat Company) is one of the project partners that is interested in investigating a novel non-destructive sensing technology. Their involvement is to provide a knowledge about the production of cured meat products, validation and commercialisation of the technique. http://www.prolongo.com/?lang=en

The concept of a_w was introduced over fifty years ago to describe the state of water in food (Ibarz and Barbosa-Canovas, 2014). In 1953 (Gustavo V. Barbosa-Cánovas, Anthony J. Fontana, Schmidt and Labuza, 2007), William James Scott showed that a_w is the parameter that governs microbial growth in food not the water content, as most people thought. Four years later, he established the concept of a minimum a_w for microbial growth. Now, food manufacturers regularly use a_w to determine whether or not a product is susceptible to microbial propagation (Carter and Fontana, 2008).

Currently, there are a number of commercially available a_w instruments (Cole-Parmer, 2016b; Labcell Ltd, 2016b; Rotronic Instruments Ltd, 2016) that are used by the meat industry and research institutions. However, the techniques have some disadvantages that limit their use in the manufacturing process. The drawbacks of the methods are as follows:

- Destructive – this is the key disadvantage, as all existing methods require a sample to be cut from a curing meat product. This causes a disturbance in the curing process owning to the area of the sample cut being unevenly cured, which would require extra time for the area to be cured. In addition, each tested sample has to be disposed of after the measurement is complete, which leads to waste of the product.
- High cost – the cost could be a problem for small manufacturers, who are the majority in cured meat industry (more detail is provided in section 2.5).
- Time-consuming – this becomes an issue when over 20-30 samples are measured, which would require over 5 hours (more detail is provided in section 2.5).

The limitations of the existing a_w measurement techniques are the drivers for this research. Therefore, the successful outcome of this investigation will provide the meat industry with a non-destructive, low cost and time-efficient technique to determine a_w in cured meat and meat products.

Electromagnetic (EM) sensors, namely those, which operate at radio or microwave frequencies, are widely used in a variety of industrial sectors. Examples include, civil engineering materials analysis (Adous, Quéffélec and Laguerre, 2006), timber imaging (Goy, Martin and Leban, 1992), chemical processing (Gradinarsky *et al.* 2006; O. Korostynska *et al.* 2014a; O Korostynska *et al.* 2014b) and medicine (Olga Korostynska *et al*. 2014c; J. H. Goh *et al*. 2013a; Mason *et al.* 2013; J H. Goh *et al.* 2013b). However, there

has yet to be a significant impact of these sensors in the food industry, with the majority of such technology there being centred on cooking or sterilisation. However, researchers from Built Environment and Sustainable Technologies (BEST) Research Institute in Liverpool John Moores University (LJMU) have demonstrated the first potentially non-invasive solution for measurement of water holding capacity (Mason *et al.*, 2016) and a_w (S. G. Bjarnadottir *et al.*, 2015) in meat products based on EM wave sensors operating at microwave frequencies. Therefore, there is the belief that further benefits could be brought to the cured meat industry; this belief is supported by other authors in the field (Clerjon and Damez, 2009). The particular benefit of the technology is its non-invasive nature, which, in contrast with current techniques, holds the potential to eliminate fears over instrumentation contributing to food contamination, which has disastrous consequences for consumers and suppliers. Another significance of the new sensor system will be a cost reduction by minimisation of the product waste, which is disposed of when the HACCP requirements are not met. In addition, meat industry is interested in time reduction of the meat curing process to reach higher annual turnover by determination of a_w in real time.

Currently, the curing process is controlled by simply measuring the solidity and weight of the product, and the key element is an experienced worker with the right instinct. The worker squeezes a meat product and estimates a_w, which may lead to human error and over drying the product. Firstly, over drying will be costly for the company, as the temperature (usually 12-14 °C) and humidity (usually 75%) of the environment has to be controlled. Secondly, over drying causes a thick crust on the surface of the meat, which prevents the inside moisture from escaping. This means that the outside of the meat product is dried and safe to consume, whereas the inside might not be as it still contains high levels of moisture (high a_w) (Wright, 2011). Thus, a non-invasive and non-destructive sensing system will solve these issues, namely providing enhanced knowledge of a_w that will reduce the timing of the drying process. This will reduce expense on energy-consuming dryers and improve the productivity.

The system will afford opportunities for dry-cured meat manufacturers to adapt and change recipes in line with healthy eating guidance, such as that offered by the World Health Organisation (World Health Organization, 2004) and the European Food Information Council (EUFIC, 2017). For example, the use of frequent or continuous a_w prediction will enable manufacturers to monitor the effect of reducing the salt levels in their products and

work toward launching low-salt derivatives. It will go further than other initiatives in this field, such as the FP7 ProCured project (Cordis, 2015), since the developed method of a_w prediction enables simple through life product monitoring. This will clearly have a huge positive impact on societal health since reducing salt intake will reduce the risk of high blood pressure, heart disease and strokes for European Union (EU) citizens, as most countries are above the 6g per day salt intake targets. Thus, the impact of this will be felt at national and European levels through reduced mortality and healthcare costs. In England and Wales alone, a recent study estimated that a 3g reduction in mean daily salt intake by adults would lead to up to 20,000 fewer deaths annually, and healthcare savings of £260 million per year (ActionSalt, 2016). In the European context, a 2015 study of 9 European countries (including Spain, Italy, UK and Scandinavia) projected that a 30% decrease in current salt intake levels would result in 632,000 fewer strokes, 708,400 fewer cases of heart disease, and 495,600 fewer deaths (Hendriksen *et al.*, 2015). Sausages, ham, bacon and other processed meats appear to increase the risk of people dying young. Diets high in processed meats are linked to cardiovascular disease, cancer and early deaths (Gallagher, 2013). The evidence shows that eating processed meat increases a risk of colorectal cancer (Canadian Cancer Society, 2016). In 2006, there were an estimated 3,191,600 cancer cases diagnosed and 1,703,000 deaths from cancer in Europe. One of the most common form of cancers was colorectal cancers (4,102,900, 12.9%) which caused 207,400 deaths (Ferlay *et al.*, 2007).

1.1. Aim and Objectives

The aim of this investigation is to develop a rapid non-destructive method to predict a_w in cured meat using microwave spectroscopy.

Objectives of this project are to:

- Research the importance of a_w measurement in the meat curing process, commercially available a_w meters and recent research undertaken for a_w prediction in cured meat.
- Investigate electromagnetic wave theory for design and simulation of electromagnetic wave sensors and theoretical model of a meat sample using High Frequency Structural Simulation (HFSS) software.

- Construct sensor and carry out an experimental work to monitor weight loss and water activity in meat.
- Develop a predictive model from the experimental data for determination of a_w in dry-cured meat.

1.2. Statement of Novelty

This thesis describes the development of a novel low-cost, time-efficient and non-invasive microwave sensor for measuring water activity in cured meat, which is currently not available for the meat industry. The research will demonstrate the potential use of the microwave sensor to provide a rapid measurement system for ensuring quality of the products.

1.3. Overview of the Thesis

In order to achieve the aim and meet the objectives of this research, the thesis is structured in chapters. The first Chapter has discussed the importance of water content and specifically a_w in meat and meat products, the problems faced in monitoring the meat drying process and determination of a_w in cured meat by the meat industry.

In Chapter 2, a literature review will start by focusing on a_w and a_w measurements. It then will describe and evaluate state of the current commercially available techniques to measure a_w in cured meat used by the meat industry. Moreover, the recent research carried out to develop non-destructive techniques to predict a_w in cured meat will be reviewed. This will lead to highlighting a need to investigate electromagnetic wave sensors to develop a non-destructive method for determination of a_w in cured meat and meat products.

In Chapter 3, the theory of electromagnetic waves will be introduced, particularly microwave sensing system as a proposed technique to monitor water activity in cured meat products. Different sensor structures and their characteristics will be described and their features will be compared in order to select the most suitable sensor for this investigation. In addition, the description of substrate and feed techniques of the microstrip sensors will be presented.

In Chapter 4, the design process of the research will be described, namely design, simulations, sample preparation, experimental approaches and data analysis. The chapter will start with the design process and provide the flow diagram of the research methodology. This will follow with the description of the samples preparation, continuous and discrete monitoring. The last section will describe the data processing and the development of the prediction models.

In Chapter 5, the sensor design, implementation and validation will be provided. The first section of the Chapter will present the HFSS models of the sensors and a meat sample. In section 5.2, the simulation results of five microwave sensors are presented. Section 5.3 walks through the detailed procedure of the physical construction of the sensors and comparison of experimental and simulation measurements of the sensors in the air. The last section will provide the validation of the theoretical model.

Chapter 6 will provide real-world experimental results obtained using sensor versions 1, 2 and 3 for continuous monitoring of weight loss of meat samples in the curing process. Results obtained from all three sensors will be processed, plotted and analysed to develop a prediction model for monitoring of the meat curing process using a microwave sensor system.

In Chapter 7, the real-world experimental results obtained from sensor versions 3, 3.1 and 3.2 for discrete monitoring for prediction of water activity will be shown; and also the results obtained from the prototype sensor version 3 in the LJMU laboratory and in the Norwegian pilot plant owned by Animalia.

Chapter 8 will summarise the objectives of the research and conclude the investigation and the recommendations for relevant future work will also be discussed.

Chapter 2 Literature Review

In this chapter, the literature review will begin by focusing on water activity (a_w) and meat curing techniques. Then, currently available a_w measurement instruments will be critically reviewed, followed by a further critical review of relevant sensors or techniques for non-invasive water activity measurement, which remain in the research domain. Finally, a summary of the key findings of the literature review will be provided, along with discussion of the need for a new method for water activity determination.

2.1. Water Activity

The accepted definition of water activity is *"the partial vapour pressure of water in a substance divided by the standard state partial vapour pressure of water"* (Food and Drug Administration, 2014). However, to understand the importance of water activity in the context of food, it is necessary to understand that the microorganisms that grow on or in food products rely on water. In addition, water activity is an indicator of the water available for the growth of microorganisms, and does not necessarily directly relate to the total water content of a product. The researchers in the food industry define the concept of water activity as follows (Al-Muhtaseb, McMinn and Magee, 2002):

$$Water\ Activity = \frac{p}{p_0} = \frac{relative\ humidity}{100} \qquad (2.1)$$

Where p is the partial pressure of water in the food and p_0 the vapour pressure of pure water at the same temperature.

Microorganisms absorb water by moving it across the cell membrane. This water movement mechanism depends on the a_w gradient — on water moving from a high a_w environment outside the cell to a lower a_w environment within the cell. When a_w outside the cell becomes low enough, it causes osmotic stress: the cell cannot take up water and becomes dormant. The microorganisms are not eliminated; they just become unable to grow enough to cause infection. Different organisms cope with osmotic stress in different ways, and therefore the minimum level of water activity for different organisms to survive varies; some types of moulds and yeasts have adapted to withstand very low a_w levels (Food and Drug Administration, 2015).

The knowledge of a_w provides a possibility to identify which bacteria (Heller, 2001; Vesterlund, Salminen and Salminen, 2012), moulds (Mathlouthi, 2001; Rosso and Robinson, 2001), or fungi (Pardo *et al.*, 2004) can grow on and in it. By reducing a_w, the growth of certain classes of microbes can be eliminated, namely E.coli, listeria and campylobacter. In 1999, over 143 people were made ill by consuming dry-fermented salami, which contained E.coli in British Columbia, Canada. In 2011, the listeria was found in a sample of imported dry-cured ham and 5,700 pounds of product were recalled (Frame, 2012).

Water activity is a control step and an integral part of many HACCP plans (López-Malo and Alzamora, 2015). Table 2.1 shows a_w limits for many common microorganisms. These well-established microbial growth limits have been incorporated into Food and Drug Administration (FDA) and other regulations (Decagon Devices, 2012).

Table 2.1. Water activity and growth of microorganisms in food (Decagon Devices, 2012).

Range of a_w	**Microorganisms**	**Products**
1.00-0.95	Pseudomonas, Escherichia, Proteus, Shigella, Klebsiella, Bacillus, Clostridium perfringens	Highly perishable (fresh) foods and canned fruits, vegetables, meat, fish, milk, and beverages
0.95-0.91	Listeria, Salmonella, Vibrio parahaemolyticus, C. botulinum, Serratia, Lactobacillus, Pediococcus, some moulds,	Cured meat (ham), some cheeses (Cheddar, Swiss, Muenster, Provolone), bread, tortillas
0.91-0.87	Many yeasts (Candida, Torulopsis, Hansenula), Micrococcus	Fermented sausage (salami), sponge cakes, dry cheeses,
0.87-0.80	Most moulds (mycotoxigenic penicillia), Staphyloccocus aureus, most Saccharomyces (bailii) spp., Debaryomyces	Most fruit juice concentrates, sweetened condensed milk, syrups, jams, jellies, soft pet food
0.80-0.75	Most halophilic bacteria, mycotoxigenic aspergilli	Marmalade, marzipan, glacé fruits, beef jerky
0.75-0.65	Xerophilic molds (Aspergillus chevalieri, A. candidus, Wallemia sebi), Saccharomyces bisporus	Molasses, raw cane sugar, some dried fruits, nuts, snack bars, snack cakes
0.65-0.60	Osmophilic yeasts (Saccharomyces rouxii), few molds (Aspergillus echinulatus, Monascus bisporus)	Dried fruits containing 15-20% moisture; some toffees and caramels; honey, candies
0.60-0.20	No microbial proliferation	Dry pasta, flour, cookies, dried vegetables

Water activity is the only moisture related measurement that is an accepted HACCP control point. It is particularly important in intermediate, shelf-stable food products. In combination with pH, a_w determines which of these intermediate-moisture foods are considered potentially hazardous by the FDA (US Public Health Service, 2013) .

2.2. Meat Curing

Meat curing is the application of salt, colour fixing ingredients, and seasoning in order to impart unique properties to the end product (Ray, 2010). Some techniques involve adding sugar, nitrite, nitrate and sometimes phosphates and ascorbates to meats for preservation, colour development, and flavour enhancement (Marriott, Graham and Extension, 2000). The functions of the most popular ingredients used in curing are as follows.

Salt:

- Provides a characteristic flavour to impart a cured meat taste.
- Acts as a preservative through growth inhibition and destruction of microorganisms.
- Enhances the transport of other cure ingredients throughout the muscle by osmotic movement of salt itself.
- Dehydrates meat tissue to reduce bacterial growth.

Sugar:

- Provides a characteristic flavour to impart a cured meat taste.
- Counteracts the harshness of salt.
- Provides an energy source for microorganisms, which convert nitrate to nitrite during a long-term cure.
- Provides a surface colour characteristic of aged ham if caramelised sugar is used.

Nitrates and nitrites:

- Contribute to the characteristic cured flavour.
- Contribute the characteristic reddish-pink colour of cured meat.

- Prevent growth of a food poisoning microorganism known as Clostridium botulinum, which can occur in foods that require heat processing.
- Retard the development of oxidative rancidity and rancid taste.
- Prevent warmed-over flavour in reheated products.

The ingredients may be in either dry or liquid form and applied either to the surface of meat or in meat by some injection techniques (artery pumping or stitch pumping). The artery pumping method involves injecting a brine solution into the meat's artery by using a long needle connected with a hose to a pump. The stitch pumping technique is based on applying the solution under the pressure to the surface of the meat with a bank of needles connected to a pump (Meats and Sausages, 2016). Dry-cure is the oldest curing method in which the curing ingredients are rubbed on the surface of the meat. The dry sugar cure method can be used under wider temperature variations and will have less spoilage problems under unfavourable curing conditions (Ray, 2010). A simple and time-tested dry-curing formula for 12-14 lbs piece of meat requires the following ingredients:

- 8 lbs salt
- 3 lbs sugar
- 2 oz. sodium nitrate
- 1/2 oz. sodium nitrite

The length of curing is typically 7 days per inch of thickness (Ray, 2010). For instance, if a ham joint weighs 12-14 lbs and measures 5 inches at its thickest point, then it should be cured for 35 days. Another important consideration is to be sure the cure is rubbed into the aitchbone joint and hock end of the ham to avoid bone sour. The temperature range should be high enough for the meat to cure properly and dry, but low enough so harmful bacteria and mould does not grow. Ideal temperatures for dry-curing are between 10-15 °C (Ray, 2010).

Prolongo is a Spanish meat company that has produced high quality sausages and hams since 1820, which is located in Valle del Guadalhorce (Prolongo, 2016). The curing process of hams in Prolongo is illustrated in Figure 2.1 that consists of four stages, namely salting, salt equalisation, washing and curing. Firstly, the hams are buried underneath a pile of salt as

shown in Figure 2.1 (a). Then, the samples are placed in large containers for salt equalisation that is demonstrated in Figure 2.1 (b). Next, the salt is washed off from the samples [see Figure 2.1 (c)], which are then hung in the temperature and humidity controlled dryers for the curing process [see Figure 2.1 (d)]. This is a multi-stage process, so there are a number of drying rooms/chambers used in different conditions. The final product is shown in Figure 2.2 (a), which is called "*Jamon Curado Duroc*" (cured ham). In addition, Figure 2.2 presents some other Prolongo's cured meat products, namely "*Salchichon Tunel Pimienta*" (Tunnel Peppered Salami), "*Chorizo Lomo Tunel Pinienta*" (Tunnel Peppered Chorizo), "Salami Extra".

(a) (b)

(c) (d)

Figure 2.1. Meat curing process at Prolongo; (a) hams buried underneath a pile of salt, (b) salt equalisation, (c) washing process and (d) curing process.

(a) (b)

(c) (d)

Figure 2.2. Cured meat products from Prolongo (2016); (a) "Jamon Curado Duroc" (cured ham), (b) "Salchichon Tunel Pimienta" (Tunnel Peppered Salami), (c) "Chorizo Lomo Tunel Pinienta" (Tunnel Peppered Chorizo) and (d) "Salami Extra".

2.3. Commercially Available Water Activity Meters

This section will present the current methods to measure a_w in food products and provide examples of commercially available instruments that are based on those methods. There are three most commonly used techniques by the manufactures of a_w meters, namely chilled mirror dew point, resistive electrolytic hydrometer and capacitive electrolytic hydrometer. The most popular a_w measurement devices in the meat industry are AquaLab, Rotronic and Novasina. The basic characteristics of the instruments and their measurement techniques (sensor type) will be provided in this section. The key features of these devises, namely the sensor type, accuracy, measurement time and cost are illustrated in Table 2.2.

Table 2.2. Water Activity meters from key manufacturers.

Device	Sensor Type	Accuracy (a_w)	Meas. Time (s)*	Non-invasive	Self-calibrate	No sample preparation	Portable	Price***(€)
AquaLab 4TEV	Dew point	±0.003	<600	✗	✗	✗	✗	10,300
AquaLab Pawkit	Capacitive	±0.02	600	✗	✗	✗	✓	2,000
Novasina LabMaster-a_w	Resistive electrolytic	±0.03	<600	✗	✗	✗	✗	10,900
Novasina LabStart-a_w	Resistive electrolytic	±0.002	420	✗	✗	✗	✗	5,850
Rotronic HygroPalm23-a_w	Dew point	±0.05	600-2100**	✗	✗	Invasive probe available	✓	3,800
Rotronic Hygrolab C1	Dew point	±0.005	600-2100**	✗	✗	Invasive probe available	✗	6,795

* Includes sample preparation (300s) where device is invasive and self-equilibration (warm-up) period stated by manufacturer is less than this period
** These devices have a "quick" mode, which automatically provides a value after 5 minutes with reduced accuracy.
*** Based on survey of distributors across Europe

2.3.1. Chilled Mirror Dew Point

Chilled mirror dew point measurement is a primary method for determining vapour pressure that has been in use for decades (Devine and M. Dikeman, 2004). Dew point instruments are accurate, fast, simple to use, and precise. The measurement range of commercial dew point meters is 0.030 to 1.000 a_w with a resolution of ±0.001 a_w and an accuracy of ±0.003 a_w. Measurement time is typically less than 5 minutes. However, the instruments must be warmed up (the standard warming up time recommended by manufacturers is 15 minutes). In addition, the verification of the equipment is strongly recommended, which can be carried out using the verification solution standards from the manufacturers. The verification requires 5-20 minutes depending on the temperature equilibration time.

The dew point instruments contain a sealed chamber with a mirror, optical sensor, internal fan and infrared thermometer. The measurement of the water activity is taken by equilibrating the temperature of a sample within the headspace of the chamber. A thermoelectric (Peltier) cooler precisely controls the mirror temperature, and a thermocouple behind the mirror accurately measures the dew point temperature when condensation starts. The exact point at which condensation appears is detected using an optical reflectance sensor. This sensor emits infrared light onto the mirror, and reflected light is detected. When condensation occurs on the mirror, a change in reflectance is registered and the dew point

temperature is measured. At the same time, the sample temperature is measured with an infrared thermometer (thermopile), and both temperatures are used to calculate water activity (Gustavo V. Barbosa-Cánovas, Anthony J. Fontana, Schmidt and Labuza, 2007).

2.3.1.1. Aqualab Pre Water Activity Meter

The Aqualab Pre (see Figure 2.3) is a robust entry-level water activity meter with stripped down form. The instrument requires minimum maintenance. The Aqualab Pre uses the dew-point method that is a primary measurement of water activity. Therefore, the calibration of the system is unnecessary; however, a verification check of the device is required for accurate results. The Aqualab Pre has a solid repeatability as it holds the sample at 25°C, thus temperature fluctuations will not affect readings of a sample. Water activity is temperature dependent; measuring at the same temperature every time assures consistency in readings. Its basic 0.01 a_w accuracy enables users to add a_w testing at the line, loading dock, or offsite facility (Labcell Ltd, 2016b).

Figure 2.3. AquaLab Pre Water Activity Meter (Labcell Ltd, 2016b).

2.3.1.2. AquaLab Series 4TE - Laboratory Specification Water Activity Monitor

Decagon's AquaLab Series 4TE (see Figure 2.4) water activity (a_w) meter is fast and precise measurements of a_w or ERH (Equilibrated Relative Humidity). The Aqualab Series 4TE is the most recent development of AquaLab. As with its predecessors, measurements are fast (typically less than 5 minutes excluding time for warming up, verification check and temperature equilibration of a tested sample) and accurate to ±0.003 a_w. The Series 4 features a "clamshell" opening sensor block design to allow easy sampling. It allows users to pre-define the sampling temperature using the keypad on the front of the instrument. Temperatures of between 15 and 50 ^oC can be set to allow samples to be warmed or cooled

to within 0.2 ^{o}C. The new design of AquaLab also features internal data storage allowing measurements to be taken, safely recorded and then downloaded to PC. Using the AquaLink 4 Software, measurements can be organised and viewed and the user can create reports based on the pertinent information.

Figure 2.4. AquaLab Series 4TE (Decagon Devices, 2017)

2.3.1.3. Rotronic HygroLab C1

ROTRONIC provides a high-end laboratory device called the HygroLab C1 (see Figure 2.5) for a_w measurements with up to four probes. Connect station probes and insertion probes for measuring a_w in cheese, meat, tobacco, building materials, animal feed, pharmaceuticals products and much more. ROTRONIC also provides a validated software HW4, which can be used for remote monitoring with charting and data recording functions (Rotronic Instruments Ltd, 2016).

HygroLab C1 has the following features

- 4 input channels for HC2 station probes or HC2 insertion probes can be connected for measurement of a_w, RH and temperature
- a_w Quick function for fast measurement results (typically 4-5 minutes)
- Audible alarm to indicate completed measurement
- Saves up to 2,000 data records with %RH, °C/°F, date and time

Figure 2.5. Rotronic HydroLab C1 (Rotronic Instruments Ltd, 2016).

2.3.1.4. Rotronic HYGROPALM - HP23-A

The HP23 is a multifunction hand-held indicator with data logging capability. The HP23 can be used in many different applications such as the spot check measurement of HVAC installations and manufacturing processes, the measurement of seeds, pharmaceutical powders and other materials in bulk, the measurement of paper stacks and rolls, etc. The HP23 is also a calibrator that can be used to read and adjust other instruments from ROTRONIC that are based on the AirChip 3000 technology.

Each of the two probe inputs can be configured to accept either a digital HygroClip 2 humidity-temperature probes (factory default) or an analogue probe measuring any signal such as barometric pressure, air velocity etc. The HP23 has a real time clock to keep track of the date and time when recording data and is powered with either a standard 9 V alkaline battery or with a rechargeable battery (Rotronic, 2012).

Figure 2.6. Rotronic HYGROPALM - HP23-A (Rotronic, 2012).

2.3.2. Resistive Electrolytic Hygrometer

Many commercial instruments based on the electric hygrometer sensor are available for measurement of water activity (a_w). One of the electric hygrometers is resistance-type sensor. The work principle of the sensor: a material (either a salt film or proprietary hygroscopic polymer film) changes its electrical response as a function of relative humidity. Depending on the water vapour pressure of the surrounding air, water will adsorb or desorb within the sensor and alter the electrical properties of the hygroscopic material. The sensor must be calibrated to convert the resistance value to units of a_w. In these instruments, a sample is placed in a sealed chamber containing the sensor. The sample, air, and sensor must come to vapour and thermal (if not temperature compensated) equilibrium for accurate a_w measurements. Overall, these instruments measure the entire a_w range from 0 to 1.0 a_w with a resolution of ±0.001 a_w and an accuracy of between 0.01 and 0.02 a_w (Gustavo V. Barbosa-Cánovas, Anthony J. Fontana, Schmidt and Labuza, 2007).

Electric hygrometers offer a reliable means for measuring a_w, provided some precautions are taken. Requirements for careful calibration, determining the equilibration time and the influence of temperature, must be considered to ensure accurate and reproducible readings. Equilibration time required for various products to reach a constant a_w value (a change of <0.01 a_w) increases at higher a_w and the following precautions must be taken for reliable measurement:

- a_w value is taken when the reading (0.001 unit) has been constant for 10 minutes
- Humidity sensors are calibrated regularly to compensate for drift
- A separate calibration curve is made for each sensor
- Sensors are calibrated at the same temperature at which samples are measured (Gustavo V. Barbosa-Cánovas, Anthony J. Fontana, Schmidt and Labuza, 2007).

Difference in temperature between the sample and sensor can cause large errors. At high a_w, a 0.1°C temperature difference results in a 0.006 a_w error. If a_w is high and sample temperature is above sensor temperature, water can condense on the sensor. The equilibration time varied from 20 minutes to 24 hours depends on the humidity range and food material due to both thermal and vapour equilibration. Sample temperature must be known to obtain accurate a_w measurements (Sablani, Rahman and Labuza, 2001). Some instruments do not measure sample temperature; thus, they require careful temperature control or have long read times to allow thermal equilibration. Without careful control and measurement of temperatures in the regions occupied by the sample and the sensor (or allowing enough time for thermal equilibration), no meaningful data can be collected (Reid, 2001). Product literature on modern electric hygrometers suggests short read times, although these claims have not been verified.

2.3.2.1. Novasina LabMaster-a_w

Novasina LabMaster-aw (see Figure 2.7) is a professional laboratory instrument for a very precise measurement of a_w in food, drugs, cosmetics etc. The temperature of the measurement chamber may be set in the range from 0^oC to 50^oC and kept consistently within an accuracy of ±0.2K. This instrument runs the most used a_w measuring technology, the electrolytic resistive principle (Cole-Parmer, 2016a).

Figure 2.7. Novasina LabMaster-a_w (Cole-Parmer, 2016a).

2.3.2.2. Novasina LabStart-a_w

The LabStart-a_w meter is simple-to-operate, which provides basic measurement functions, yet still having built-in automatic equilibrium detection and the well-proven resistive-electrolytic sensor technology as employed in all Novasina a_w meters. As standard, the LabStart-a_w is supplied with one re-useable humidity calibration standard, which provides a very economical solution to precision a_w measurements in one simple kit. Furthermore, the calibration standard is an easy method for verification of the instrument's high performance.

The LabStart-a_w is a typical starter instrument and should be used where a rough idea about a_w level is required, like in production. As higher a_w-levels require a temperature-controlled measurement chamber, the LabStart-a_w should be used for measuring samples in the medium range up to 0.8 a_w maximum.

The accuracy of ±0.03 a_w might be too low for quality assurance requirements, so it is not recommended to use it for that purpose.

It comes with the automatic equilibrium detection, 1 re-usable SAL-T standard and the Novasina electrolytic resistive sensor technology.

Anywhere that a quick and reasonable a_w reading is required without being too concerned about accuracy and repeatability. Water activity in the range of 0.4-0.6 a_w gives the best results, so mainly powders and drier materials should be measured with the LabStart-a_w (Novasina, 2016).

Figure 2.8. Novasina LabStart-a_w (Novasina, 2016).

2.3.3. Capacitive Electrolytic Hygrometer

Some a_w instruments use capacitance sensors to measure a_w. An example of such an instrument is the 4-inch AquaLab Pawkit a_w meter (see Figure 2.9), which was originally designed for government inspectors. It is a reliable a_w instrument for use on-the-go (Labcell Ltd, 2016a).

Changes in the electrical capacitance of the polyamide layer of the sensor occur as the RH of the chamber changes. Such instruments compute the RH of the headspace by monitoring the change in electrical capacitance. When the a_w of the sample and the RH of the air are in

equilibrium, the measurement of the headspace humidity gives the a_w of the sample (Labcell Ltd, 2016a).

Figure 2.9. AquaLab Pawkit (Labcell Ltd, 2016a).

In addition to equilibrium between the liquid phase water in the sample and the vapour phase, the internal equilibrium of the sample is important. If a system is not at internal equilibrium, one might measure a steady vapour pressure (over the period of measurement) which is not the true a_w of the system. An example of this might be a baked good or a multi-component food. Initially out of the oven, a baked good is not at internal equilibrium; the outer surface is at a lower a_w than the centre of the baked good. One must wait for a period of time (could take up to 40 minutes depending on the temperature of the sample) in order for the water to migrate and the system to come to internal equilibrium. It is important to remember the restriction of the definition of a_w to equilibrium. Temperature plays a critical role in a_w determination. Most critical is the measurement of the difference between sample and capacitance sensor temperature. Accurate measurements with this type of system require good temperature control (Decagon Devices, 2015).

2.4. Water Activity Measurement in the Research Domain

In this section, different investigations to develop non-destructive methods to predict a_w in cured meat will be discussed. These techniques are: Computed Tomography (CT), Near Infrared (NIR) and the Hyperspectral Imaging (HSI). Furthermore, in section 2.4.4 the microwave cavity sensor developed by the researchers from Liverpool John Moores University (LJMU) to predict a_w in cured meat will also be presented. Although, the cavity

type sensor demonstrated good results for a_w determination, the technique is destructive, leading to the aim of this work to develop and demonstrate a non-destructive method for determination of a_w in cured meat and meat products. The comparison of these methods are summarised in Table 2.3.

Table 2.3. Comparison of research based methods for a_w prediction.

Device	Sensor Type	R^2	RMSECV	Non-invasive	Self-calibrate	No sample preparation	Portable	Price(€)
Computed Tomography	X-Ray	0.832	0.0099	A sample placed inside the system	✓	✓	✗	>50,000
Near Infrared	Near Infrared Spectroscopy	0.618	0.0141	A sample placed under the system	✓	✓	✗	>7,000
Hyperspectral Imaging	Visible Light	0.906	0.0090	A sample placed under the system	✓	✓	✗	>20,000
Microwave Cavity Sensor	Microwaves	0.910	N/A	A sample placed inside the system	✓	✓	✗	>1,000

2.4.1. Computed Tomography

Computed tomography (CT) is an imaging procedure that uses special X-ray equipment to create detailed pictures, or scans, of areas inside the body. This method is mostly used in medicine (National Cancer Institute, 2016). However, CT has also been used in food science for different purposes (Santos-Garcés *et al.*, 2010) as it is able to distinguish biological tissues (Seeram, 2009). This shows that CT technology can be used for a wide range of applications, namely to estimate pig carcass composition (Font Furnols, Teran and Gispert, 2009) or to determine moisture content and water holding capacity in Atlantic cod fillets (Kolstad, Morkore and Thomassen, 2008). Segtnan (2009) used CT to study curing and salting processes in salmon fillets as there is a strong correlation between salt content and CT values. The method was also used to study curing and salting processes in cod (Haseth *et al.*, 2009) and dry-cured ham (Vestergaard, Risum and Adler-Nissen, 2004; Vestergaard *et al.*, 2005)

Santos-Garcés in his paper (Santos-Garcés *et al.*, 2010) states that a_w in meat products is highly correlated with moisture and salt contents, which can be predicted using CT. Based on this statement, he expected that CT technique (see Figure 2.10) could be used to develop a predictive model for a_w determination in cured meat products. Therefore, the objective of

his work (Santos-Garcés *et al.*, 2010) was to develop models for the local prediction of salt, water and a_w within dry-cured hams during the drying process using CT.

Figure 2.10. Scan of dry-cured ham using computed tomography (Font, Fulladosa and Garcia-Gil, 2013).

Santos-Garcés (2010) selected three different Regions of Interest (ROIs) from each tomogram: Biceps femoris muscle (BF), Semimembranosus muscle (SM) and Semitendinosus muscle (ST) (see Figure 2.11).

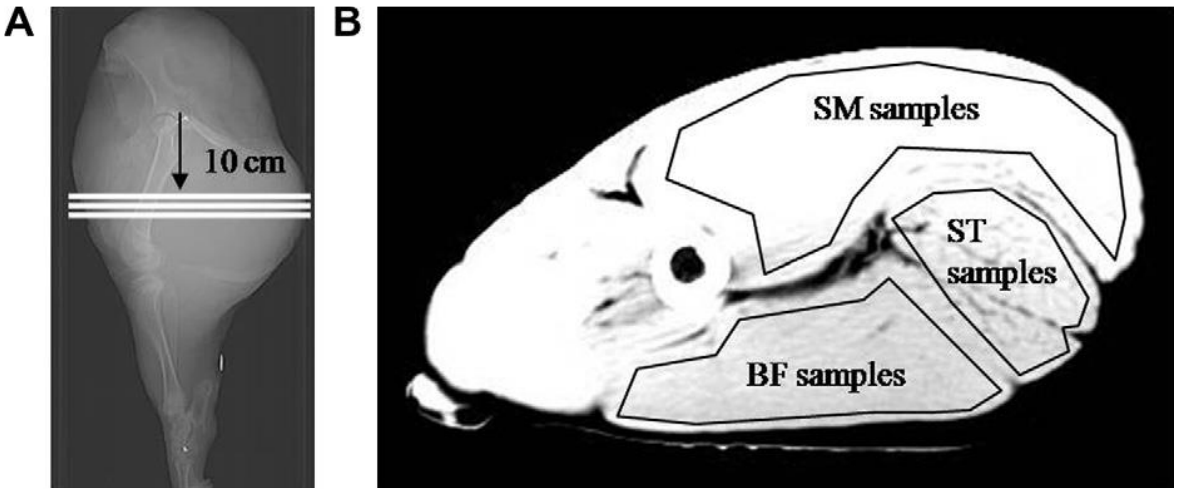

Figure 2.11. The location of the slice was at 10 cm from the aitchbone in the distal direction, at the widest part of the ham. A CT image (tomogram) showing a cross-sectional slice of a dry-cured ham at the end of the resting period. (Santos-Garcés *et al.*, 2010).

Santos-Garces *et al.* (2010) developed the predictive model for a_w using samples from all three regions *Biceps femoris* (BF), *Semimembranosus* (SM) and *Semitendinosus* (ST) samples (muscles) of the meat. During the study, it was investigated whether the fat content of the samples produces an essential disturbance in the predicted parameters. Thus, two different approaches were used: one including fat content as a covariate in the regression models; and the second approach removing ST samples (as they contained the highest level of fat) from the calibration samples set to improve the models. In addition, specific models were developed for each type of muscle as the chemical characteristics of muscles are different and can influence the predictions.

Table 2.4. Prediction models for a_w using different sets of samples.

Data Set	RMSEC	R^2	RMSECV
All Data	0.01	0.832	0.0099
All Data + fat (with ST samples)	0.0074	0.908	0.0076
BF	0.0053	0.949	0.0091
SM	0.0051	0.956	0.0082
ST	0.0087	0.842	0.0089

(Santos-Garcés *et al.*, 2010) concluded that model for prediction of a_w during the drying process was accurate enough (as it can be seen in Table 2.4) to consider CT as a useful tool for controlling and optimising the dry-cured ham elaboration processes. However, a fat content had a negative impact (RMSECV = 0.0099 and RMSECV = 0.0076 for samples without and with fat consideration, respectively) on the accuracy, which makes this method unreliable if the fat content is not considered.

2.4.2. Near Infrared

Near Infrared (NIR) spectroscopy is a part of the electromagnetic spectrum with the wavelength range of 780-2526 nm, which corresponds to the wave number range 12820-3959 cm^{-1}. The most prominent absorption bands occurring in the NIR region are related to overtones and combinations of fundamental vibrations of -CH, -NH, -OH (and -SH) functional groups (Reich, 2005).

NIR spectroscopy is well suited for measurement of moisture because water shows strong absorption bands in NIR, namely the first overtone of -OH stretching at around 6800–7100 cm^{-1} (1470–1408 nm) and the combination band of -OH stretching and bending at around 5100–5300 cm^{-1} (1960–1887 nm). However, the NIR method must be carefully calibrated against a reference method, and appropriate reference calibration standards of known moisture content have to be generated. This calibration phase is time consuming and requires the use of chemometrics (Corredor, Bu and Both, 2011). Additionally, NIR suffers from poor sampling due to the low penetration depths of NIR waves (Green *et al.*, 2005; Austin *et al.*, 2013).

Collell (2011) in his paper describes the ability of NIR reflectance spectroscopy to predict moisture, a_w and NaCl content at the surface of dry-cured ham during the process. He conducted a test on the surface of 98 hams using a Fourier Transform (FT) NIR spectrometer (see Figure 2.12) and two probes (on-contact and remote) during the process.

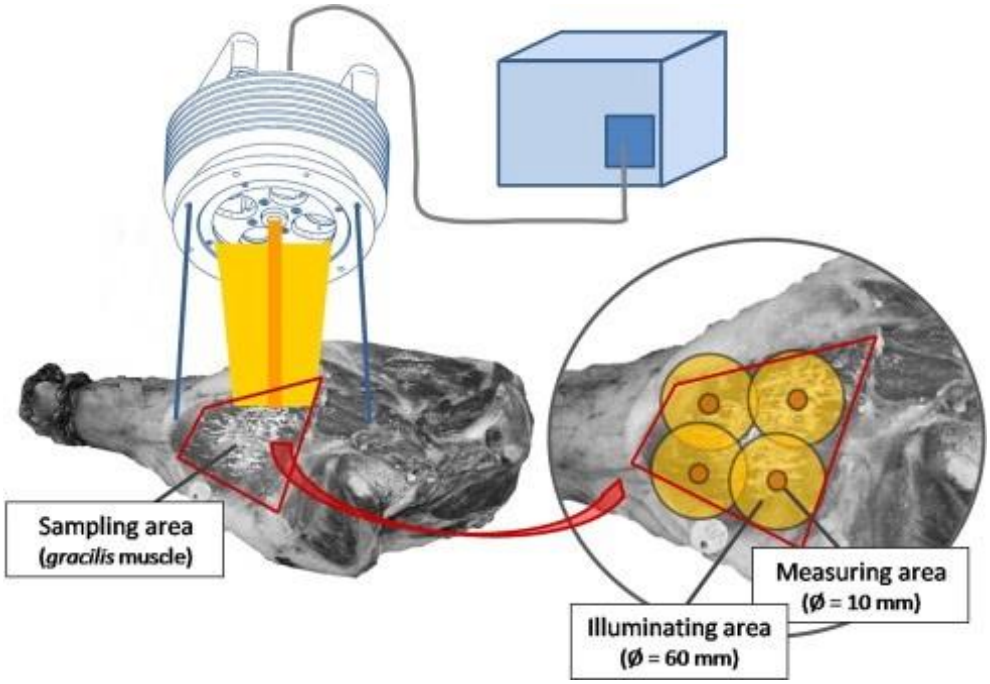

Figure 2.12. Remote measurement probe: Spectral acquisition setup on the gracilis muscle (Collell *et al.*, 2011).

Prediction models of a_w for both remote and on-contact measurements are demonstrated in Table 2.5. The model based on the remote measurement probe yielded poor results with determination coefficient R^2 = 0.62 and RMSECV = 0.0141. The prediction model developed based on data from on-contact measurements showed even weaker results, with R^2 = 0.451 and RMSECV = 0.0169. Based on this investigation, it can be concluded that NIR spectroscopy is not capable of predicting a_w. Perhaps the technique requires an improvement or further investigation.

Table 2.5. Prediction models for a_w determination of dry-cured ham samples.

Probe	R^2	RMSECV
Remote	0.618	0.0141
On-contact	0.451	0.0169

2.4.3. Hyperspectral Imaging

Hyperspectral remote sensing exploits the fact that all materials reflect, absorb, and emit electromagnetic energy, at specific wavelengths, in distinctive patterns related to their molecular composition. Hyperspectral imaging (HSI) sensors in the reflective region of the

spectrum (sometimes referred to as imaging spectrometers) acquire digital images in many contiguous and very narrow (nominally about 0.010 µm wide) spectral bands that typically span the visible, near-infrared, and mid-infrared portions of the spectrum (0.4-2.5 µm). This enables the construction of an essentially continuous radiance spectrum for every pixel in the scene. Thus, HSI data exploitation makes possible the remote identification of ground materials-of-interest based on their spectral signatures (Manolakis and Shaw, 2002).

Liu *et al.* (2013) from South China University of Technology and National University of Ireland carried out an investigation on non-destructive prediction of a_w of porcine meat slices by HSI during the salting process. Experimental work was undertaken by placing pork samples on the conveyer belt and then moving them to the field of view of the camera and scanning line by line for each salting period. The experimental setup is shown in Figure 2.13.

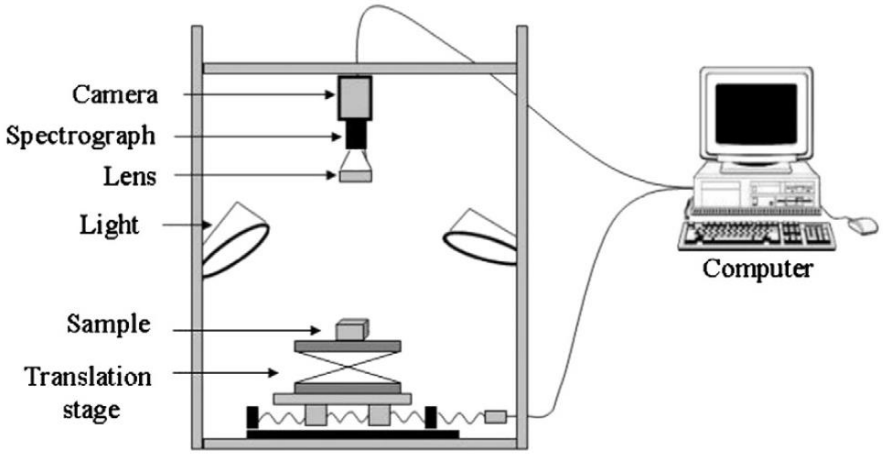

Figure 2.13. Schematic diagrams of main components of the hyperspectral imaging system (Liu *et al.*, 2013).

Once the data was collected from the sensor system, a prediction model was developed to determine a_w of meat slices during salting process. HSI (400-1000 nm) of pork slices were acquired at different periods of the salting process. The first model to predict a_w was developed by using Partial Least Squares Regression (PLSR). The model provided acceptable results with $R^2_{prediction} = 0.909$ for a_w. Based on the identification of the optimal wavelengths weighted using regression coefficients from the PLSR models, they compared three linear calibration algorithms including PLSR, Principle Component Regression (PCR) and Multiple Linear Regression (MLR). The comparison of the algorithms demonstrated that the optimized regression models had better performance with MLR model with $R^2_{prediction}$ =

0.914 and Root Mean Square Error of Prediction (RMSEP) = 0.007 for prediction of a_w. The performance of PLSR (full and simplified), PCR and MLR models for a_w parameters is shown in Table 2.6.

Table 2.6. Performance of PLSR (full and simplified), PCR and MLR models for salt and a_w parameters.

		Calibration		Cross-validation		Validation	
Parameter	Model	R^2_c	RMSEC	R^2_{cv}	RMSECV	R^2_p	RMSEP
a_w	PLSR-full	0.916	0.008	0.906	0.009	0.909	0.007
	PLSR	0.932	0.007	0.922	0.008	0.91	0.007
	PCR	0.925	0.008	0.918	0.008	0.913	0.007
	MLR	0.942	0.007	0.927	0.008	0.914	0.007

Based on the outcome of this study, Liu *et al.* (2013) concluded that the prediction models were accurate enough to consider HSI as a useful tool for controlling and optimizing the meat salting process. Industrial relevance: This feasibility study demonstrated that hyperspectral imaging offers the possibility for process monitoring and control and for optimization of key parameters during salting process in the meat industry.

2.4.4. LJMU Microwave cavity sensor

Researchers from the BEST Research Institute at LJMU have developed a microwave cavity type sensor that is illustrated in Figure 2.14. The sensor showed the potential of using microwaves in determination of Water Holding Capacity (Abdullah *et al.*, 2014; Mason *et al.*, 2016) and measuring a_w in dry-cured ham (Bjarnadottir *et al.*, 2014). The latter investigation was undertaken between BEST Research Institute (LJMU) and Animalia (Norwegian Meat and Poultry Research Centre, Oslo). The results obtained from this study demonstrated an acceptable linear correlation (R^2 = 0.91) between a_w and amplitude shift at 4.93 GHz (see Figure 2.15). These results indicate that microwave measurements might be a promising technique for determination of a_w for the process control of dry-cured hams, however this is a destructive measurement, which requires further investigation (Bjarnadottir *et al.*, 2014).

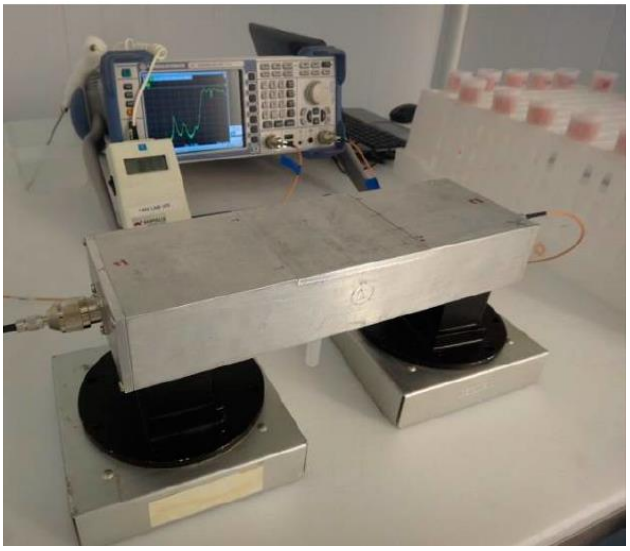

Figure 2.14. Microwave cavity sensor (Mason *et al.*, 2016).

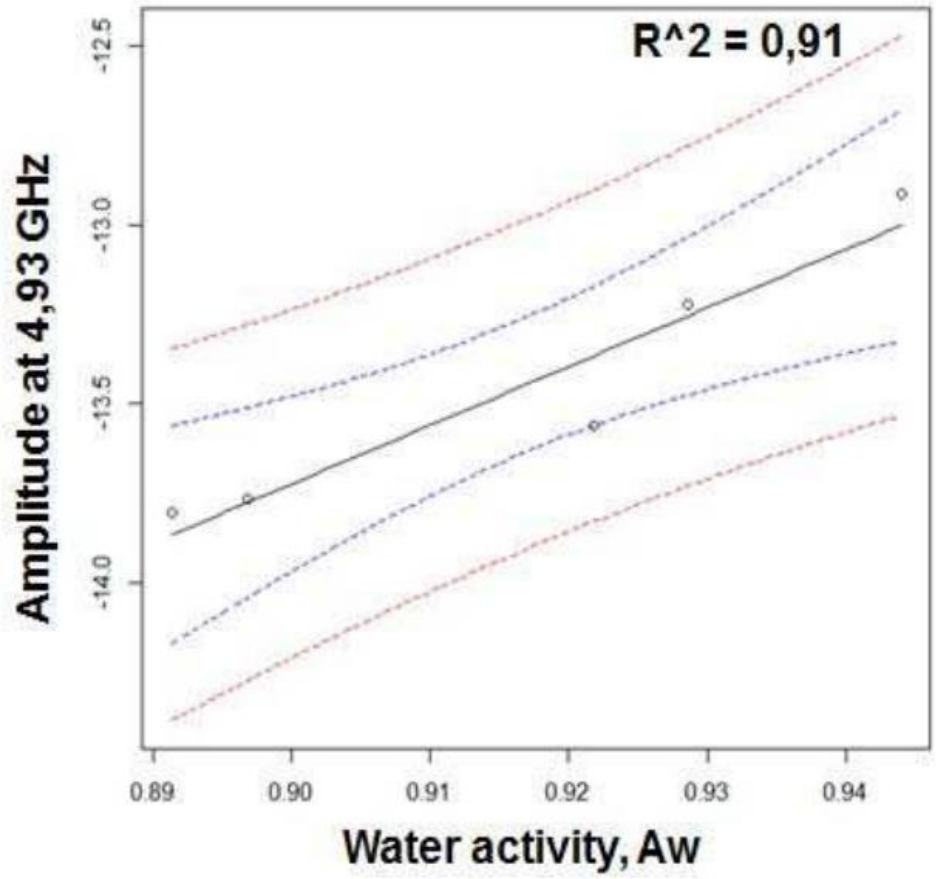

Figure 2.15. The correlation between the amplitude at 4.93 GHz and the water (Bjarnadottir *et al.*, 2014).

2.5. Summary

Water activity (a_w) is the only moisture related measurement that is an accepted HACCP control point. It is a management system, which regulates procedures to make sure the food produced is safe to eat. Based on the requirements of the HACCP system a_w is used as the main factor to determine shelf life of the product in food industry. Since a_w influences different chemical reactions in the product as well as the survival and the resistance of microorganisms. This makes a_w essential in production of cured meat, as it becomes an indicator of when the curing process is completed, and the product is ready for sale. This is important for safety reasons, but also for energy optimisation since curing requires high temperature and humidity. Currently commercially available a_w meters provide high accuracy. However, all existing methods to determine a_w in meat and meat products are destructive, which limits their continuous use during production, as samples must be disposed of after the measurement is complete. Additionally, the destructive nature is not the only disadvantage of the current techniques. The cost of the commercially available desktop a_w meters based on received quotations varies between £5,000 and £13,000 (e.g. Novasina LabTouch a_w Instrument cost £6,685.20 (Cole-Parmer, 2016b) and Novasina LabMaster Advanced a_w Meter cost £12,514.80 (Cole-Parmer, 2016a)), however a portable a_w meter is also available from AQUALAB (cost £2,000) (AQUALAB, 2016). The destructive manner of the measurement and high-cost are not the only limitations of this technology. To obtain an accurate measurement, the meters have to be calibrated or validated and the temperature of the sample has to be equilibrated as well. Figure 2.16 illustrates a flow chart of a_w measurement process used by commercially available instruments. As can be seen in the Figure 2.16, the whole process of a_w measurement can take 40-100 minutes, which makes the technology time-consuming.

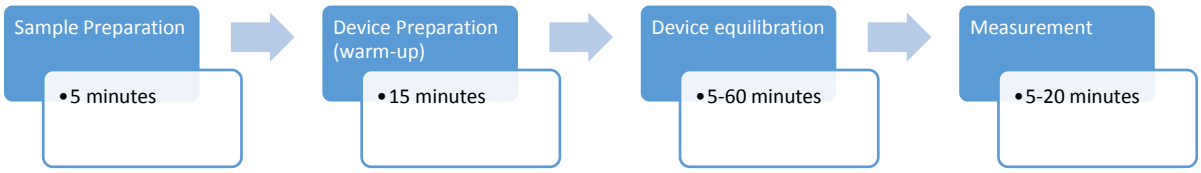

Figure 2.16. Flow chart of a_w measurement by commercially available devices.

This motivated researchers to investigate into developing non-destructive methods to determine a_w in cured meat products using X-Ray, Computed Tomography (CT), Near-Infrared (NIR) and Nuclear Magnetic Resonance (NMR). Although the investigation showed the potential of using these techniques to predict a_w in cured meat products, the cost of the instrumentation required is very high. In addition, the size of this equipment (specifically NMR and CT) is large and is not practical for rapid measurements. Finally, none of these technologies has gone further than an experimental work and they are not commercially available for the meat industry. Thus, the meat industry still requires a non-destructive method to determine a_w in cured meat.

Chapter 3 Introduction to Electromagnetic Waves and Design Considerations of Microwave Sensor

This chapter will introduce the electromagnetic waves, particularly microwave sensing system as a proposed technique to monitor water activity in cured meat products. Different sensor structures and their characteristics will be described and their features will be compared in order to select the most suitable sensor for this investigation. The desired frequency range for this investigation is 2-6 GHz owing to potential results obtained using the cavity sensor (see Figure 2.14) in previous work by the Built Environment and Sustainable Technologies (BEST) Research Institute (LJMU) in collaboration with the Norwegian Meat and Poultry Research Centre. Selected sensor structure will be studied in more detail to obtain satisfactory experimental results. The experimental work will be carried out with two approaches, namely discrete and continuous measurements. The discrete approach will be undertaken to determine water activity, which is an indicator of the safety of a product. The continuous measurements will be carried out for weight loss determination of cured meat, as it is the current industrial method to track the drying process of the product.

3.1. Electromagnetic radiation

In a tremendous intellectual leap, in 1873 James Clerk Maxwell suggested the existence of electromagnetic waves and predicted mathematically their properties before anybody had ever observed, or even thought of, such a phenomenon. Since then, scientists and communications engineers have used this radiation for a myriad of purposes. Electromagnetic waves can typically be described by any of the following three physical properties: the frequency f, wavelength λ, or photon energy E. The Figure 3.1 shows the electromagnetic spectrum and some of the applications for which they are used. The spectrum covers an enormous range with wavelengths ranging from the size of an atom to almost the size of the universe. The corresponding photon energies occupy a similar range, from the unmeasurable to the highly dangerous (Lawson, 2005).

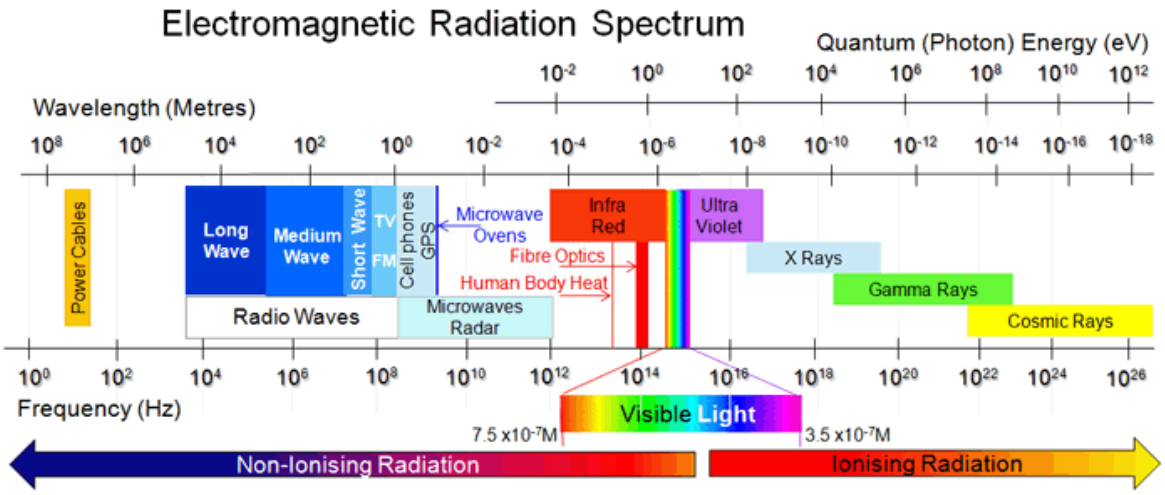

Figure 3.1. Electromagnetic Radiation Spectrum (Lawson, 2005).

Microwaves are electromagnetic waves that operate in the frequency range between 0.3GHz to 300GHz. Currently, microwaves are used in many applications but the first use was as a microwave radio telephone system in 1934 that was operated between England and France at 1.8GHz. In addition, the magnetron was developed in 1937, and found its use in a high-power microwave generation system, which is currently used in microwave ovens. Another important application based on the microwave spectroscopy is a radar system that is used by the military (Stutzman and Thiele, 2013).

3.2. Microwave Sensor Systems

Microwave sensing technology is a developing approach successfully used in various industrial applications, namely for real-time non-destructive measurements. The principle of this method is based on the interactions of microwaves with a material under test (MUT), which changes the velocity of the signal, i.e. attenuates or reflects the signal. Due to these changes, the permittivity of the material also changes and results in frequency shifts or attenuation of the incident electromagnetic signal. By considering how transmitted (S_{21}) and reflected (S_{11}) microwave powers vary at discrete frequency intervals, the change in the signal can be linked to the composition of the object under test (Korostynska *et al.* 2014).

Buschmüller (2008) investigated use of microwave resonance technology, which utilises the interaction between water molecules and changing electromagnetic fields. The measuring

frequency of the employed sensor was predetermined by the resonance wavelength of the microwave-induced resonator. The resonance frequency depends on the geometries of the employed sensors. If the resonator is loaded with materials, an increasing storage of electric field energy can be observed, which leads to a decreasing resonance frequency. The permittivity, which gets excited by the storage of energy, significantly changes in relation to the water content. In addition, the wet material disposes energy of the resonator, which results in an increasing width of the resonance waves.

Since resonators respond very sensitively, a high accuracy of measurement is possible. While an increasing water content leads to a decreasing resonance frequency, the frequency bandwidth increases simultaneously (see Figure 3.2). The broadening of the detected resonance frequency band is caused both by the product moisture and by the material load in the focus of the sensor. By considering frequency and bandwidth simultaneously and comparing it to the unstressed resonator in air, two independent properties become available, which enable the determination of the moisture content of a MUT. Therefore, a moisture content of a material can be obtained using microwave spectroscopy (Buschmüller *et al.*, 2008).

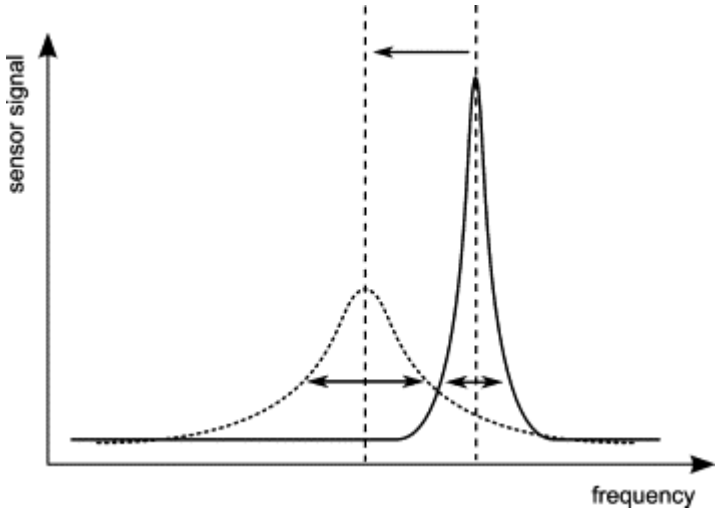

Figure 3.2. Microwave resonance curves. With increasing water content, the microwave resonance frequency decreases, while the frequency bandwidth increases. Resonance curves in air (solid line). Resonance curve in wet material (dash line) (Buschmüller *et al.*, 2008).

A standard microwave sensor system consists of three parts, namely a sensor head, vector network analyser (VNA) and graphical user interface (GUI). A block diagram of a microwave sensor system is demonstrated in Figure 3.3. VNA is an instrument that is widely used for Radio Frequency (RF) design applications and enables the performance of RF and microwave devices to be characterised in terms of network scattering parameters, or S parameters. VNA offers high number of sweep points, which provides more sensitive signal readings. The VNA data can be presented using magnitude, phase and complex data (real and imaginary).

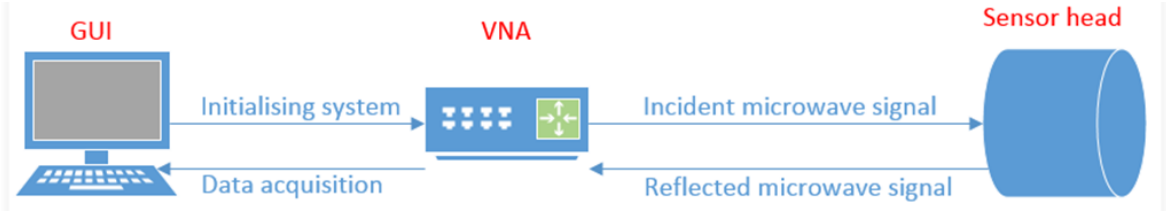

Figure 3.3. Block diagram of microwave sensor system.

The GUI has full control of the system, i.e. it initialises the VNA, configures desired parameters (e.g. S-Parameters, frequency range etc.), captures key information from a sensor head via VNA, analyses data/reflected signal and displays suitable parameters/information on a PC/laptop screen (e.g. Plotted/numerical data or predicted values of measurements).

3.3. Design Considerations for a Microwave Sensor

In this section, design considerations for a microwave sensor will be discussed. This work borrows heavily from antenna theory, however since the aim is to develop a sensor, structure and devices are referred to as such and the design considerations may vary owing to the different operating requirements. An antenna is defined by the IEEE as a "transmitting or receiving system that is designed to radiate or receive electromagnetic (EM) waves" (Antenna Standards Committee, 1983).

There are different types of EM sensors, which can be designed in different shapes and sizes, namely, a cavity resonator, wire (dipole, loops), aperture, microstrip and arrays. These are the most common EM sensors and a configuration of each one of them has a radiation pattern

and design parameters, in addition to their benefits and drawbacks (Fung, 2011). In sub-section 3.3.1, advantages and disadvantages of these sensors will be described in order to select the most suitable sensor for this investigation. The selection will be based on three main aspects, namely low cost, low profile and easily reproducibility of the sensor. The cost of the device must be competitive with the current commercially available instruments as the majority of the cured meat companies are small or medium-sized. Therefore, the companies cannot afford expensive equipment. The second aspect is low profile that is a significant design consideration owing to a nature of the product, i.e. varies sizes/shapes of cured meat products (see Figure 2.2). The final parameter of the sensor's design is its ability for high scale production.

Sub-section 3.3.2 will present patch type sensors, their structure and mathematical equations, which are necessary to calculate dimensions and resonance frequency of sensors. Another essential consideration in designing patch sensors are feeding techniques that will be discussed in sub-section 3.3.3. Finally, the third important aspect in the sensor design is its substrate, which will be introduced in sub-section 3.3.4.

3.3.1. Electromagnetic Sensors

A dipole is one of the most popular sensors as a modelling building block and in direct application, specifically the half-wave dipole. The structure of the sensor is simple with a straight wire fed in the centre that makes it a widely used sensor in communication and other applications. The amplitude distribution of the sensor is sinusoidal with a maximum at the centre owing to the simple and accurate model of the sensor as shown in Figure 3.4 (Stutzman and Thiele, 2013).

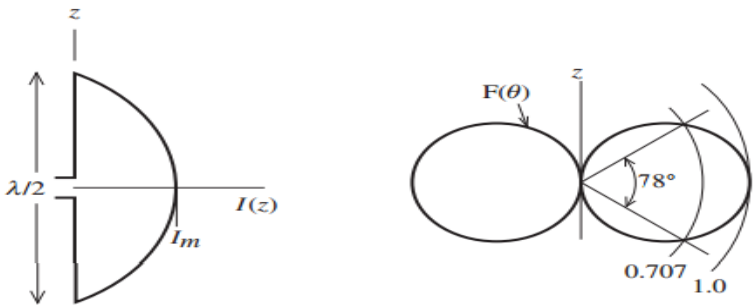

Figure 3.4. The half-wave dipole. (left) Current distribution. (right) Radiation pattern (Stutzman and Thiele, 2013).

A dipole antenna that is split in half at its centre feed point and fed against a ground plane called **monopole antenna**. The monopole antenna has the same currents and charges as on the upper half of its dipole counterpart. However, the dipole antenna has twice the terminal voltage. This behaviour is caused by the gap width of the input terminals, i.e. the dipole antenna has twice the input terminals and the same electric field over twice the distance that gives twice the voltage. Thus, the monopole antenna has half the input impedance that of the dipole counterpart (Stutzman and Thiele, 2013). A traditional monopole antenna is shown in Figure 3.5.

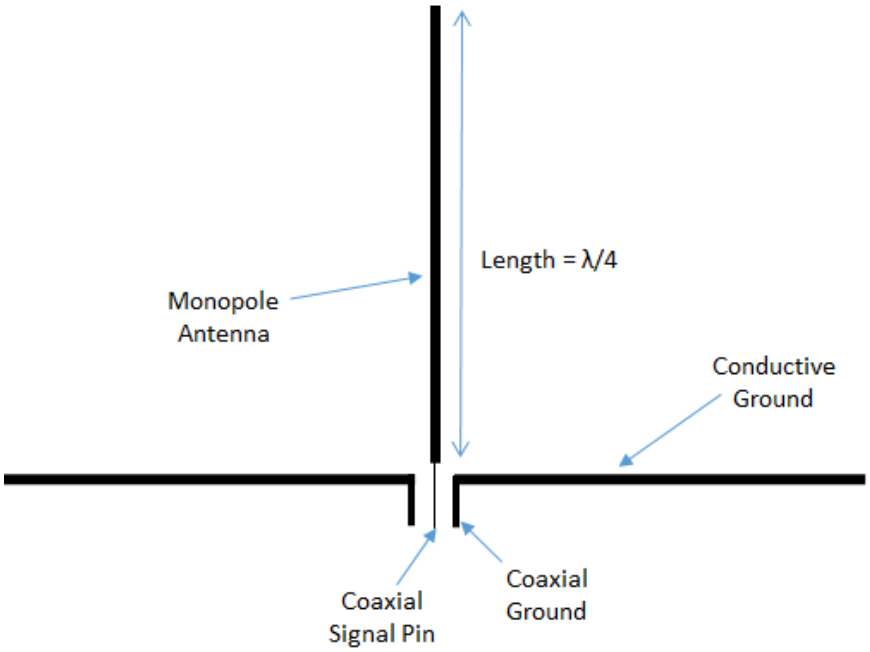

Figure 3.5. A traditional monopole antenna (Stutzman and Thiele, 2013).

Loop antenna is a simple and low-cost antenna type that can take many different forms, namely rectangular, square, triangle, ellipse and circle. Loop antennas are usually classified into two categories, electrically small and electrically large. Electrically small antennas are those whose overall length (circumference) is usually less than about one-tenth of a wavelength ($C < \lambda/10$). However, electrically large loops are those whose circumference is about a free-space wavelength ($C \sim \lambda$). Most of the applications of loop antennas are in the HF (3–30 MHz), VHF (30–300 MHz), and UHF (300–3,000 MHz) bands (Balanis, 2005). The loop sensor found its application in the water industry for water pipe leak detection using electromagnetic waves (Goh *et al.*, 2011).

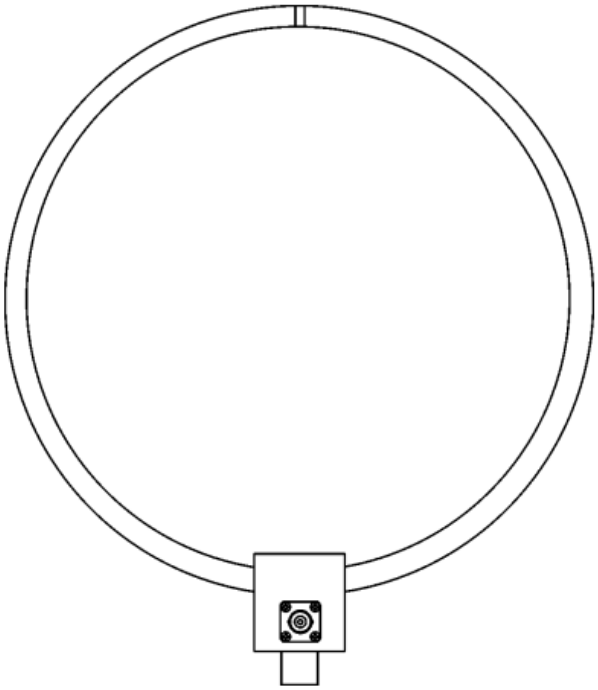

Figure 3.6. Loop sensor [Adopted from (Mess-Elektronik, 2016)].

The **helical antenna** is characterised by high gain, wide bandwidth and circular polarisation. Theses parameters make helical antenna unique in a wide range of applications, namely satellite communications, radio astronomy, TV signal transmission and wireless networking. The helical antenna combines two radiating elements, such as the dipole and loop antennas.

A helix becomes a linear antenna when its diameter approaches zero or pitch angle goes to 90^o. However, a helix of fixed diameter can be seen as a loop antenna when the spacing between the turns vanishes ($a = 0^o$). The rigorous analysis of a helix is extremely complicated. Therefore, radiation properties of the helix, such as gain, far-field pattern, axial ratio, and input impedance have been investigated using experimental methods, approximate analytical techniques, and numerical analyses (Ogherohwo and Barnabas, 2015).

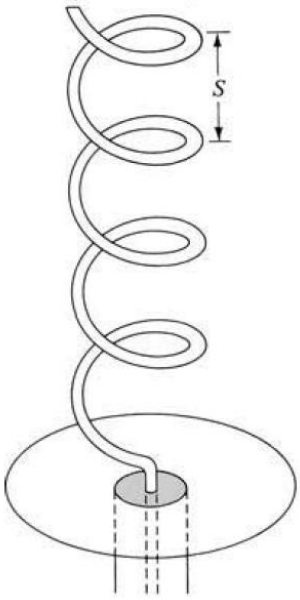

Figure 3.7. Helical sensor (Balanis, 2005)

The **microstrip patch sensor** is a single-layer design, which consists generally of four parts, namely patch, ground plane, substrate, and the feeding part. The sensors can be classified as single element resonant sensors. The sensor is a very radiating metal strip located on one side of a thin non-conducting substrate, the ground plane is the same metal located on the other side of the substrate. The metallic patch is normally made of thin copper foil plated with a corrosion resistive metal, such as gold, tin, or nickel (Alsager, 2011). The most common microstrip patch sensor is presented in Figure 3.8. This type of sensor has found its application in underwater wireless sensor networks (Abdou *et al.*, 2013).

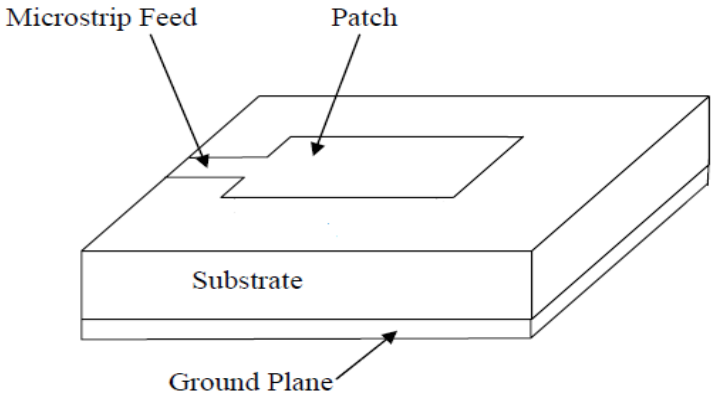

Figure 3.8. Microstrip patch sensor (Nitikanikks, 2017).

Phased array is a sensor system that consists of multiple sensor elements. Usually an array sensor is a combination of two or more patch sensors that are collected with a networking technique. The sensors have been traditionally used for military applications for the last few decades. Nowadays, they are used in other industries, namely for communication and radar applications (Ehyaie, 2011). A common design of the phased array sensor is shown in Figure 3.9.

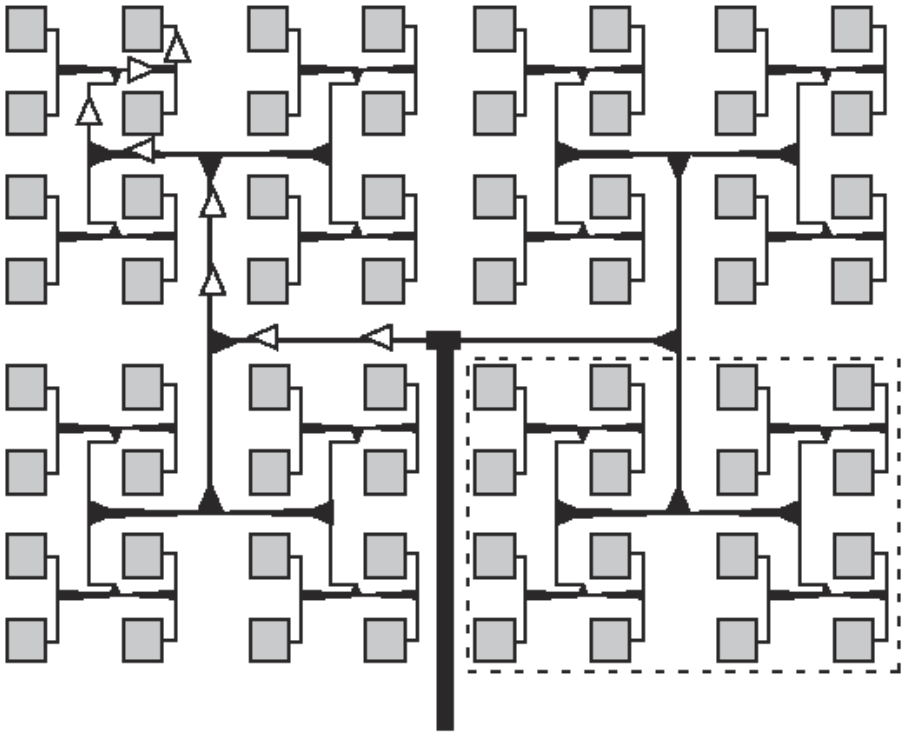

Figure 3.9. Phased array sensor (Ehyaie, 2011).

Aperture sensors were introduced to increase more sophisticated forms and the utilisation of higher frequencies. The sensors can be very conveniently flush-mounted on solid materials, namely on the skin of aircraft and spacecraft and covered with a dielectric materiel for protection in hazardous conditions of the environment. Therefore, the sensors are often used for aircraft and spacecraft applications. Figure 3.10 presents a pyramidal horn sensor, which is one of the forms of aperture antennas (Balanis, 2005). This type of sensor found its application in monitoring water infiltration on concrete flat roofs (Kot *et al.*, 2016).

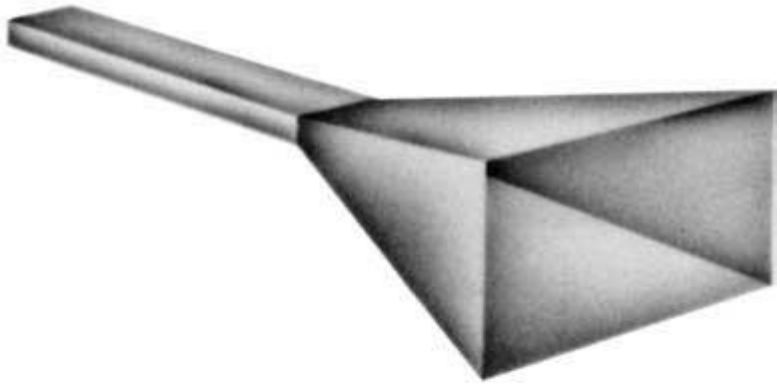

Figure 3.10. Aperture antenna (Balanis, 2005).

Phased array sensors are expensive to produce with the cost increasing with more radiating elements. Phase shifters, numerous feeds, and multiple cables are required. In addition, the building and assembly of a phase array will require more time than other sensor configurations being considered. Aperture sensors also can be very expensive depending on what type of material is used. Dimensions of a horn sensor are more complicated and may be hard to manufacture. Microstrip sensors can be built at a low cost by using cheaper substrate material (see section 3.3.4 for more details on substrate materials), and conductor material for the radiating elements and ground plane. Laser cutters can be used to cut out the shapes of the design and this can be quick. Moreover, microstrip sensors are lightweight as they can be made with a thin substrate and conductive foil (Fung, 2011).

Microstrip patch sensor is selected over other sensors for this investigation owing to meeting the criteria chosen for suitable sensor development. Microstrip sensor is lightweight and can be designed in a flexible size and shape, which enables one to conduct measurements with different sized meat and meat products. In addition, the production cost of the sensor can be

reduced by using low cost substrate material, which makes the overall price of the sensor affordable for small businesses.

3.3.2. Patch sensor design

3.3.2.1. Structure

The patch type sensors belong to the class of resonant sensors. A rectangular patch sensor is presented in Figure 3.11. It is resonant when the length, *L* is around half multiples of the resonance frequency. The patch type sensor consists in general of three major layers, ground plane, substrate and patch (Balanis, 2005).

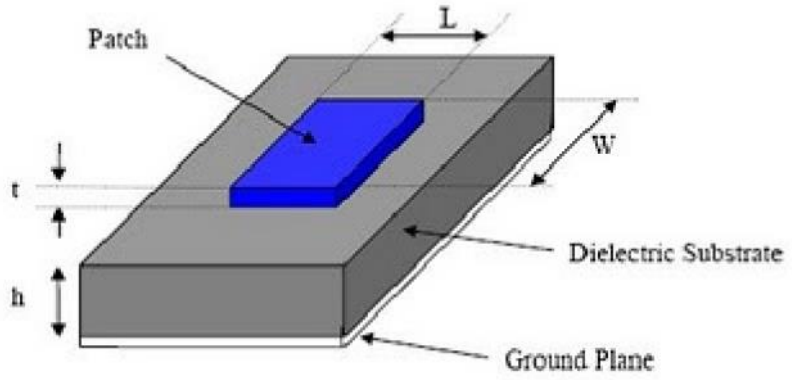

Figure 3.11. Structure of a rectangular patch sensor (Balanis, 2005).

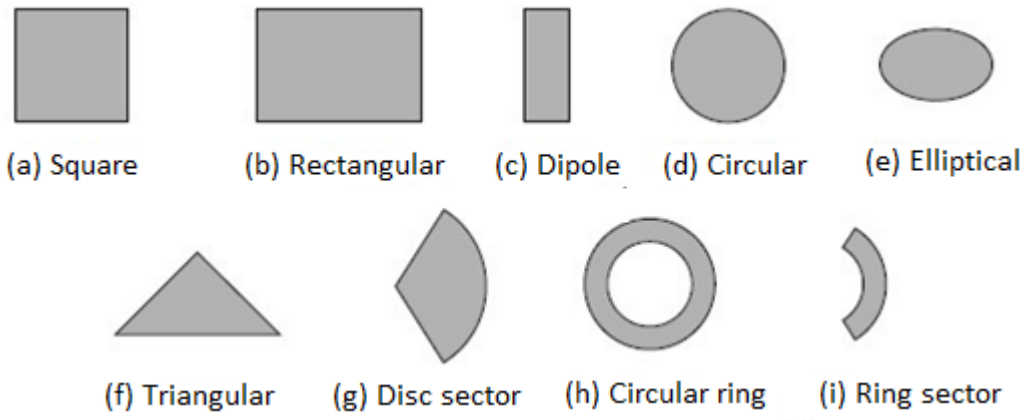

Figure 3.12. Common forms of patch layer (Balanis, 2005).

Figure 3.11 shows that the patch layer is rectangular but other common forms of patch layer are shown in Figure 3.12. Rectangular and circular patch layers are used often instead of triangular because it is easier to derive the mathematical expression for the model (Balanis, 2005). Therefore, the first sensor will be designed in rectangular shape.

3.3.2.2. Size Reduction of Patch Sensors

Meat products can be found in a variety of sizes depending on the type of the meat products as well as industrial marketing. The required sensor must be able to align with a size of a specific meat product. Consequently, the size reduction methods of patch sensors will be presented.

The common method for reducing the size of the patch sensor is to utilize a high permittivity dielectric substrate. However, the sensor are more expensive and have narrow bandwidth. To solve the above issues, many design techniques of the patch sensor have already been proposed, such as the inserted slot (Wong and Wu, 1997) the corrugation structure (Lee *et al.*, 2003), the iris structure (Seo and Woo, 2004), and the shorting pin (Waterhouse, 1995). But, these design methods have drawbacks in their design, namely a complex structure and low performance for miniaturisation (Jang, Kim and Kim, 2012). Therefore, the design methods of the size reduced patch sensor with metamaterial technology have been investigated by a number of authors (Lee *et al.*, 2007; Zhao, Lee and J. Choi, 2011; Garg, Verma and Samadhiya, 2012), specifically split ring resonators (SRRs) or complementary split ring resonators (CSRRs) (Jang, Kim and Kim, 2012).

Metamaterials are artificially engineered materials designed to provide material properties not readily available commercially. They can be designed to realise materials with near zero values of permittivity; negative permittivity or permeability; or simultaneous negative permittivity and permeability. The concept of metamaterials as well as metamaterials structures have also been used to design various types of antennas with enhanced performance, such as high gain as well as improved efficiency. Additionally, they have been used for the miniaturisation of antennas (Sharawi, Khan and Mittra, 2015).

The SRR was originally proposed by Pendry in 1999, and is the metamaterial resonator having the negative permeability (Pendry *et al.*, 1999). Two concentric metallic rings with a split on opposite sides form the SRR structure. This behaves as an LC resonator with distributed inductance and capacitance that can be excited by a time-varying external magnetic field component of normal direction of resonator. This resonator is electrically small LC resonator with a high quality factor. Based on the Babinet principle (Tan and Mcdonald, 2012) and the duality concept, the CSRR is the negative image of SRR, and the basic mechanism is the same for both resonators except for the excited axial electric field. With adjustment of the size and geometric parameters of the CSRR, the resonance frequency can be easily tuned to the desired value (Jang, Kim and Kim, 2012).

3.3.2.3. Calculations for a rectangular patch sensor dimension.

To design one simple rectangular patch sensor the following parameters need to be calculated: length, width and eventual feed line for microstrip sensor.

Length of sensor:

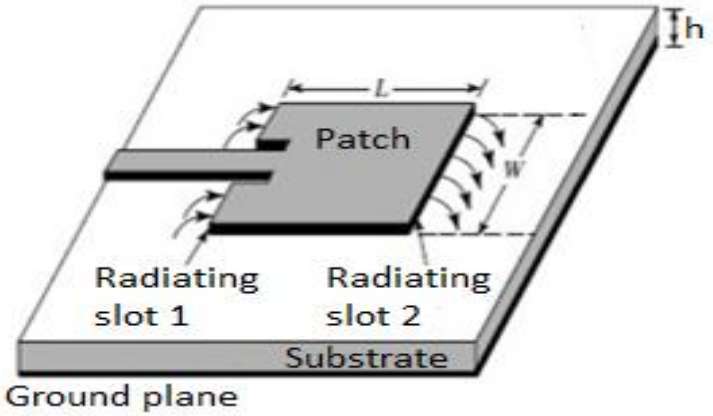

Figure 3.13. Fringing field (Balanis, 2005).

To calculate the length of the patch sensor, the fringing fields that occur need to be taken into account. The fringing field occurs at the end of the patch. The electric field does not end abruptly at the edges and therefore creates the "fringing fields". These fields can be represented as two radiation slots, which means that the patch looks electrically larger than

the physical size. Therefore, the calculated length needs to be extended with the fringing factor ΔL so the sensor design is for patch with $L = \lambda/2$ and no fringing (Balanis, 2005).

For a half - and quarter wave patch the resonate frequency is given in (3.1) (Balanis, 2005).

$$f_r = \frac{1}{2\sqrt{\varepsilon_0 \mu_0}(L+2\Delta L)\sqrt{\varepsilon_{eff}}} \tag{3.1}$$

Where:

ε_0 is the permittivity in vacuum

$\mu_0$is the permeability in vacuum

ΔL is the fringing factor

e_{eff} is the effective electric constant which take the fringing field outside the patch into account (Garg, 2001).

Effective electric constant given by formula (Balanis, 2005)

$$\varepsilon_{eff} = \frac{\varepsilon_r+1}{2} + \left(\frac{\varepsilon_r-1}{2}\right)\sqrt{1+12\frac{h}{W}}, \quad \frac{W}{h} > 1 \tag{3.2}$$

Fringing factor given by formula

$$\Delta L = 0.412h\left[\frac{\varepsilon_{eff}+0.3}{\varepsilon_{eff}-0.258}\right]\left[\frac{\frac{W}{h}+0.264}{\frac{W}{h}+0.8}\right] \tag{3.3}$$

To optimise the length and resonance frequency with formula (3.1), a praxis value for L is used.

$$L = 0.48\lambda_g \sim 0.49\lambda_g \tag{3.4}$$

$$\lambda_g = \frac{c}{f_r\sqrt{\varepsilon_r}} \tag{3.5}$$

where c is the velocity of light in vacuum.

The width of the patch gives by formula:

$$W = \frac{1}{2f_r\sqrt{\mu_0\varepsilon_0}}\sqrt{\frac{2}{\varepsilon_r+1}} \tag{3.6}$$

It is recommended that the width of the patch is in following interval (Al-Sajee and Hamad, 2011)

$$L < W < 2L \tag{3.7}$$

3.3.2.4. Calculations for a circular patch sensor dimension

The actual radius of the circular patch sensor can be obtained by

$$a = \frac{F}{\sqrt{\left\{1+\frac{2h}{F\pi\varepsilon_r}\left[\ln\left(\frac{\pi F}{2h}\right)+1.7726\right]\right\}}} \tag{3.8}$$

Where,

$$F = \frac{8.791E+09}{f_r\sqrt{\varepsilon_r}} \tag{3.9}$$

f_r = operating frequency

a = patch radius

h = thickness of the substrate

ε_r = dielectric permittivity of the substrate

3.3.3. Feed techniques

There are many methods to feed the patch and all have their advantages and disadvantages. These feeding methods can be classified into two groups, contacting and non-contacting. For the contacting methods, the patch sensor feeds directly to the patch and for the non-conducting method, electromagnetic field coupling is used to transfer the power to the patch. The most essential characteristics to be considered for this investigation are simplicity of a fabrication to reduce the cost and complexity as the main goal is to commercialise the sensing system. However, also retaining good reliability of the sensor's performance as low-

cost does not compensate low performance. Therefore, the justification of the selection of the feeding technique was based on these two aspects.

3.3.3.1. Microstrip Line Feeding

The microstrip line consists of a conducting strip connected to the patch. The microstrip line has often the same thickness as the patch but the width is smaller. The technique is very simple to design and analyse, and that is why this method is widely used. In addition, the technique is very easy to manufacture (Alsager, 2011). Figure 3.14 shows how to use microstrip as feed technique.

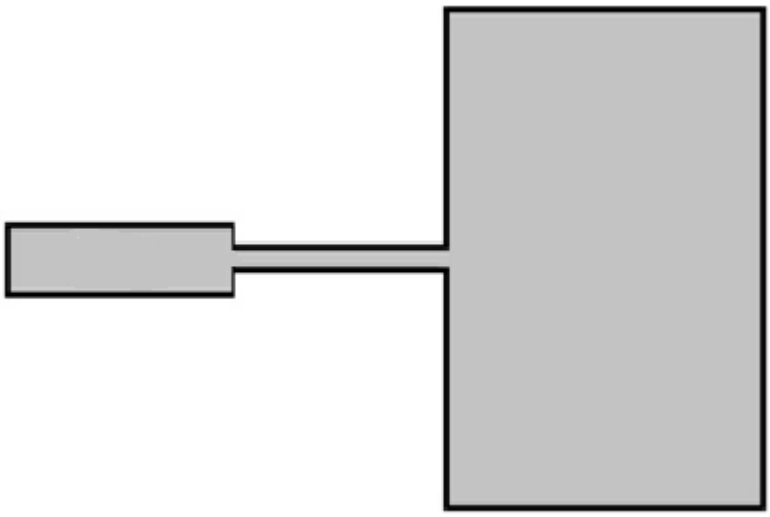

Figure 3.14. Microstrip line feed (Balanis, 2005).

3.3.3.2. Coaxial Feeding

The coaxial feed method is one of the most common feed techniques. The inner conductor of the coaxial goes through the substrate from ground to the patch and the outer conductor is connected to the ground plane (Balanis, 2005). Figure 3.15 shows how to use coaxial probe as feed technique.

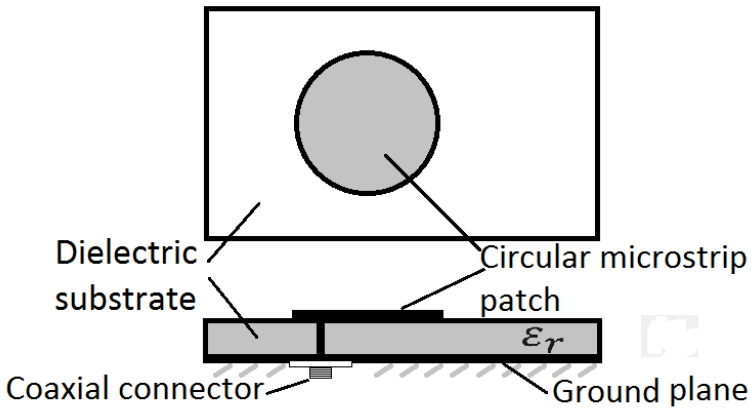

Figure 3.15. Coaxial feeding method.

3.3.3.3. Coaxial probe with capacitive feed

The difference between the usual coaxial feed and this method is that the inner conductor of the coaxial does not go the whole way up to the patch and the end of the inner conductor is connected to a circular plate. If a regular probe were used, a larger inductance would be introduced, which results in impedance mismatch. To cancel the inductance a reactance needs to be added. This feeding method with the capacitive disk does that (Balanis, 2008). Figure 3.16 shows how to use coaxial probe with capacitive feed as feed technique.

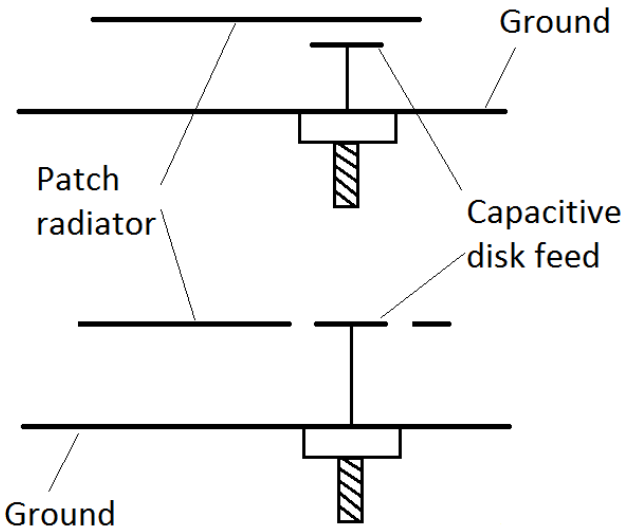

Figure 3.16. Coaxial probe with capacitive feed method.

3.3.3.4. The aperture-coupled patch

There are two layers of substrate below the patch. The substrate layers are separated with a ground plane. A microstrip line is placed below the lower substrate layer. The energy is coupled to the patch from the microstrip line by a slot in the patch. Figure 3.17 shows how to use the aperture-coupled patch as feeding technique (Balanis, 2005; Edling, 2012).

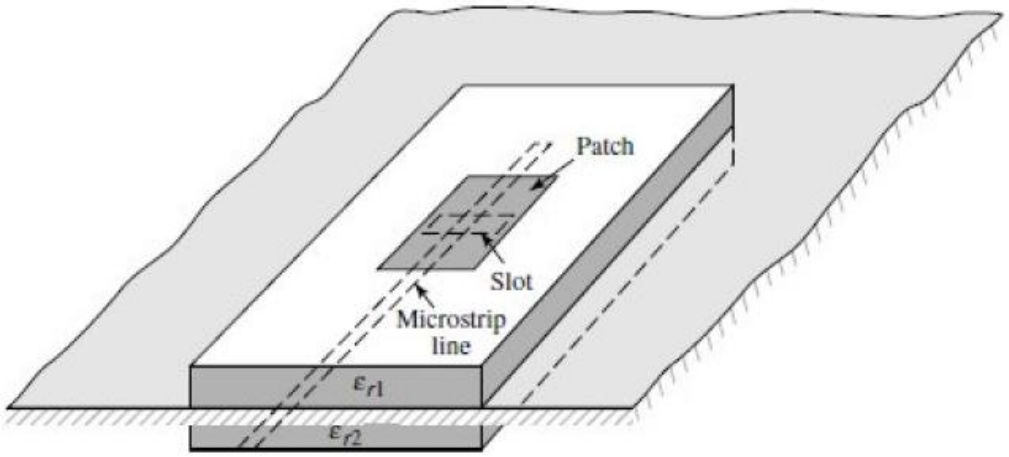

Figure 3.17. The aperture-coupled patch (Balanis, 2005).

3.3.4. Substrate

Substrate materials play an essential role for the patch sensor design. The substrates have many properties that should be considered: the dielectric constant, loss tangent, their variation with temperature and frequency, homogeneity, isotropic, thermal coefficient and temperature range, dimensional stability with processing and temperature, humidity and aging, and thickness uniformity of the substrate. One of the properties that the substrate has is permittivity. The permittivity is associated with how much electrical charge a material (substrate) can store in a given volume. The permittivity (ε) is complex and has one real part (ε') and one imaginary part (ε'') (Edling, 2012).

$$\varepsilon = \varepsilon' - j\varepsilon'' \tag{3.8}$$

The loss tangent ($\tan\delta$) measures the amount of electrical energy converted to heat in the dielectric and accounts for the power losses in passive devices such as the transmission line

or patch sensor and defined as the ratio between the real part and imaginary part of the complex permittivity (James and Hall, 1989; Edling, 2012).

$$\tan(\delta) = \frac{\varepsilon'}{\varepsilon''} \tag{3.9}$$

The relative permittivity or dielectric constant (ε_r) is the ratio between the real part of the complex permittivity and the permittivity of vacuum ($\varepsilon_0 = 8.854 \cdot 10^{-12} F/m$).

$$\varepsilon_r = \frac{\varepsilon'}{\varepsilon_0} \tag{3.10}$$

Since the speed of propagation in a given medium is:

$$c = \frac{1}{\sqrt{\varepsilon\mu}} = \frac{1}{\sqrt{\varepsilon_0\varepsilon_r\mu_0\mu_r}} = \frac{c_0}{\sqrt{\varepsilon_r\mu_r}}[m/s] \tag{3.11}$$

The dielectric constant affects the speed, it will also affect the wavelength and frequency:

$$\lambda = \frac{c}{f} = \frac{c_0}{f\sqrt{\varepsilon_r}}[m] \tag{3.12}$$

One common type of substrate is dielectric substrates. The substrate is used to fulfil two different factors, mechanical support for the structure and determining the electrical characteristics of the circuit or sensor (Edling, 2012).

Five different substrates Bakelite, FR4 Glass epoxy, RT-Duroid 5880, Taconic TLC and Benzocyclobuten, which are used for the fabrication of microstrip patch sensors, have been studied. A rectangular patch type sensor was modelled and simulated with the substrates using High Frequency Structural Simulation (HFSS) software. The purpose of this simulation was to select the most suitable substrate for this investigation and the criteria used in the selection were performance (namely return loss) and the dimensions of the sensor. The HFSS model of the sensor is shown in Figure 3.18.

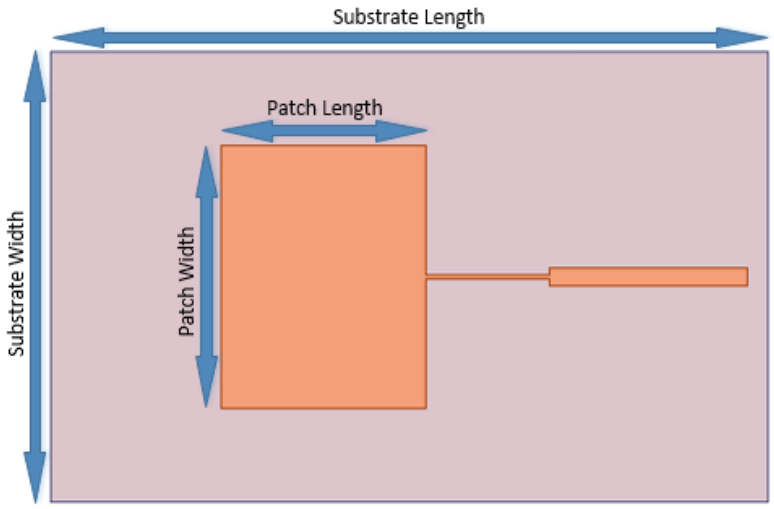

Figure 3.18. HFSS model of rectangular edge-fed patch sensor.

The return loss of the five substrates are plotted against frequency and displayed in Figure 3.19. FR4 substrate provides better return loss (-15 dBm) as compared to the other four substrates for the same resonant frequency.

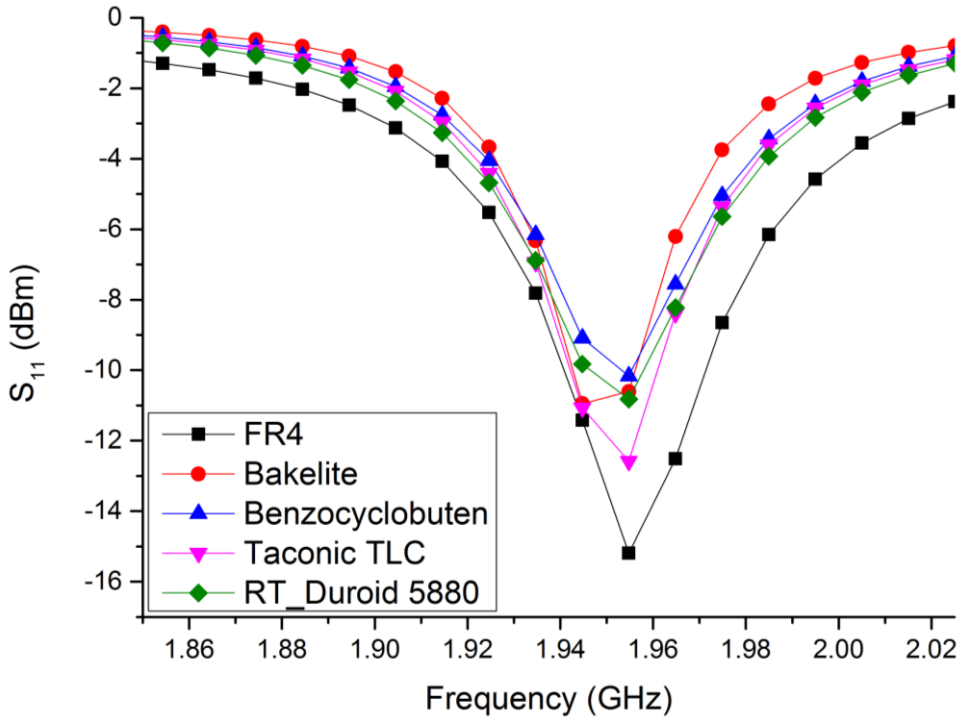

Figure 3.19. Return loss vs. frequency from the five substrates.

Characteristics of the substrates are shown in Table 3.1, namely the parameters and dimensions of a rectangular patch sensor with five different substrates. As can be seen from this table, FR4 substrate has better performance and in addition has the second smallest dimensions among the substrates after Bakelite. However, the return loss of Bakelite substrate is 4 dBm (about 5%) less than the return loss of FR4. Thus, the FR4 substrate will be given preference over other four substrates in this investigation.

Table 3.1. Characteristics of common substrates.

Characteristics	**FR4**	**RT-Duroid 5880**	**Taconic TLC**	**Bakelite**	**Benzocyclobuten**
Dielectric Constant (ε_r)	4.4	2.2	3.2	4.8	2.6
Loss Tangent (tanδ)	0.02	0.0009	0.003	0.002	0
Frequency (GHz)	1.95	1.95	1.95	1.94	1.95
Return Loss (dBm)	-15	-11	-12	-11	-10
Return Loss (%)	96.84	92.06	93.69	92.06	90.00
Patch Length (mm)	35.45	49.82	41.47	33.96	45.92
Patch Width (mm)	45.64	59.29	51.75	44.04	55.90
Substrate Length (mm)	77.90	98.40	87.10	75.50	93.30
Substrate Width	154.43	207.27	176.95	148.76	193.21
Substrate Height (mm)	1.57	1.57	1.57	1.57	1.57

3.4. Summary

This chapter introduced the electromagnetic waves, which could be potentially used to determine water activity in cured meat and meat products. As a part of electromagnetic waves, microwave spectrum was highlighted as the most suitable frequency range for this investigation, particularly the 2-6 GHz frequency range owing to a previous study (see section 2.2.4). Theory and concepts for the most common electromagnetic sensors were presented. Patch was chosen as the most suitable type/structure of sensor owing to its capability, low-cost of its production and most importantly its design flexibility. The latter is an essential criterion in the design consideration due to the nature of the cured meat products, i.e. various shapes and sizes of the product (see Figure 2.2). In addition, different structures of patch sensors and their characteristics were described, namely feeding techniques, dimensions and equations to calculate the size and resonant frequency were provided. Finally, the most common dielectric substrates for the sensor were reviewed and FR4 substrate was selected for this investigation owing to the simulation results illustrated in sub-section 3.3.4. The simulation results showed the lowest return loss (-15 dBm) and the second smallest dimensions among all five substrates. The sensor utilized for this simulation was a rectangular planar type with a transmission line feeding technique that resonates at 2 GHz, which demonstrated good performance in the simulation.

The preliminary experimental work will be conducted using this sensor; however, the frequency range between 1-6 GHz will be recorded in order to analyse the full spectrum of the desired frequency range (2-6 GHz). Frequencies from 1 GHz will be included owing to the potential of a resonant frequency shift (decrease) when the sensor is loaded with a wet material (meat sample) based on the theory in section 3.2. An additional advantage of this frequency range is it contains two ISM (industrial, scientific and medical) band frequencies, namely 2.45 GHz and 5.8 GHz. This means that the sensor can be commercialised as an industrial (meat industry is the main target), scientific or medical application/device.

Chapter 4 Research Methodology

The aim of this investigation is to develop a rapid non-destructive method to predict water activity (a_w) in cured meat using microwave spectroscopy. In this chapter, the design process of the research will be described, namely design, simulations, sample preparation, experimental approaches, data analysis and how to validate the theoretical models. The chapter will start with the design process and provide the flow diagram of the research methodology. Then, section 4.2 will introduce the HFSS (High Frequency Structural Simulation) software. In section 4.3, the sample preparation of the meat samples will be provided in detail. Section 4.4 will demonstrate the experimental setup of the continuous monitoring (monitoring of drying process) approach undertaken in this investigation. This section will be followed by the illustration of the second experimental approach, i.e. discrete monitoring for prediction of a_w in cured meat products. Finally, section 4.6 will describe procedures of data processing and prediction models development based on collected data.

4.1. Design process

A flow diagram of the research methodology is demonstrated in Figure 4.1. The first stage of this investigation was to review the literature on the existing methods/techniques to monitor the meat curing process and mainly to determine the water activity (a_w) parameter. Based on the literature review, it was ascertained that commercially available techniques to determine a_w are high-cost, time-consuming and destructive. In addition, new methods for a_w determination were reviewed and it was concluded that they still have not met the industrial requirements, i.e. some of them were more expensive than the current state of the art and others impractical owing to sample preparation requirements of the techniques. Build Environment and Sustainable Technology (BEST) research institute developed a cavity type sensor and conducted a research to determine a_w in cured meat samples. Although, the results were promising and showed a potential for a_w determination, the technique did not meet one of the requirements, i.e. the technique was destructive. Therefore, microwave technology systems were explored to develop a non-destructive sensing technique to determine a_w in cured meat products.

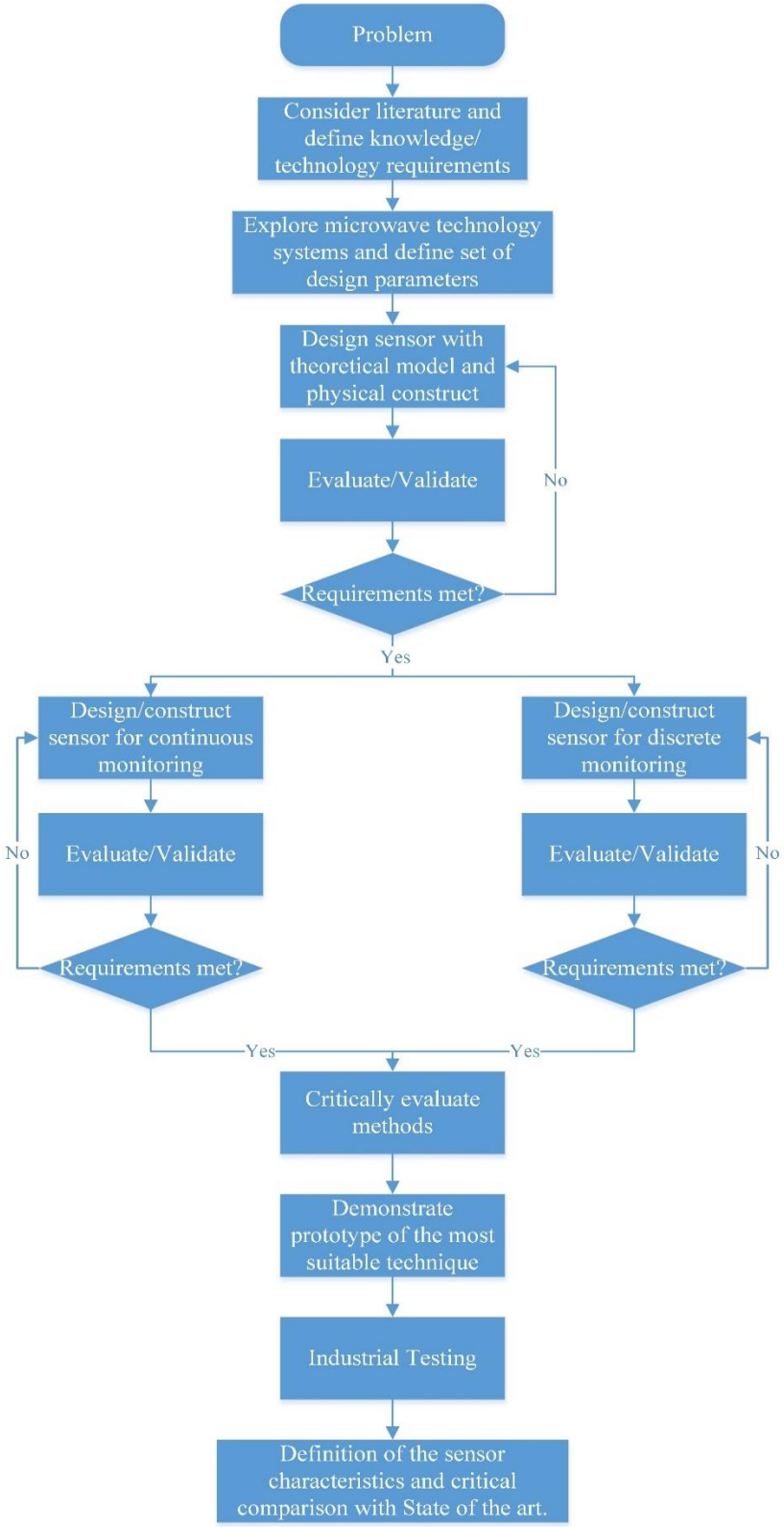

Figure 4.1. Flow diagram of a methodology.

Various structures of microwave sensors were investigated and the most suitable type was selected for this investigation. The main criterion of selection was based on the design

flexibility of the structures owing to the nature of the product, which comes in various shapes and sizes (e.g. shown in Figure 4.2). Thus, a number of patch type sensors were modelled, constructed and tested. A theoretical model of a meat sample was also designed, simulated and then validated. The validation of the model was carried out monitoring the drying process of fresh meat using the sensor. The validation process is presented in section 5.4 in more detail. The requirements for the validation was an agreement with the results obtained from a simulation of the theoretical models, which are presented in sections 5.2 (model with salt) and 5.4.1 (model without adding salt).

Figure 4.2. Cured meat products from *Roma's* (Romas, 2016).

Once the requirements were met, i.e. a good agreement between simulation results from a theoretical model and a real-world experimental work, the main experimental work was conducted. This was carried out in two approaches, namely continuous monitoring of the drying process and discrete monitoring for a_w prediction. The first approach is a current industrial technique to track the curing process and the second approach is an indication of the safety of a product. The experimental setups of both approaches are illustrated in sections 4.4 and 4.5 for continuous and discrete monitoring, respectively.

The next stage of the process was analysis of collected data and development of prediction models, which is demonstrated in section 4.6. Finally, after completing the experimental work and data analysis, a prototype of the most suitable technique was tested in the meat industry. The industrial testing was conducted in the Norwegian pilot plant owned by Animalia.

4.2. Design and Simulations

ANSYS HFSS software is the industry standard for simulating 3-D, full-wave, electromagnetic fields. Its gold-standard accuracy, advanced solvers and high-performance computing technologies make it an essential tool for engineers tasked with executing accurate and rapid design in high-frequency and high-speed electronic devices and platforms. HFSS offers state-of the-art solver technologies based on finite element, integral equation, and asymptotic and advanced hybrid methods to solve a wide range of microwave, RF and high-speed digital applications (ANSYS, 2016).

A relationship between dielectric properties and moisture content of foods has been studied by a number of authors (Sharma and Prasad, 2002; Sipahioglu and Barringer, 2003; Venkatesh and Raghavan, 2004; Lizhi, Toyoda and Ihara, 2008). When the field changes its polarity rapidly, only the water molecules can follow this change as they are small and have a strong dipole. This movement requires energy, which is drawn from the electromagnetic field. This loss of energy, which depends on the number of water molecules, is detected. When the product containing water is passed over the sensor, the resonance frequency decreases and the bandwidth of the resonance curve increases (due to losses of microwave energy inside the material) (Corredor, Bu and Both, 2011). This means that if a meat sample is placed on the sensor (see section 5.3.2) similar changes are expected to occur on the resonance frequency.

4.3. Sample preparation.

Sample preparation for all experiments followed the same procedure. The experimental design is shown in Figure 4.3. Pork loins from 60 pigs were purchased from a local slaughter house for this investigation. Each loin was deboned, back fat removed and cut into

approximately 100 × 70 × 50 mm pieces (each loin produced two samples). Sliced meat samples are shown in Figure 4.4 (a).

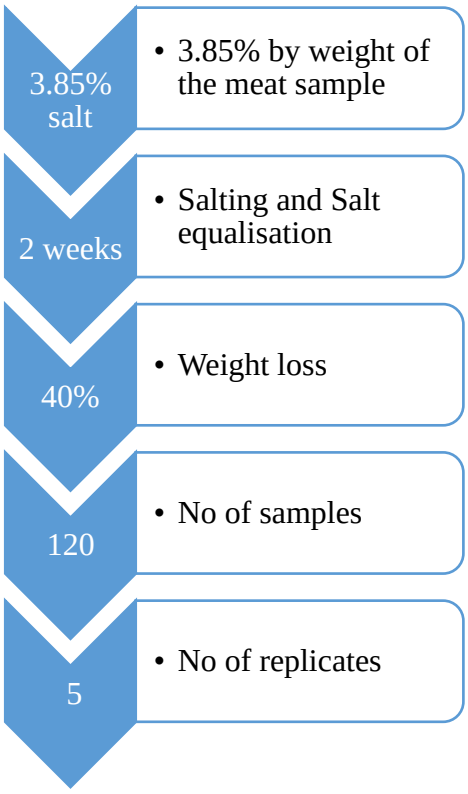

Figure 4.3. Design of experiment for the dry-cured ham model analysed in this study.

The desired weight loss was 40 % of initial weight as, generally, dry-cured meat products have 30-35 % weight loss in the final product (Fellows, 2000). In order to achieve a final salt concentration of approximately 5.5 % in the 30 % weight loss, all pieces had 3.85 % [see Figure 4.4 (b)] salt added prior to vacuum packing. Then all pieces were stored vacuum packed [see Figure 4.4 (c)] for two weeks at 4°C [see Figure 4.4 (d)] during salting and salt equalization. After salt equalisation, the pieces were unsealed and placed inside an incubation system (see Figure 4.5) at 12-14°C and 72-74 % relative humidity (RH) for microwave measurements until the samples obtained the desired weight loss.

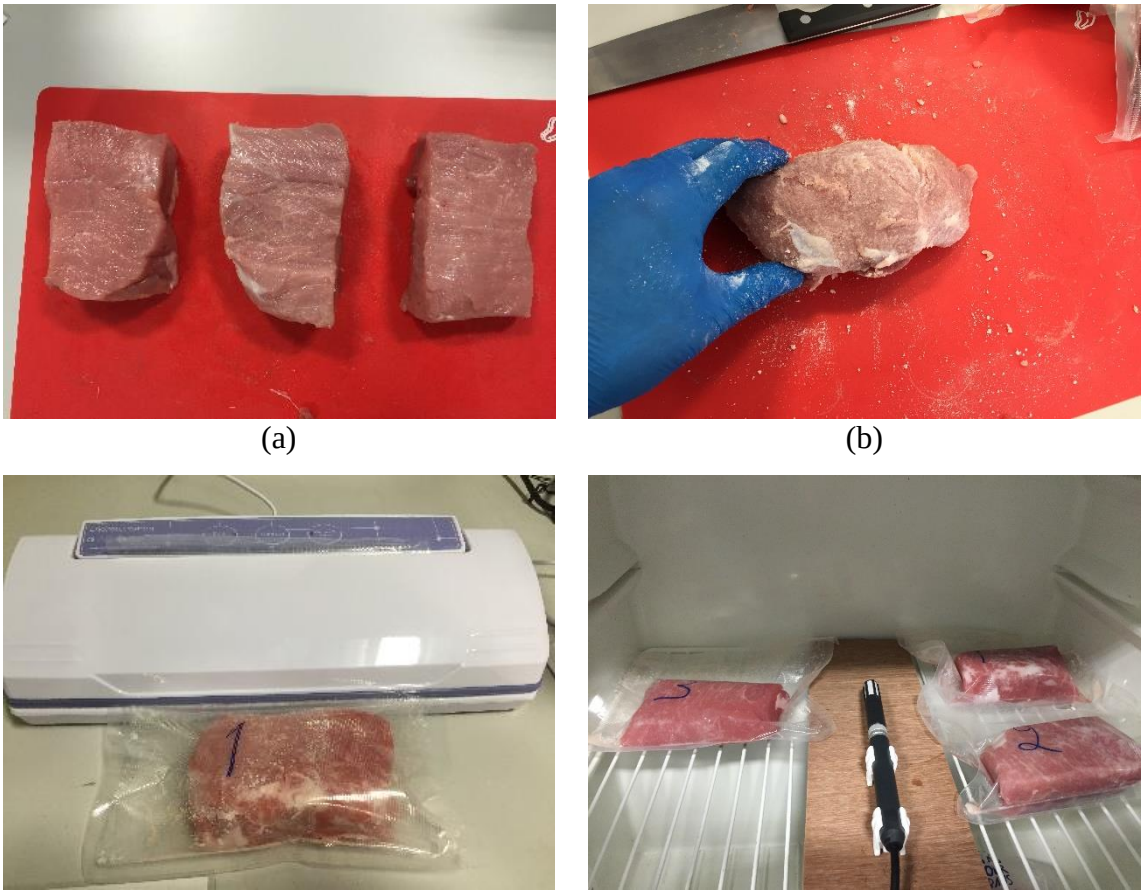

(a) (b)

(c) (d)

Figure 4.4. (a) Sliced meat samples, (b) salted meat sample (c) vacuum sealed sample and (d) meat samples inside temperature and humidity monitored refrigeration system.

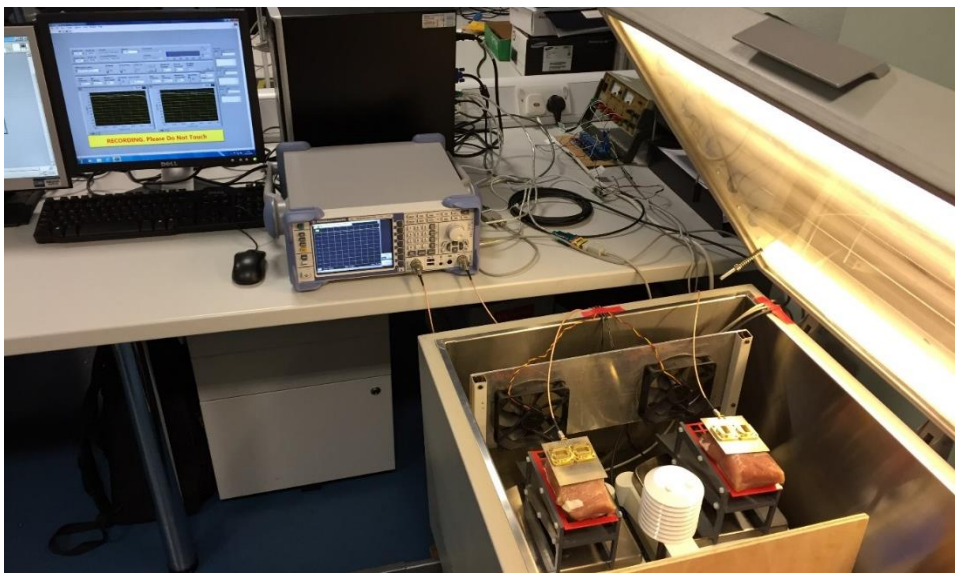

Figure 4.5. Incubation system.

4.4. Continuous Monitoring of Drying Process

The aim of this part of the investigation was to monitor the drying process of a meat, i.e. weight loss as it is the current method of tracking curing in industry. Currently, the weight loss of meat samples/products is determined by using weighing scales. A common meat-drying chamber is shown in Figure 4.6. The picture was taken in a Spanish meat company called Prolongo. As can be seen in Figure 4.6, there are hundreds of legs curing in the chamber, which makes the weighing task time-consuming and complicated. Therefore, a real-time monitoring of weight loss of the product would be beneficial for the meat industry which is currently lacking such a technique.

Figure 4.6. Dry-curing lambs' legs in Prolongo, Spain.

The experimental setup (shown in Figure 4.8) comprises two patch sensors mounted on top of two electronic weighing scales. Both sensors are connected to a PC via a Vector Network Analyser (VNA). The VNA and both weighing scales are connected to a computer for data acquisition via the LabVIEW interface, and are placed inside an incubation system to maintain a consistent temperature (approx. 13°C, ± 1°C). Temperature and humidity inside the incubation system are monitored by the temperature and humidity sensor, which is attached to the wooden board in the middle of the incubation system.

The sample is placed on a bespoke plastic "water runoff system" designed to prevent water pooling on the weighing scales once lost from the meat. The sensors are fixed on top of the samples with a weight (see Figure 4.8) to prevent the sensors from moving and falling off the samples. The sensor version 3 [see Figure 4.8 (b)] is taped to the "water runoff systems" as the weights used for the sensors version 1 and version 2 could not keep it on the meat sample. The weights and the tape did not have any effect on the sensors' readings.

To promote air circulation and promote water loss two fans are fixed inside the incubation system, pointed at the meat samples and the "water runoff systems". Both fans are connected to a power supply via a relay that is used to switch off the fans while the measurements are taken. The purpose of this is to avoid incorrect weight measurements as the scale is sensitive to small changes in air pressure. The fans are switched off for 10 seconds (it takes about 10 seconds for them to fully stop) in order to take the measurements and then the fans are turned back on. The scales are zeroed once the sensors and two "water runoff systems" are fixed to them, before placing the meat samples on them. The block diagram of the experimental setup is shown in Figure 4.7.

Measurement from the sensors is provided by using the S_{11} parameters from the VNA. Data acquisition (i.e. S_{11}, temperature and weight) took place once per hour over a period of 7 days (at this point the samples lost >40% of the initial weight). General weight loss of the final product is in the range of 30-35% of the initial weight loss. Therefore, the experimental work is stopped when the weight loss of the meat samples reaches 40%. The VNA was configured to record the full spectrum (from 9kHz to 13.6GHz) with 4000 sweep points (maximum points available on this instrument, i.e. ZVL 13GHz). Prior to the experiment, the coaxial cables, that connect the sensors to the VNA, are calibrated using the calibration kit for the ZVL 13GHz VNA instrument.

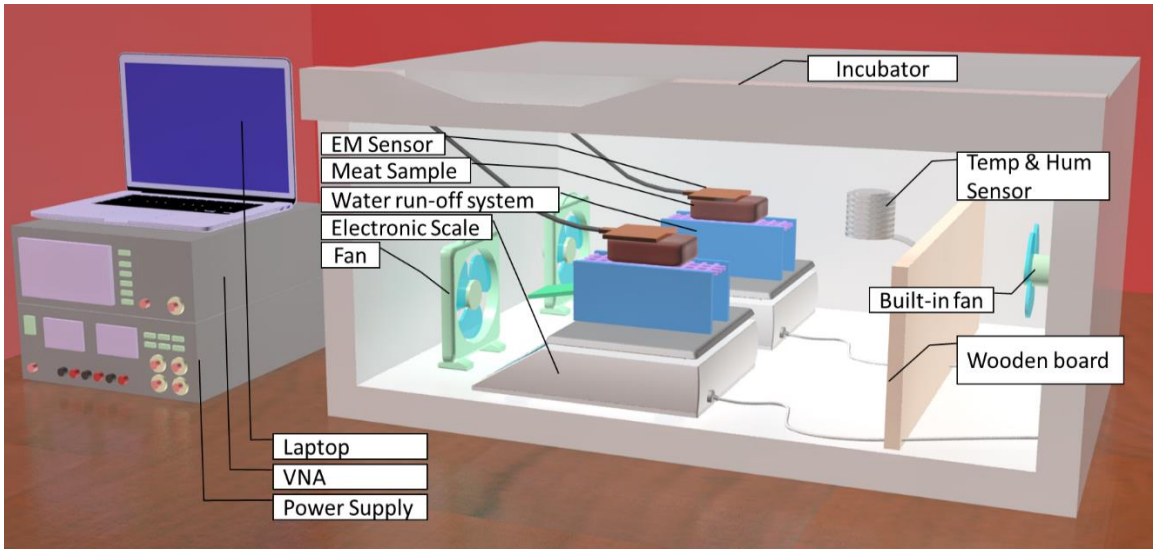

Figure 4.7. Block diagram of the incubation system.

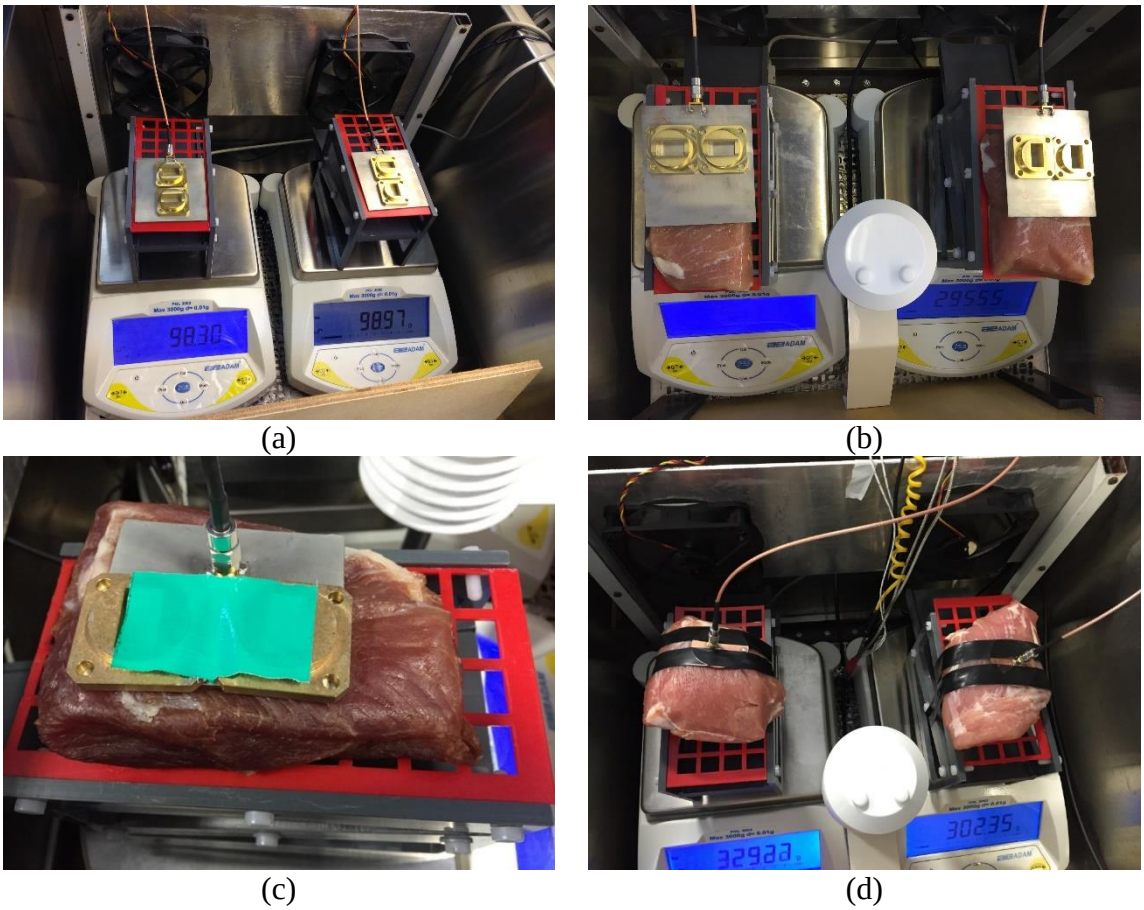

(a) (b)

(c) (d)

Figure 4.8. Experimental setup for monitoring of the meat drying process with (a) scales for monitoring weight loss, drip catchers/fans to move excess moisture away from sensor ((a) and (b) version 1, (c) version 2 and (d) version 3) and (b) humidity/temperature sensing to monitor drying condition inside incubation system.

4.5. Discrete Monitoring for Prediction of Water Activity in Cured Meat

This section presents an experimental work, which was undertaken to predict a_w in cured meat products. The sensors version 3, version 3.1 and version 3.2 were used for this experimental work that was replicated eleven times in which each measurement was made five times. In total, 83 samples (24-hour post slaughter meat samples/pork loins from the same slaughter house) were measured with the sensors. Moreover, once the measurements from the sensors were completed, a_w measurements were taken using AquaLab a_w meter [see Figure 4.9 (c)]. In addition, the sensor was tested on 14 cured meat products in the meat industry (Norwegian pilot plant owned by Animalia).

Measurements were provided by using the S_{11}-parameter from the Vector Network Analyser (VNA) since the sensor is a single port structure. Data acquisition (i.e. S_{11} and a_w) took place once every 24 hours over a period of 7 days; at this point the meat samples obtained the desired drop of a_w-value that is below 0.85. Figure 4.9 (b) shows the experimental setup (the sensor is connected to a VNA, which in turn is connected to a desktop computer running a bespoke LabVIEW interface) and Figure 4.9 (c) illustrates AquaLab a_w meter.

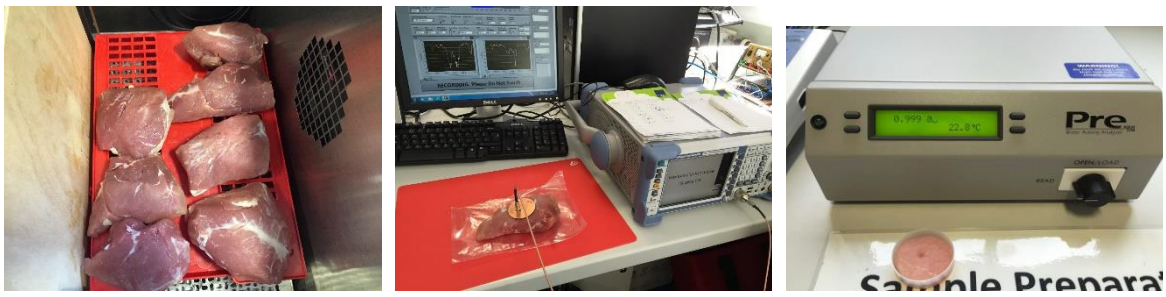

(a) (b) (c)

Figure 4.9. (a) Meat samples placed inside an incubation system at 12-14°C and 72-74 % RH for curing process, (b) experimental setup for measurement of S_{11} parameter using sensor and (c) AquaLab a_w meter used for correlation purposes.

4.6. Data Processing and Prediction Models

Once the data gathering is completed, the next stage of the investigation is data processing/analysis. Each measurement was replicated five times or more and then the mean value was calculated from the data owing to the general trend of the repeated measurements. One of the essential parts of the data processing was to compare the real measurements with the simulation results to examine the agreement between the two. The initial comparison was undertaken with the shift of the resonant frequency and then the changes in attenuation of the spectrum (i.e. S_{11}-Parameter).

One of the challenges during data processing was selecting the strongest correlation between the reflected signal and changes in meat samples (i.e. weight loss and water activity) as the spectrum contained 4000 sweep points. Therefore, a LabVIEW program was developed for the purpose of automatically correlating x variable (weight loss or water activity) against y variable (electromagnetic spectrum). The program correlates two variables and saves the R-squared values (4000 in this case) in an excel file in less than 20 minutes. The LabVIEW program is shown in Figure 4.10.

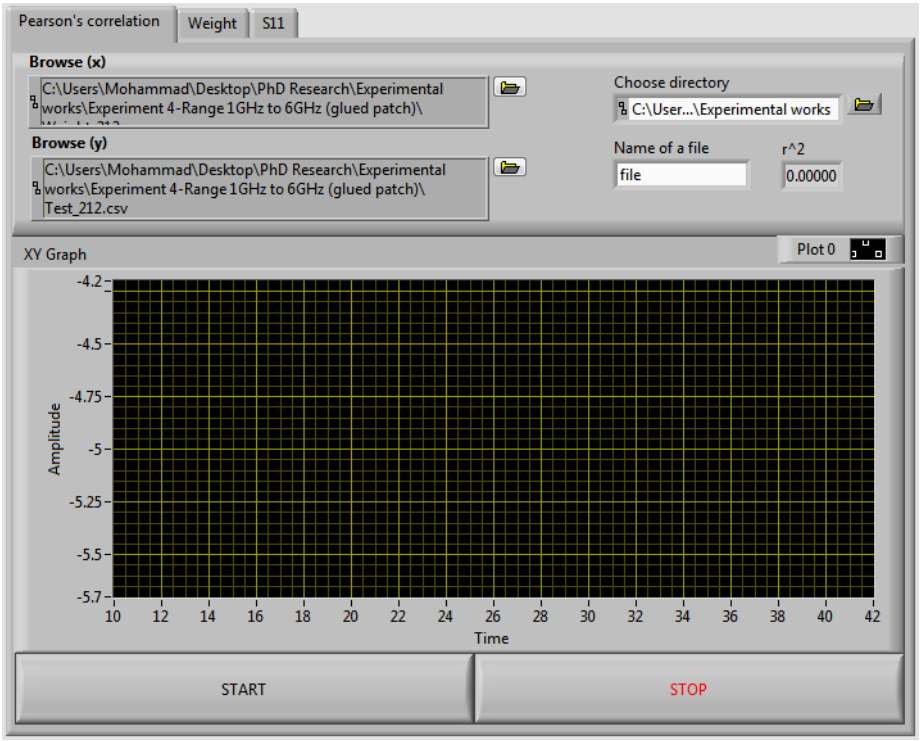

Figure 4.10. LabVIEW program for R-squared determination.

Once the data was pre-processed, Partial Least Squares Regression (PLSR) analysis was applied to create a prediction model. The PLSR technique was selected for this investigation owing to its ability to handle many independent variables, even when predictors display multicollinearity, i.e. predictor variables (electromagnetic spectrum in this case) in a multiple regression model are highly correlated, meaning that one can be linearly predicted from the others with a substantial degree of accuracy.

The PLSR has a number of advances, which include creating independent latent variables directly based on cross products involving the response variable(s), making for stronger predictions, robustness in the face of data noise and missing data and ability to model multiple dependents as well as multiple independents (Garson, 2016). PLSR method is implemented as a regression model in numerous analytical software packages, namely SPSS, SAS, PROC PLS and can also be used in such a powerful software development tool as MATLAB.

The PLSR analysis was carried out using MATLAB (R2013b version) software. In order to conduct the analysis, the PLS library was downloaded and then added to the search path of MATLAB as shown in Figure 4.11. The library and source codes are written by (Li, Xu and Liang, 2014) MATLAB 7.10.0 (R2010a) and freely available for scientific use. The MATLAB codes and instructions how to apply this PLSR technique is provided in Appendix B.

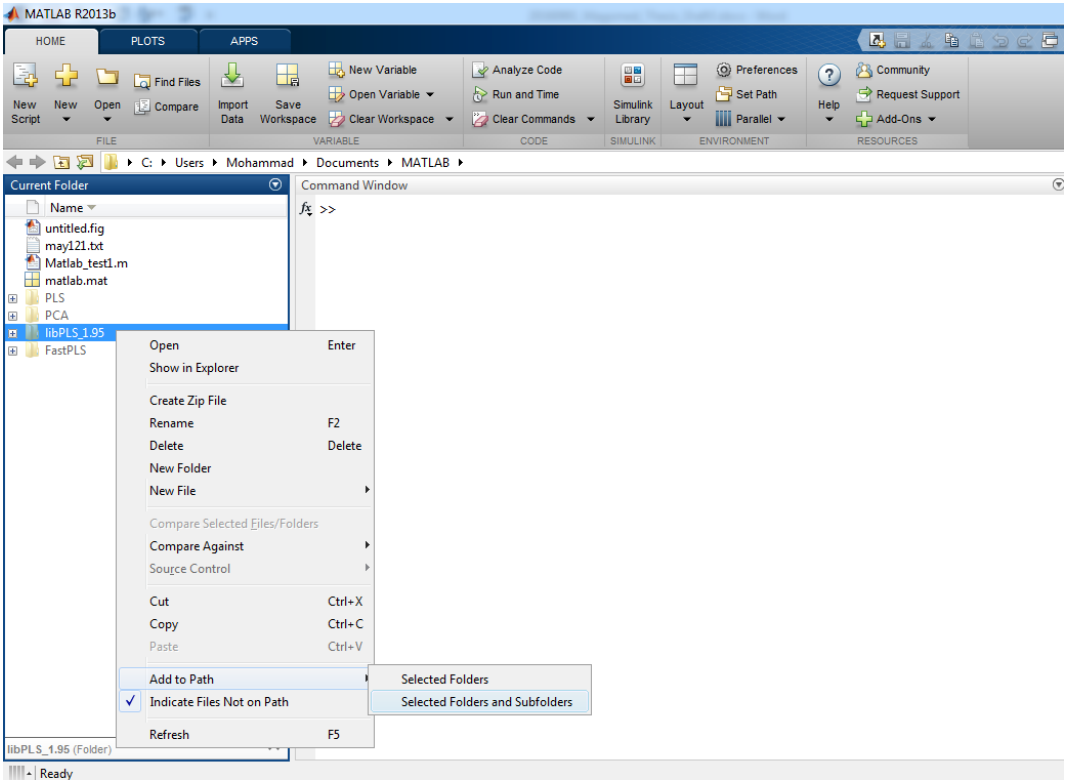

Figure 4.11. Adding PLSR library to the search path of MATLAB.

4.7. Summary

This chapter described the design process of the research methodology, which will be implemented to complete this investigation. There are two different approaches that will be taken in this study, namely continuous monitoring of the drying process and discrete monitoring to determine water activity in cured meat products. The first approach is to monitor the weight loss of the product, as it is a current method to track the drying process used by the meat industry. The second approach, i.e. discrete monitoring for water activity determination, is an indicator of the safety of a product. It introduced the HFSS simulation software and what is expected from the simulation work. Finally, it illustrated the techniques of data processing and prediction used in this study.

Chapter 5 Sensor Design, Implementation and Validation

This chapter will provide design of utilised sensors, their implementation and validation of the sensors and theoretical models for this investigation. Section 5.1 will present the HFSS models of the sensors and theoretical model of meat samples. The simulation results obtained from the sensors with the theoretical model will be demonstrated in section 5.2. Sensor implementation, i.e. EAGLE models, printing procedure and comparison between simulation and experimental results of the sensors in air will be illustrated in section 5.3. The following section 5.4 will present validation of the theoretical model, including HFSS simulation results, experimental setup and real-world experimental results.

5.1. Sensor Design

The initial sensor utilised in this study was a rectangular patch type sensor, which resonates at 2 GHz [see Figure 5.1(a)]. The shape and resonant frequency of the sensor has followed the methodology used during previous research undertaken by LJMU and Animalia Research Centre (S G Bjarnadottir *et al.*, 2015). Dimensions and resonant frequency of the sensor were calculated using equations/formulas from section 3.3.2.2. The dimensions of the second sensor [see Figure 5.1 (b)] were adjusted to increase the resonant frequency to 2.4 GHz as this is an ISM (Industrial Scientific and Medical) band, which enables the proposed sensor prototype to be commercialised. The sensor version 3 [see Figure 5.1 (c)] was calculated using equations in section 3.3.2.4. The sensors version 3.1 and 3.2 were developed by reducing the size of the sensor version 3.

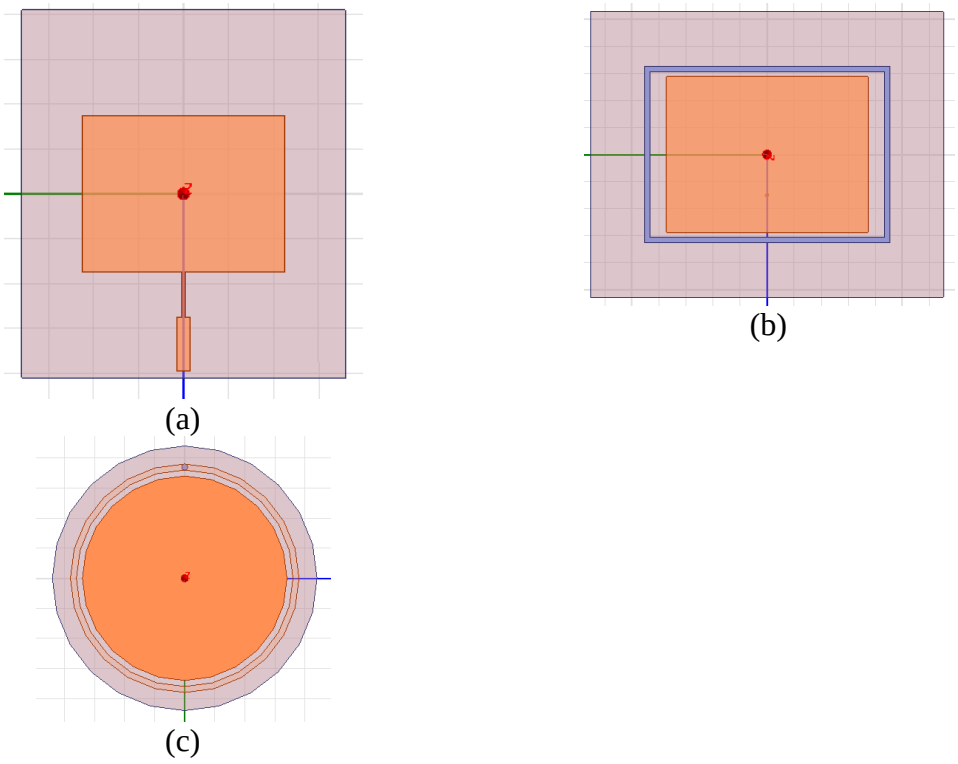

Figure 5.1. Top view of sensors (a) version 1, (b) version 2 and (c) version 3.

The top and bottom view of the HFSS models of version 3.1 and version 3.2 is illustrated in Figure 5.2 (a) and Figure 5.2 (b), respectively.

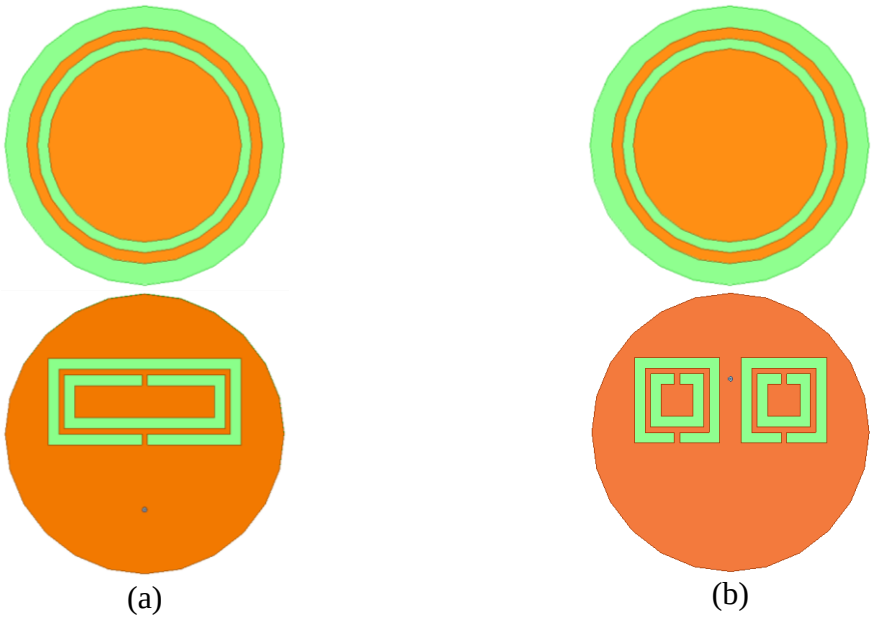

Figure 5.2. Top and bottom view of HFSS models of sensors (a) version 3.1 and (b) version 3.2.

Return loss of the sensors with and without the CSRR (see sub-section 3.3.2.2 for more detail) cells is shown in Figure 5.3 (a) and Figure 5.3 (b) for version 3.1 and version 3.2, respectively. The version 3.1 has three high performing (return loss below -10 dB is desirable as above 90% of the power is reflected) resonance frequencies at 2.87 GHz (-34 dB), 4 GHz (-17 dB) and 5 GHz (-21 dB) with the CSRRs, whereas the return loss of all troughs of the sensor without the CSRR cell is above -7 dB, that means less than 80% of power is reflected. The return loss of the version 3.2 is also improved to -32 dB (99.94% reflected power) at the 2.58 GHz resonance frequency. Additionally, as can be seen in the Figure 5.3, the resonance frequencies are decreased when the CSRR cells are etched on both sensors.

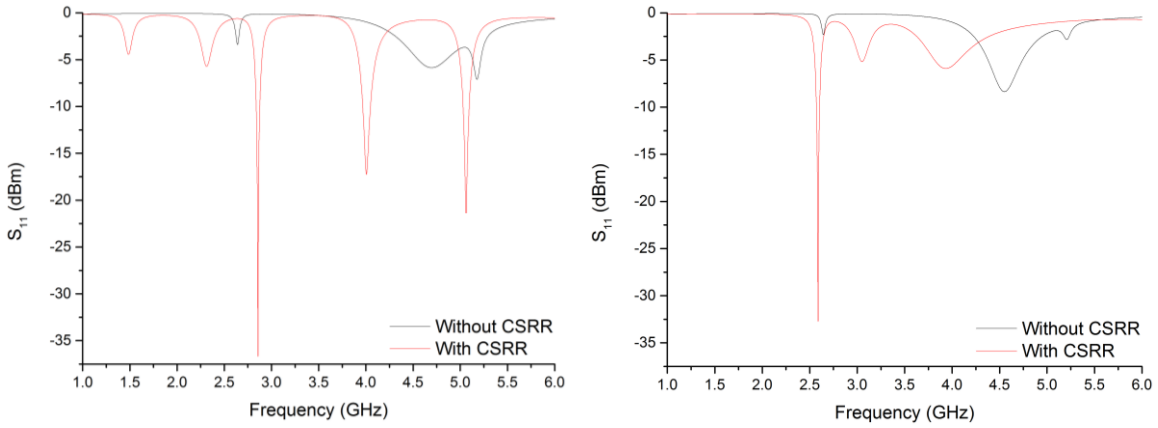

Figure 5.3. Return loss of sensors (a) version 3.1 and (b) version 3.2 with CSRR and without CSRR cells.

The dimensions (length = 60 mm, width = 60 mm and height = 10 mm) of the sample are setup so it would cover the patch area of the sensor as demonstrated in Figure 5.4. The material was assigned as water because raw meat consists of approximately 75% of water. However, relative permittivity and dielectric loss tangent of pure water are 81 and 0 respectively at 2.45 GHz, while relative permittivity and dielectric loss tangent of raw pork meat are 54 and 0.33, respectively.

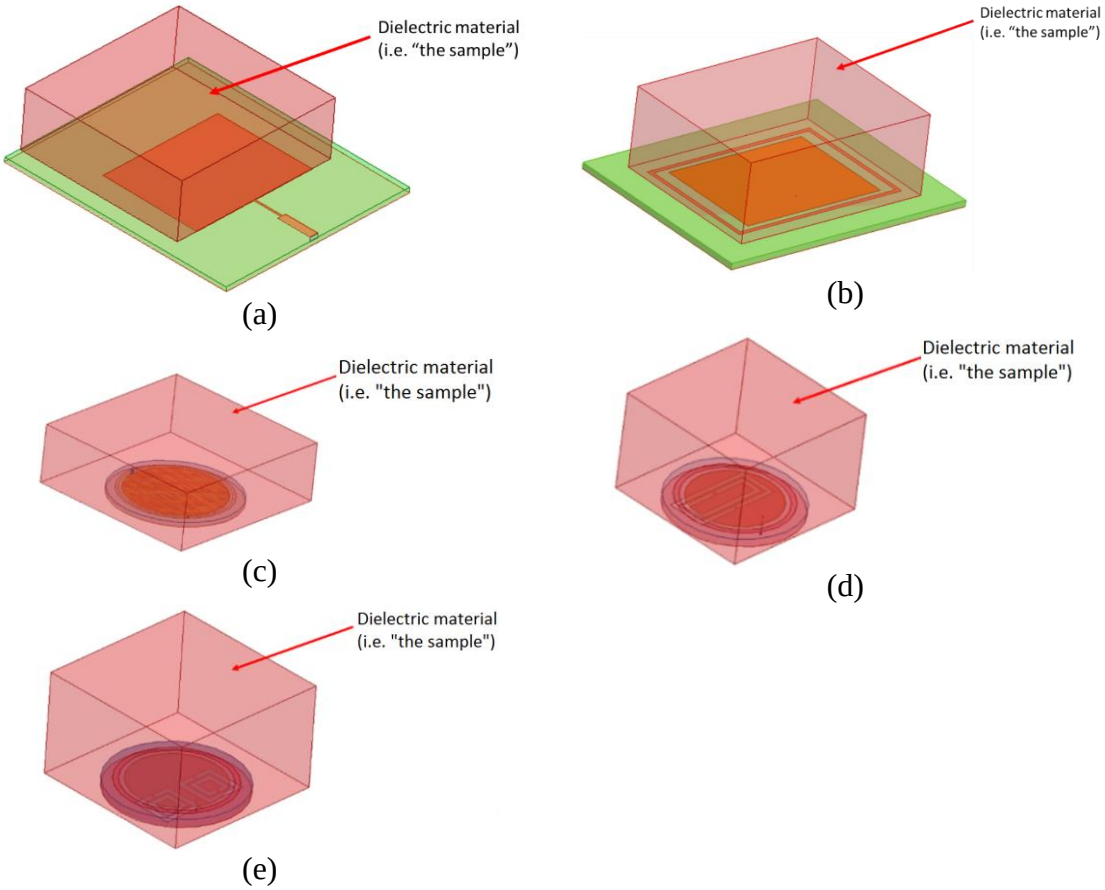

Figure 5.4. Theoretical models of sensors (a) version 1, (b) version 2, (c) version 3, (d) version 3.1 and (e) version 3.2.

5.2. Sensor Simulation Results

The water activity of a product could be derived from its dielectric properties. The water molecule is the main component that relaxes, and it can be assumed that dielectric values correspond to the average behaviour of the water molecules. The higher the binding of water to food matrices such as protein chains, the lower the water activity and lower the relaxation frequency because this prevents water molecule from easily following the alternative electric field. Hence a study of dielectric relaxation spectra and in particular relaxation frequency, is likely to offer a solution to access water activity (Clerjon, Daudin and Damez, 2003).

Thirteen simulations were completed in HFSS by decreasing the relative permittivity of the sample (from 54 to 30, decrementing by two values) and one more simulation without the sample (sensor in an air vacuum). Figure 5.5, Figure 5.6, Figure 5.7, Figure 5.8 and Figure 5.9 demonstrate HFSS simulation results from sensors version 1, 2, 3, 3.1 and 3.2. The

results are provided by S-Parameter (i.e. $S_{11,}$ reflection coefficient). The resonance frequency of all sensors is decreased and bandwidth is increased when a modelled meat sample is placed on the microwave resonance sensors owing to dielectric constant of loaded material. The theory behind this behaviour of the resonant frequency and bandwidth is provided in section 3.2: "*If the resonator is loaded with wet materials, an increasing storage of electric field energy can be observed, which leads to a decreasing resonance frequency. The permittivity, which gets excited by the storage of energy, significantly changes in relation to the water content. In addition, the wet material disposes energy of the resonator, which results in an increasing width of the bandwidth*."

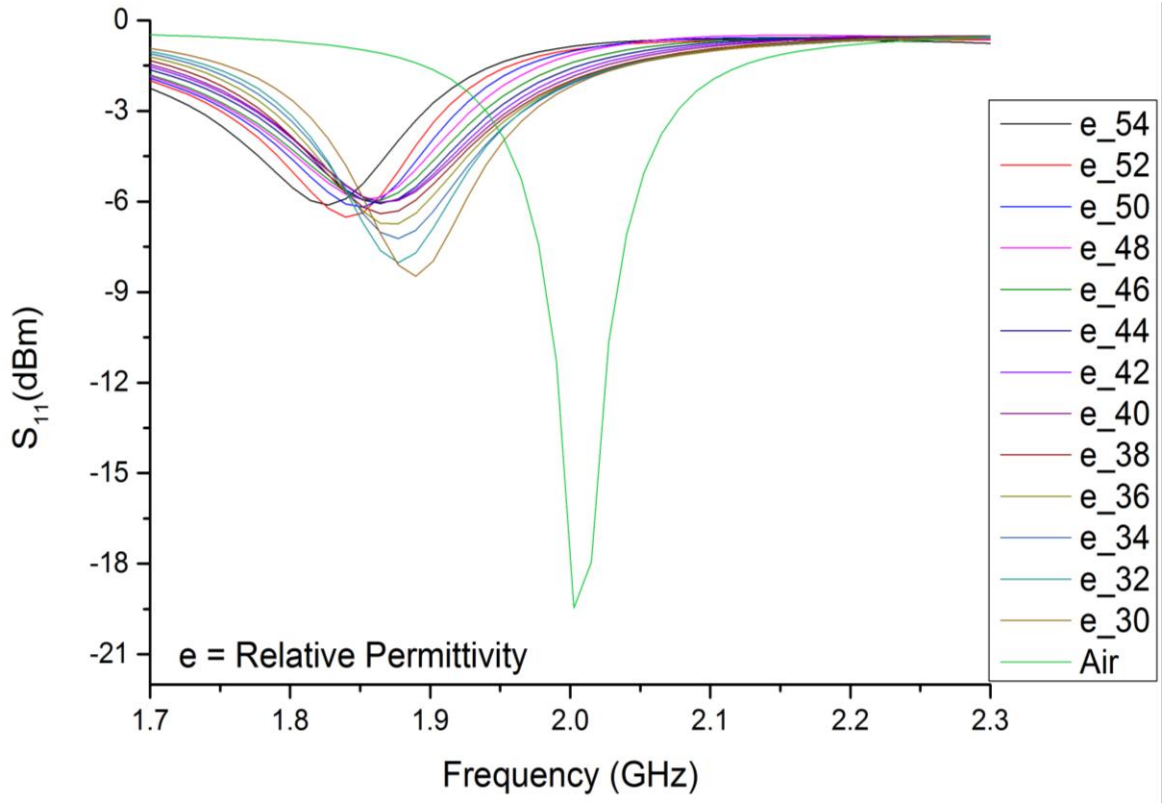

Figure 5.5. HFSS simulation results for sensors version 1.

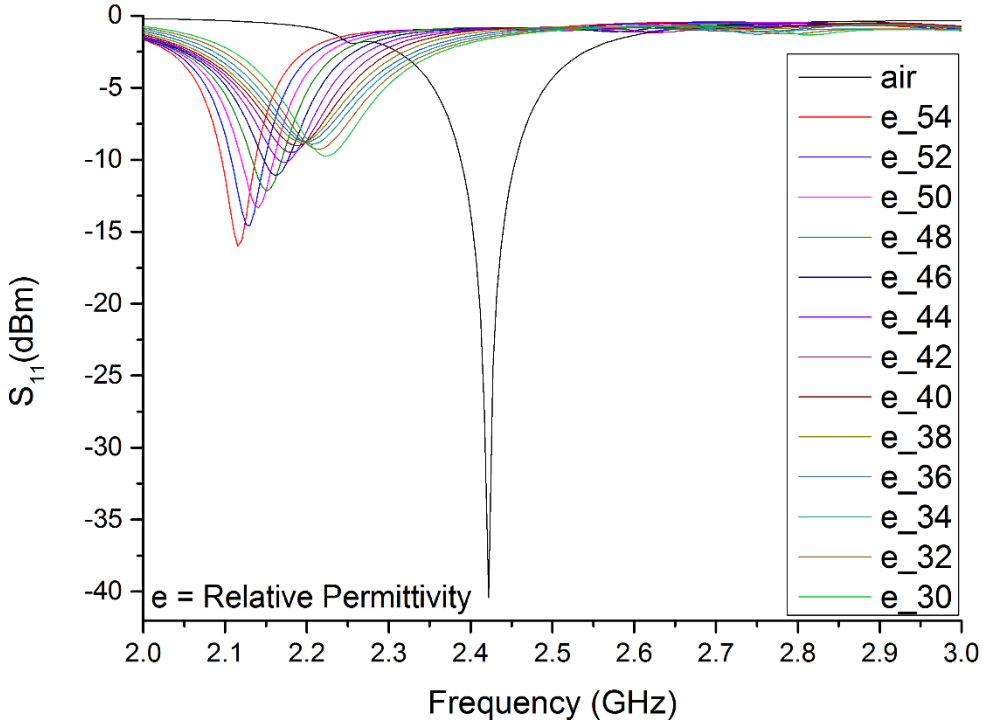

Figure 5.6. HFSS simulation results for sensors version 2.

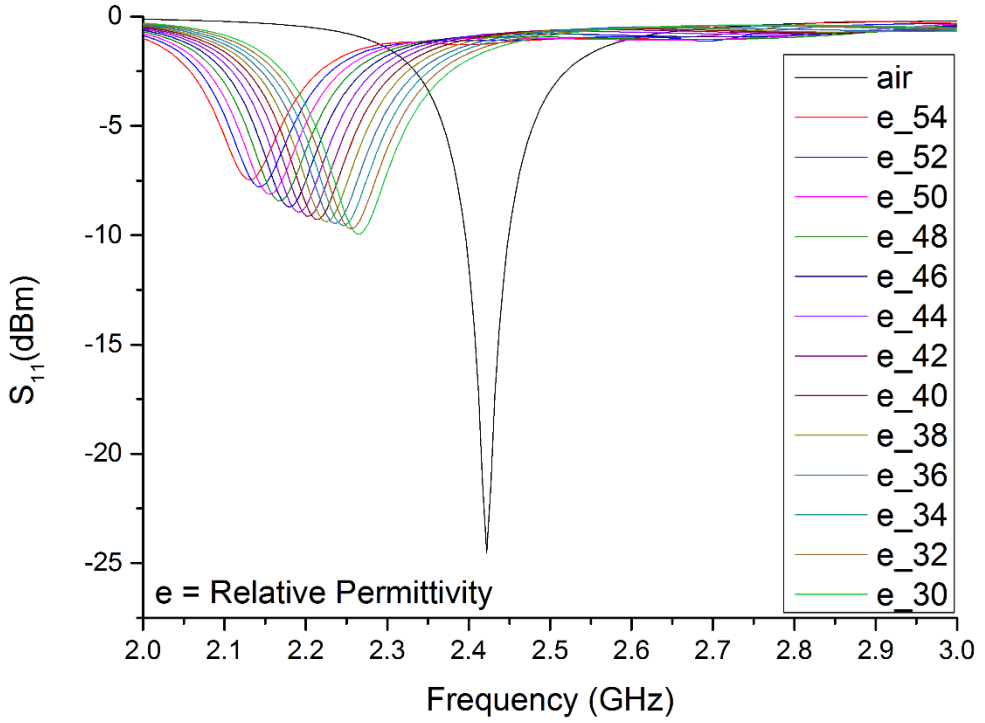

Figure 5.7. HFSS simulation results for sensors version 3.

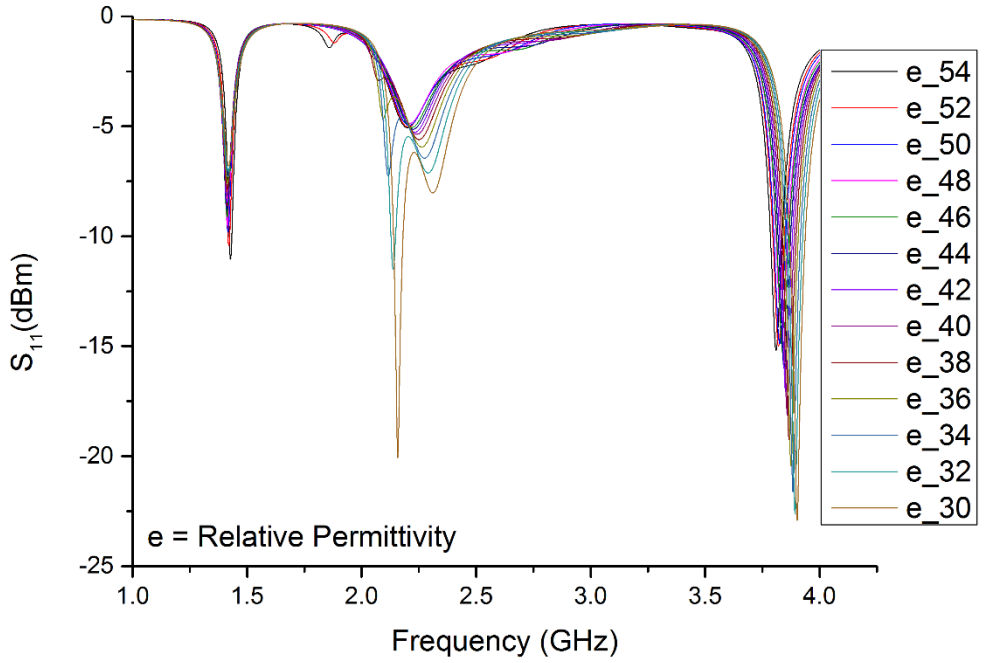

Figure 5.8. HFSS simulation results for sensors version 3.1.

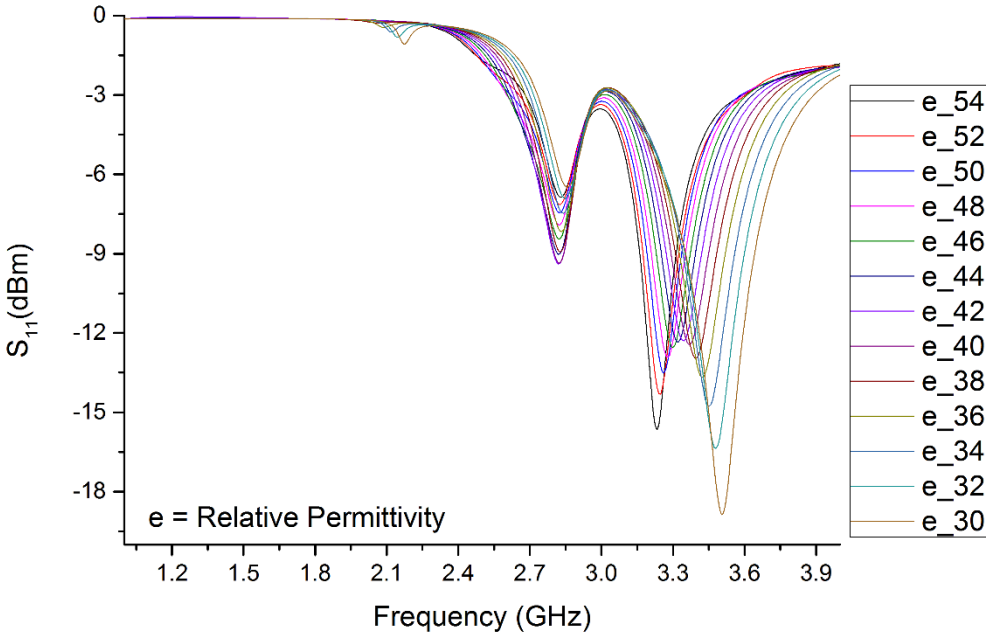

Figure 5.9. HFSS simulation results for sensors version 3.2.

The changes that occurred during the simulation (resonance frequency shift and changes of the attenuation) were correlated against relative permittivity to understand whether there is a relationship between these changes. Figure 5.27 (a) demonstrates a very strong linear correlation (R^2 = 0.87, R^2 = 0.99 R^2 = 0.99 R^2 = 0.94 R^2 = 0.99 for sensors version 1, 2, 3,

3.1 and 3.2, respectively) between relative permittivity and resonance frequency shift. Figure 5.27 (b) illustrates a strong linear relationship (R^2 = 0.99, R^2 = 0.99 R^2 = 0.95 R^2 = 0.98 R^2 = 0.96 for sensors version 1, 2, 3, 3.1 and 3.2, respectively) between amplitude changes and the relative permittivity. As was mentioned earlier, the dielectric constant of a material relates to its water content. The simulations demonstrated a linear relationship between changes of the resonance frequency and the dielectric constant of the material. This means that the sensor can be used for monitoring the meat drying process by creating a linear prediction model.

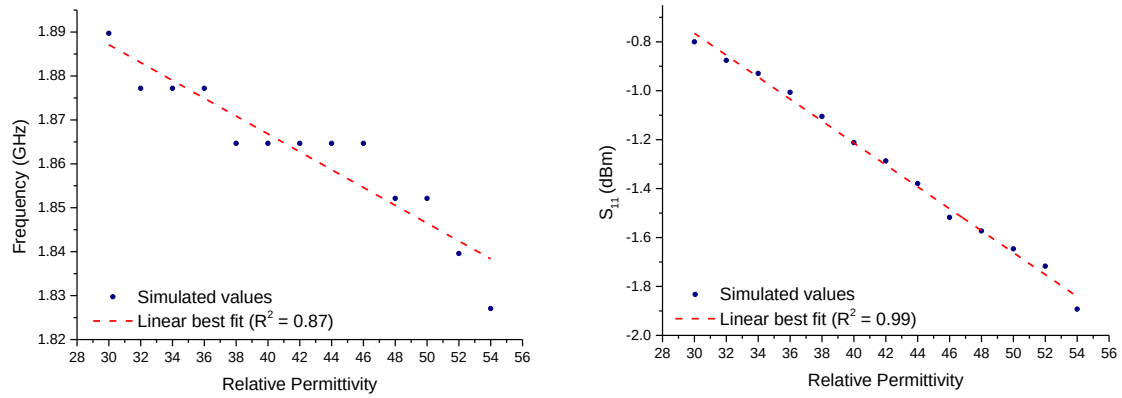

(a) (b)

Figure 5.10. Results from HFSS simulation of meat curing process imitation using sensor version 1; correlation between relative permittivity and (a) resonance frequency shift, with R^2 = 0.87 and (b) S_{11} change at 1.7 GHz, R^2 = 0.99.

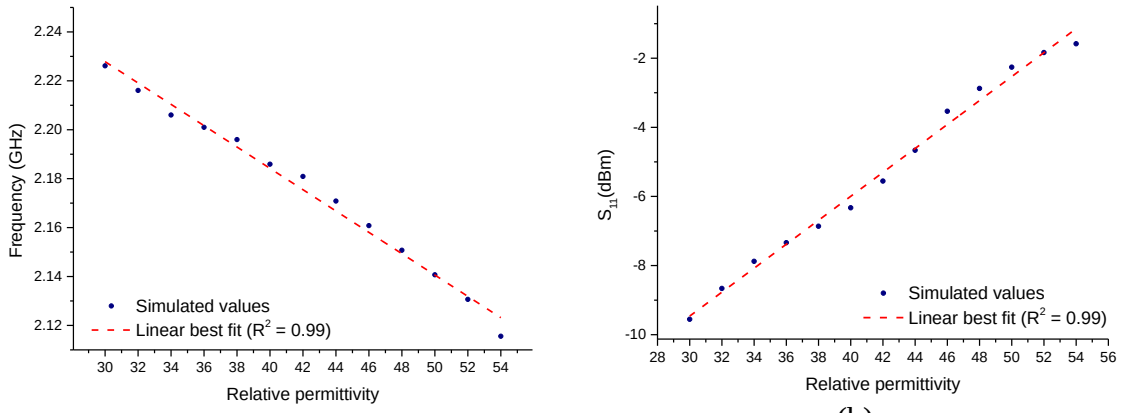

(a) (b)

Figure 5.11. Results from HFSS simulation of meat curing process imitation using sensor version 2; correlation between relative permittivity and (a) resonance frequency shift, with R^2 = 0.99 and (b) S_{11} change at 2.2 GHz, with R^2 = 0.99.

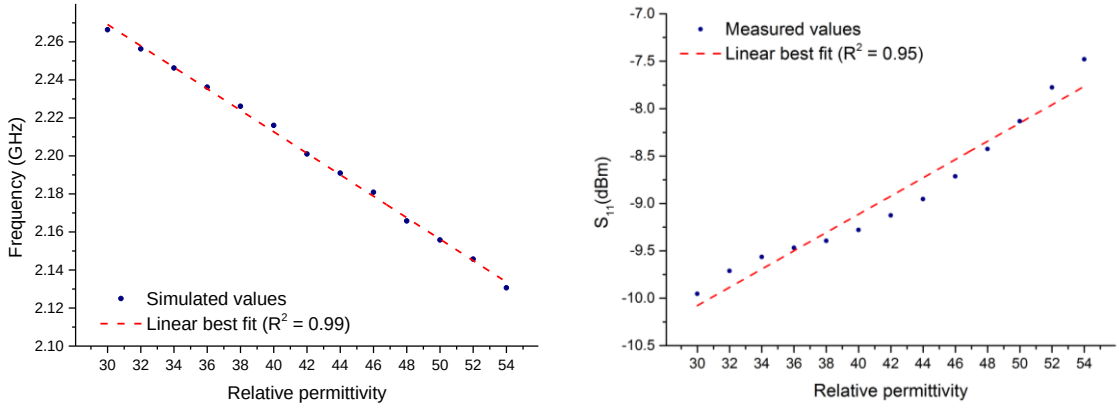

(a) (b)

Figure 5.12. Results from HFSS simulation of meat curing process imitation using sensor version 3; correlation between relative permittivity and (a) resonance frequency shift, with $R^2 = 0.99$ and (b) S_{11} change at 2.4GHz, with $R^2 = 0.95$.

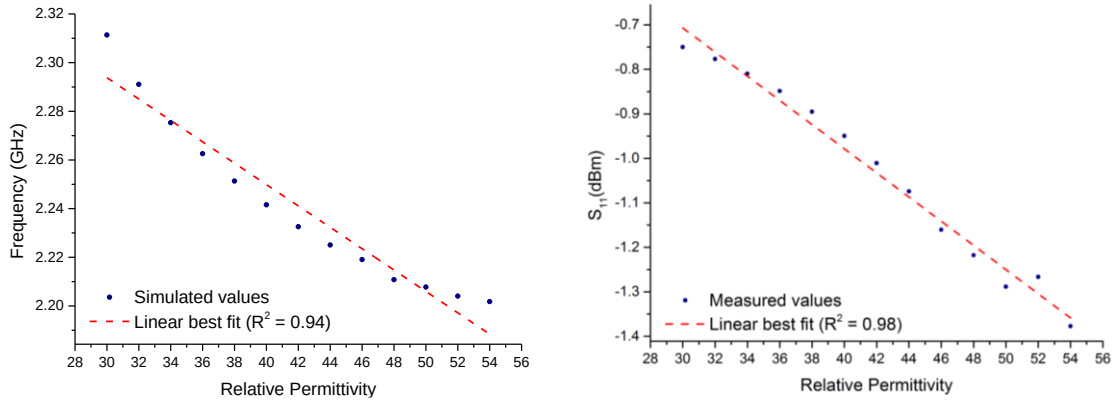

(a) (b)

Figure 5.13. Results from HFSS simulation of meat curing process imitation using sensor version 3.1; correlation between relative permittivity and (a) resonance frequency shift, with $R^2 = 0.94$ and (b) S_{11} change at 3.67GHz, with $R^2 = 0.98$.

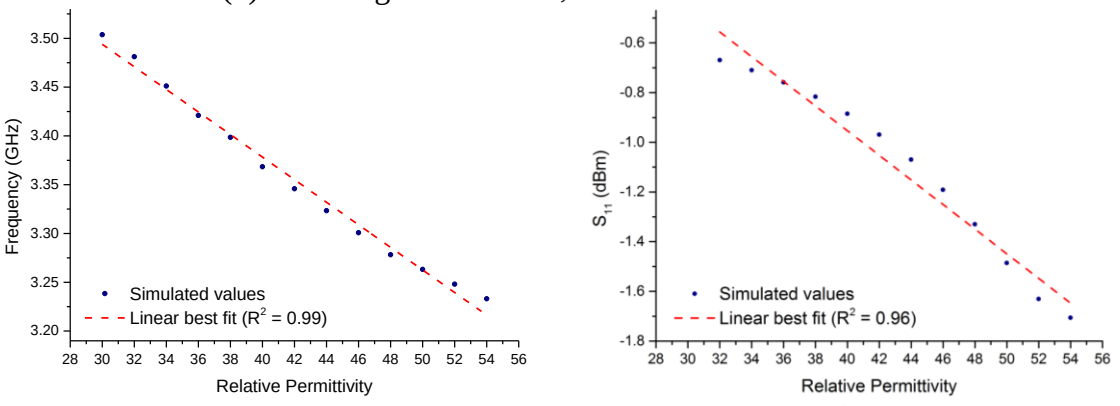

(a) (b)

Figure 5.14. Results from HFSS simulation of meat curing process imitation using sensor version 3.2; correlation between relative permittivity and (a) resonance frequency shift, with $R^2 = 0.99$ and (b) S_{11} change at 2.5GHz, with $R^2 = 0.96$.

5.3. Sensor Implementation

Once the simulation stage was completed, the physical construction of the sensors was conducted. The process consisted of two main steps, namely designing the sensors on EAGLE software and etching the copper with a CNC routing machine.

5.3.1. EAGLE Models of the Sensors

EAGLE (Easily Applicable Graphical Layout Editor) is a PCB (Printed Circuit Board) design software, which is developed by CadSoft (CadSoft US, 2016). The software contains a number of functions, such as a schematics editor, a PCB editor and auto-router module. The most common use of this software is a design of electronic schematics and layouts of PCB boards. As the sensors do not require any electronic schematics at this stage of the investigation, only the PCB layout editor is used. All five sensors were drawn separately using the EAGLE software as it can be seen in Figure 5.15 and Figure 5.16.

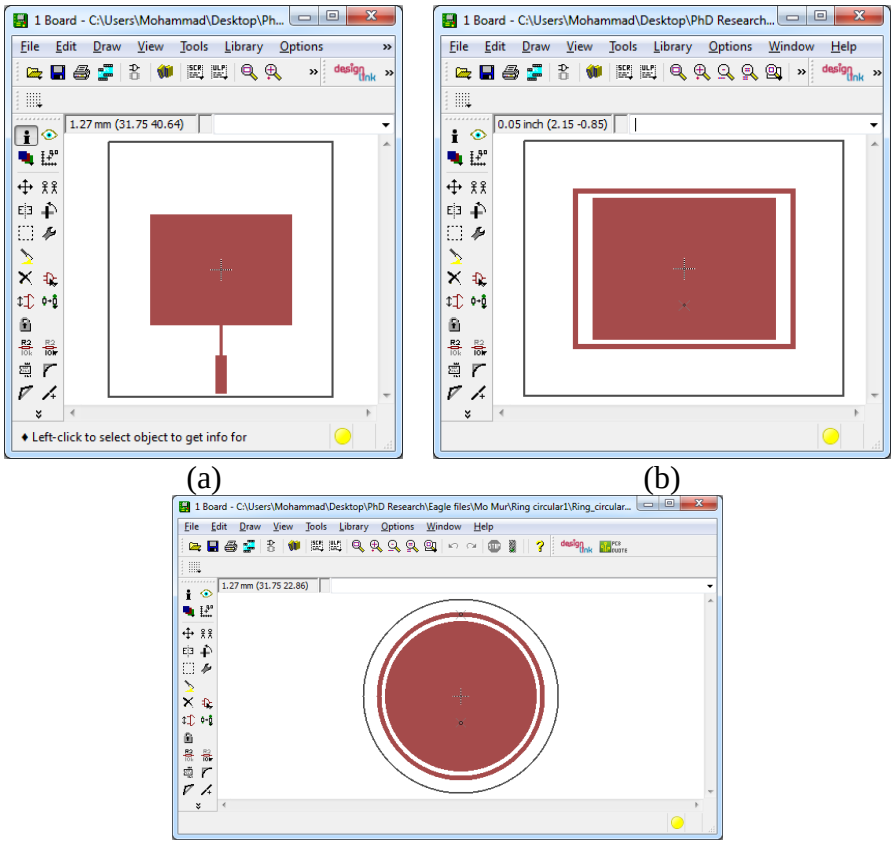

Figure 5.15. PCB layouts of sensors (a) version 1, (b) version 2 and (c) version 3 in EAGLE software.

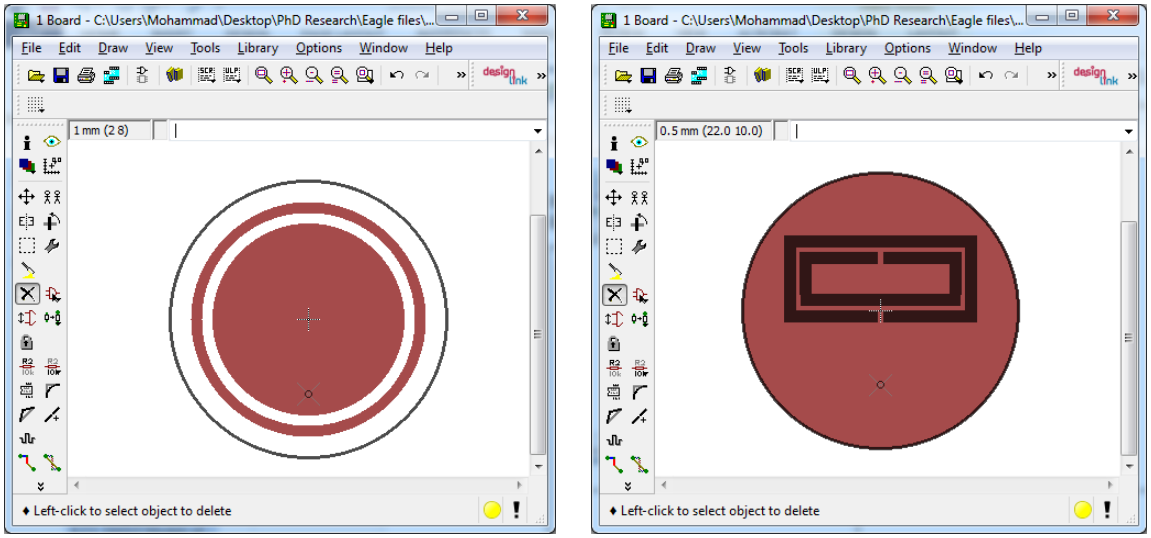

(a)

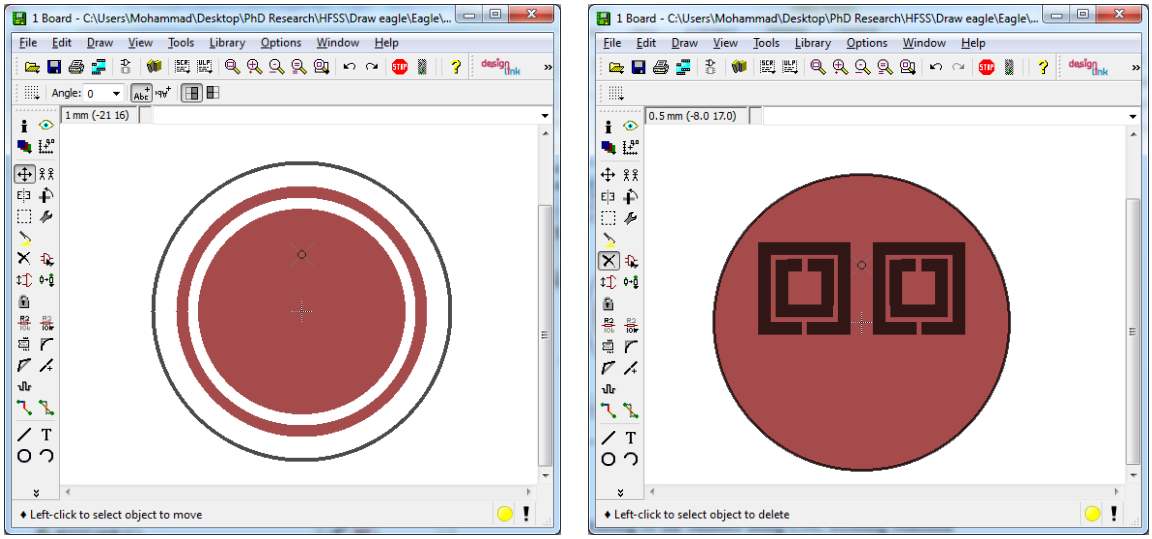

(b)

Figure 5.16. PCB layouts of sensors (a) version 3.1 ((*left*) top and (*right*) bottom) and (b) version 3.2 ((*left*) top and (*right*) bottom) in EAGLE software.

5.3.2. Printing of the Sensors using CNC Routing Machine

The physical construction of the sensors was carried out by printing them on PCB boards using a Bungard CCD2 Computer Numerical Control routing machine, which is shown in Figure 5.17. The machine is connected to the PC that contains RoutePro 2000 CCD-control software where sensors' layout files were loaded for drilling and the routing. The eagle files, i.e. board layout files were converted to Hewlett-Packard Graphical Language format in order to load them into the machine. Then, ABViewer software was used to open the files prior to loading them in the CCD-control software.

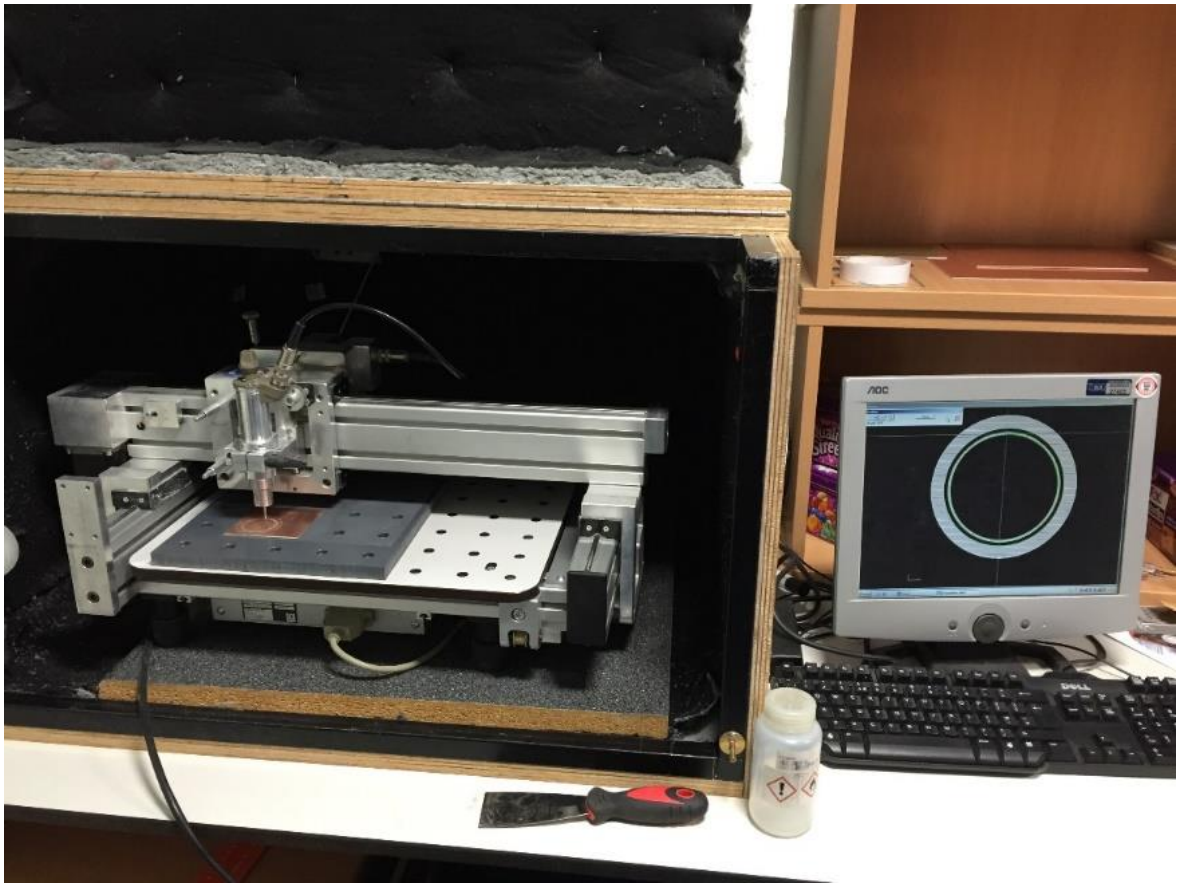

Figure 5.17. CNC Routing machine connected to a PC.

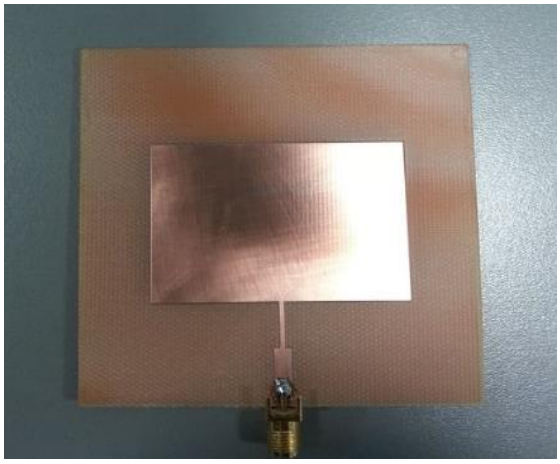

(a)

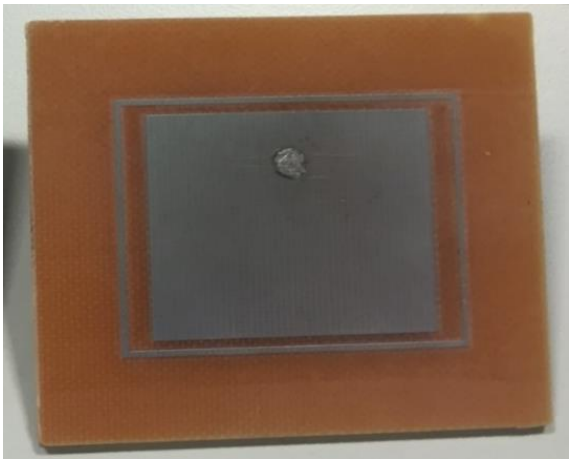

(b)

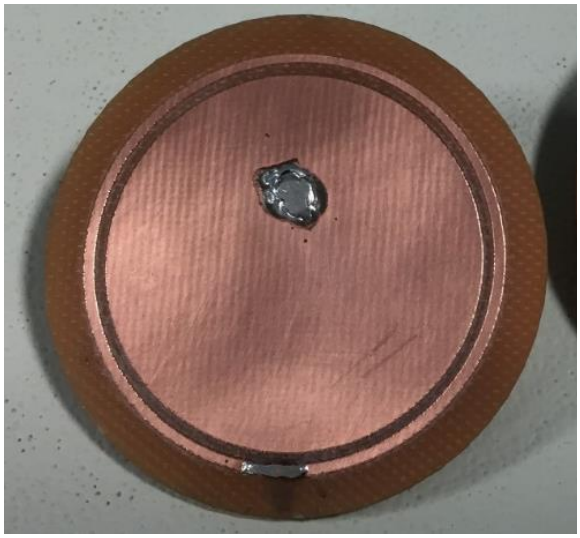

(c)

Figure 5.18. Top view of the sensors (a) version 1, (b) version 2 and (c) version 3 fabricated with the CNC Routing machine.

(a) (b)

Figure 5.19. (a) Top and (b) bottom views of the Sensor version 3.1.

(a) (b)

Figure 5.20. (a) Top and (b) bottom views of the Sensor version 3.2.

5.3.3. Simulation and Experimental Measurements of the Sensors in Air.

This sub-section provides the simulated and measured results of return loss for sensors version 1, 2, 3, 3.1 and 3.2 (results are shown in Figure 5.21, Figure 5.22, Figure 5.23, Figure 5.24 and Figure 5.25, respectively). The relatively good agreement is seen between the measured and simulated return loss curves.

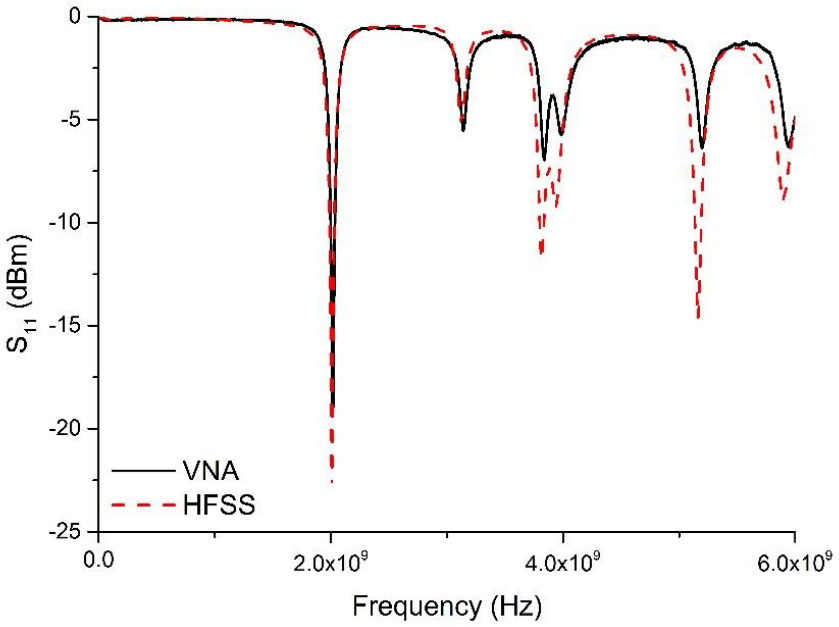

Figure 5.21. Demonstrating the modelled and measured return loss of sensor version 1.

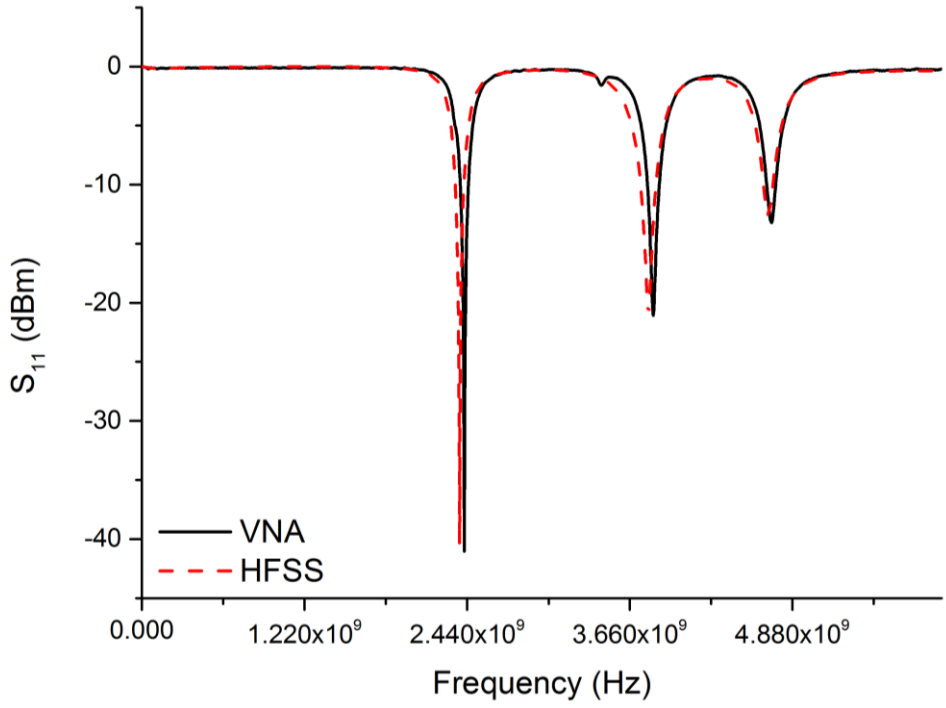

Figure 5.22. Demonstrating the modelled and measured return loss of sensor version 2.

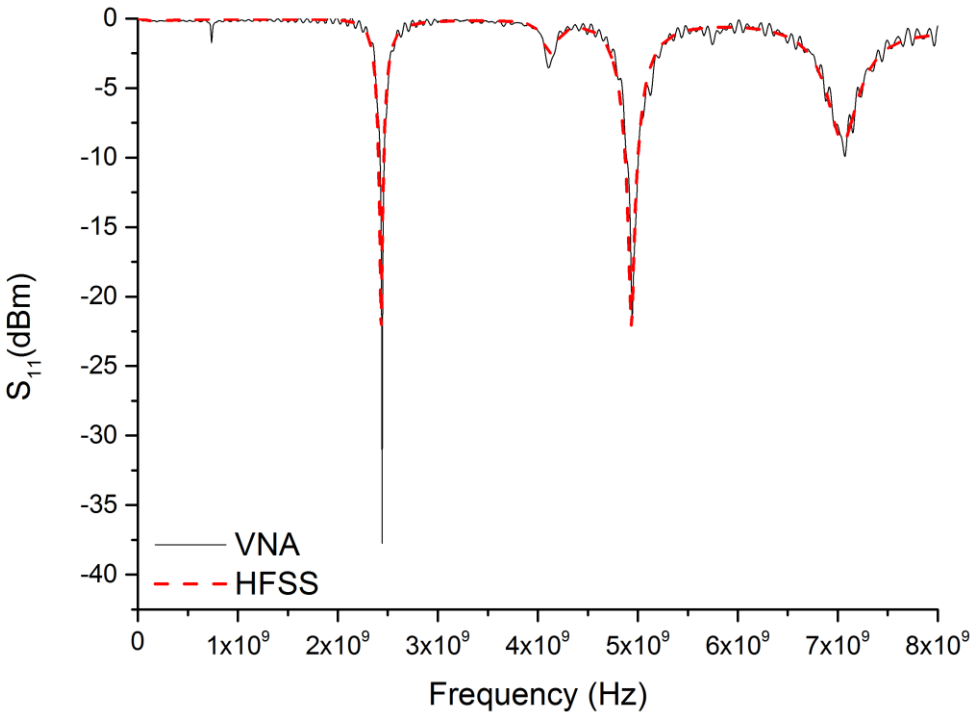

Figure 5.23. Demonstrating the modelled and measured return loss of sensor version 3.

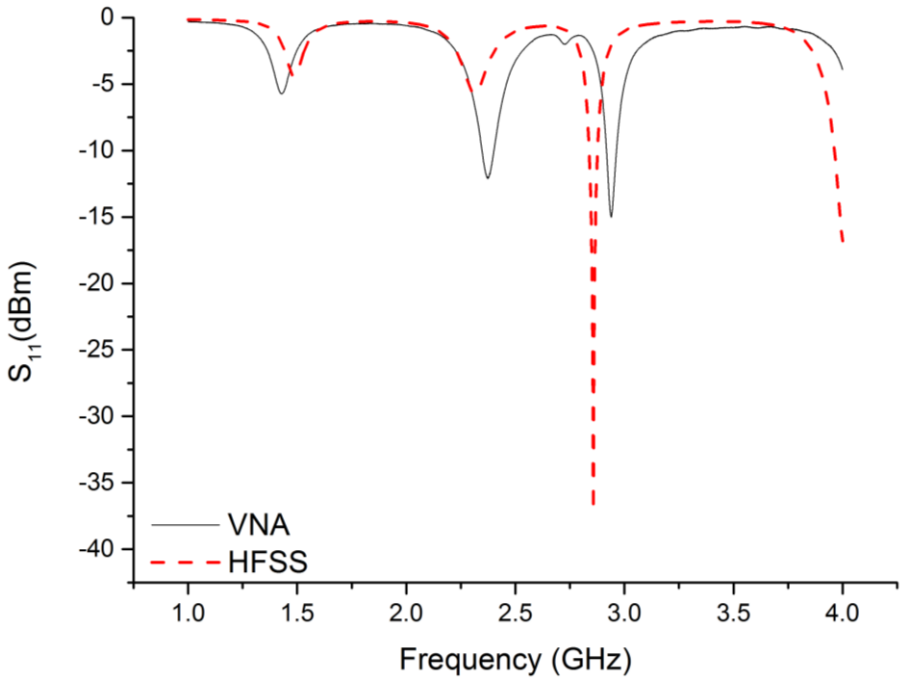

Figure 5.24. Demonstrating the modelled and measured return loss of sensor version 3.1.

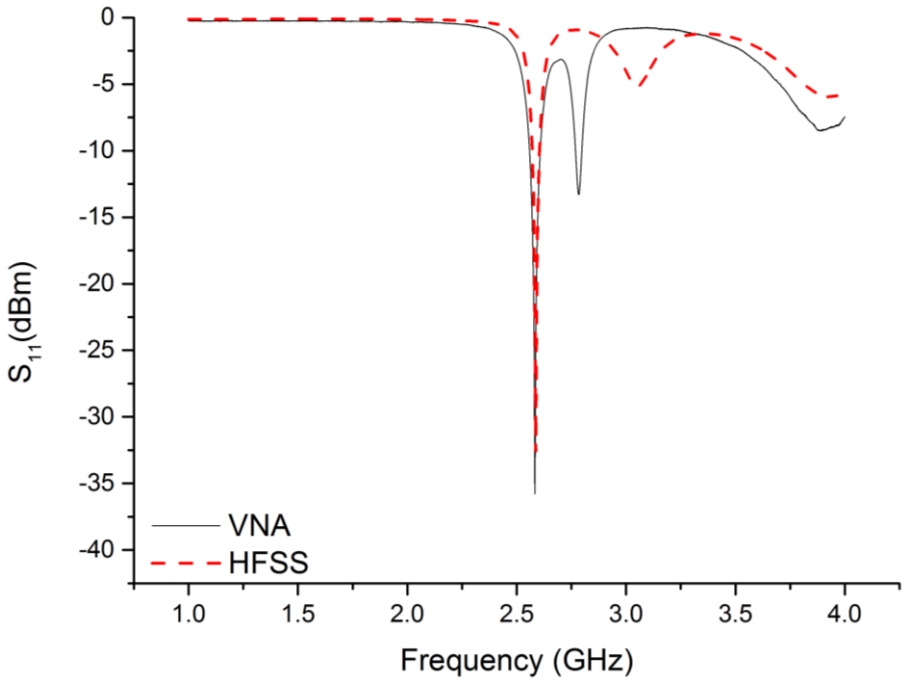

Figure 5.25. Demonstrating the modelled and measured return loss of sensor version 3.2.

5.4. Validation of the Theoretical Model

5.4.1. HFSS Simulation

HFSS simulation was undertaken prior to preliminary experiment to validate a potential of the electromagnetic sensors to determine the weight loss of a meat sample. Figure 5.26 illustrates HFSS results obtained using a theoretical model of sensor version 1. It can be seen in Figure 5.26 that a resonant frequency decreases when a relative permittivity of a dialectic material increases. This imitates moisture loss of a modelled meat sample, i.e. the drying off process. Figure 5.27 shows a very strong linear relationship between frequency shift and decrease of relative permittivity, with $R^2 = 0.99$.

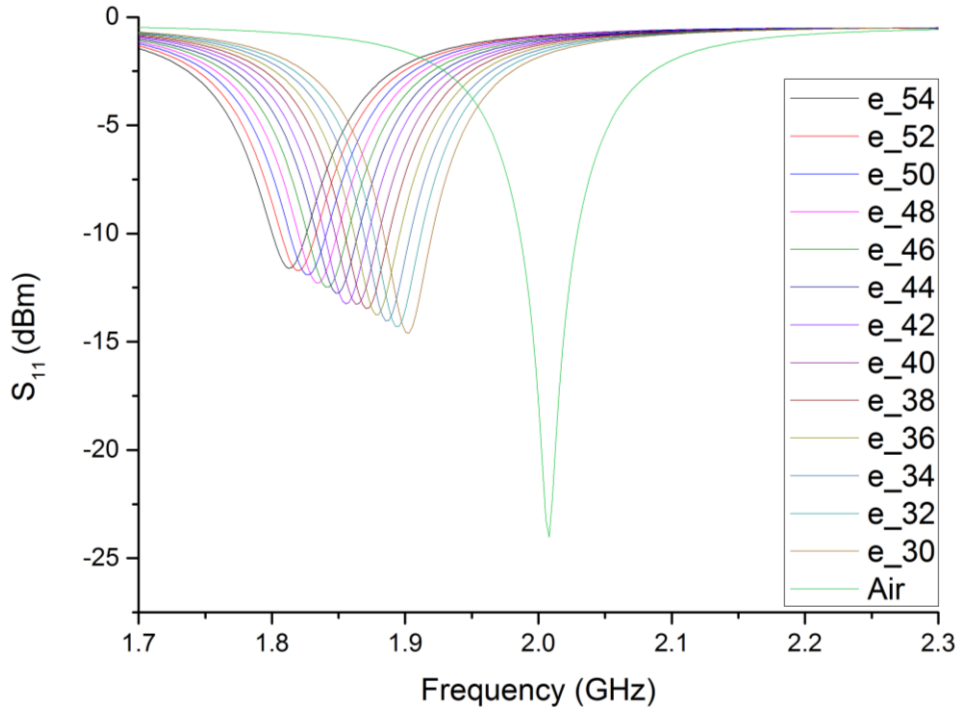

Figure 5.26. HFSS simulation that imitates a meat drying process (e represents an epsilon, i.e. relative permittivity).

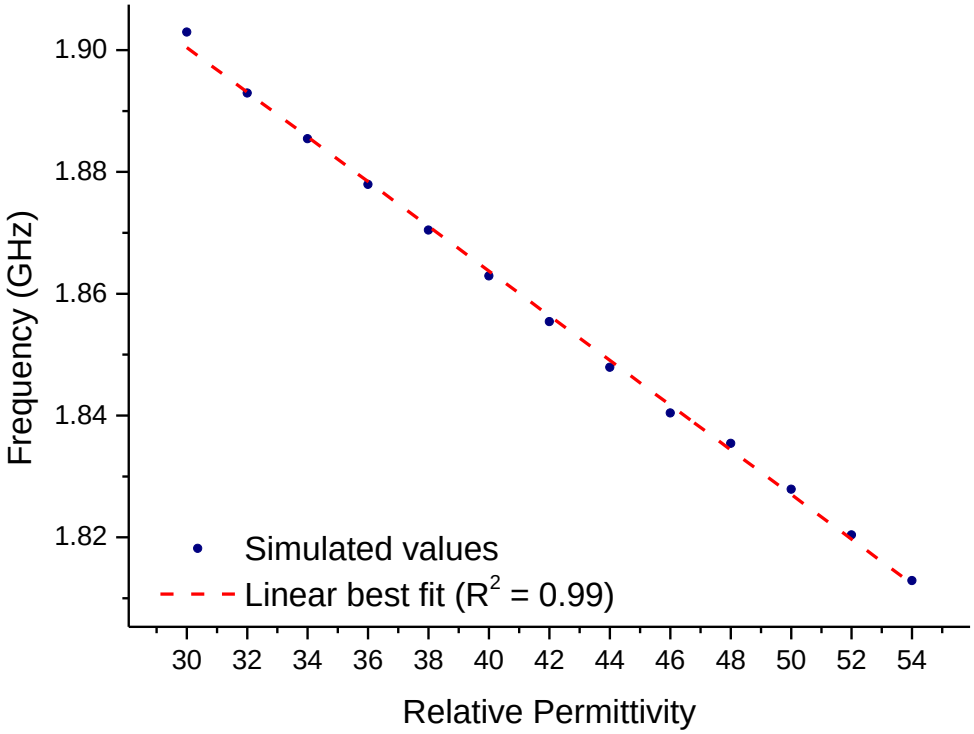

Figure 5.27. Results from HFSS simulation of meat drying process imitation; correlation between relative permittivity and resonance frequency shift, with R^2 = 0.99.

5.4.2. Experimental Setup

Pork loin steaks were acquired from a local supermarket for a preliminary experimental work, and stored at 5 °C. Rather than salting the meat at this stage, it was the intention to let the meat dry naturally to determine the sensor response in the unsalted condition and compare the results with the theoretical model.

The meat samples were cut into approximately 70 × 50 × 15 mm pieces and placed on top of a bespoke water run-off system, designed for rapid removal of drips from the meat, which would otherwise skew weight measurements. The tray was situated on top of a set of digital scales so that the weight of the sample could be continuously recorded during the drying process. This arrangement was placed within a refrigerator which was set to approximately 5°C, ± 2°C. The temperature was monitored throughout the experimental procedure. The block diagram of the experimental setup is illustrated in Figure 5.28.

To promote air circulation and water loss, a fan (a standard PC fan) was fixed inside the fridge. The fan was connected to power supply via a relay (see Figure 5.29) which is used to switch off the fan while the measurements are taken. The relay was under control of LabVIEW program, which was turning the relay off for 10 seconds prior to the measurements. The purpose of this is to avoid incorrect weight measurements as the scale is sensitive to small changes in air pressure. The scale was zeroed once the sensor and "water runoff" system were fixed to it, and before placing the meat sample on it.

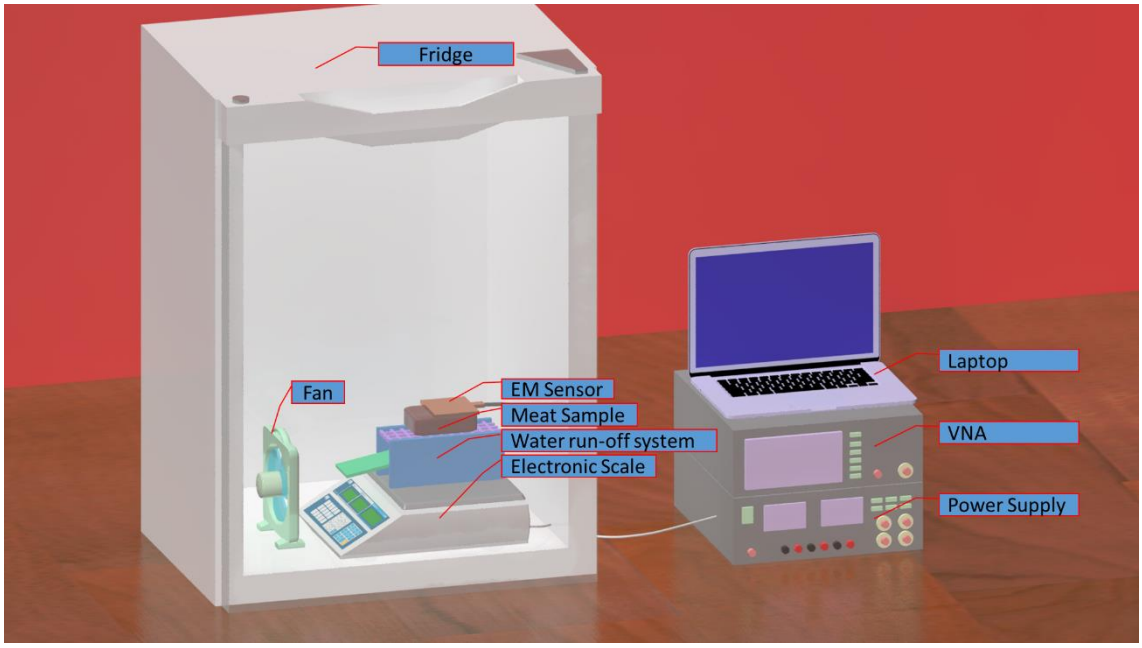

Figure 5.28. Block diagram of the experimental setup.

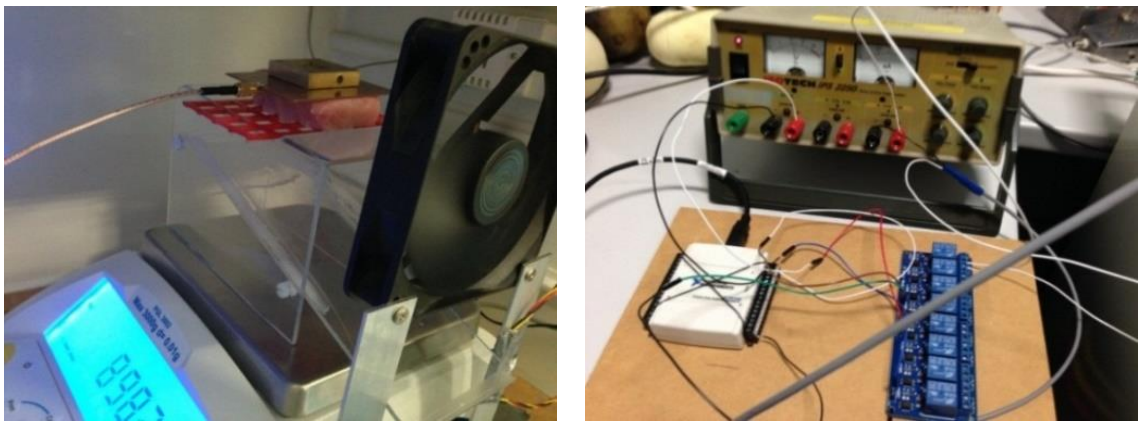

(a) (b)

Figure 5.29. (a) Experimental setup inside the refrigerator, showing the water run-off system, digital scales, meat sample, sensor and fan system used to promote rapid drying and reduce water residue; (b) the relay system for controlling fan via LabVIEW.

Once the meat was in place, the sensor was positioned on top of the sample and fixed in place. A conformal polypropylene based spray coating was applied to the sensor (both radiating and ground planes) to eliminate issues with corrosion, which could cause damage to both the meat sample and the sensor.

The sensor was connected to a Vector Network Analyser (VNA, model Rohde and Schwarz ZVL13), which in turn was connected to a desktop computer running a bespoke LabVIEW interface (see Figure 5.30) for continuous capture of S-Parameters (namely S_{11}). The system was utilised in order to conduct an experimental work over a period of 28 days.

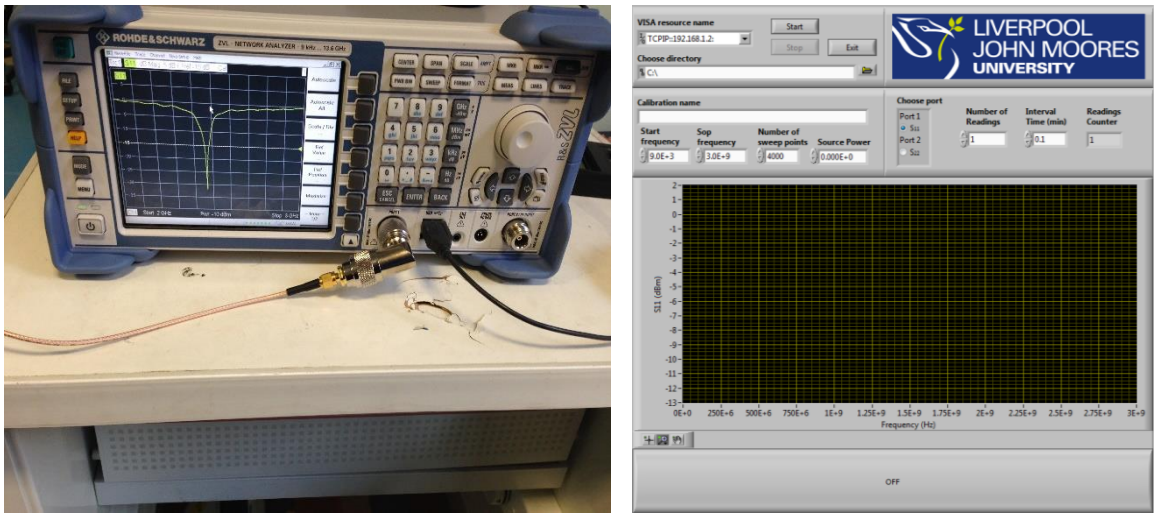

(a) (b)

Figure 5.30. (a) Vector Network Analyser and (b) LabVIEW interface utilised for continuous automated measurements over the experimental period of 28 days.

Measurement from the patch sensor was provided by using the S_{11}-parameter from the VNA since the sensor is a single port structure. Data acquisition (i.e. S_{11}, temperature and weight) took place once per hour over a period of 5 days; at this point typically, the loin samples have lost > 40% of their original weight through shedding of loosely bound and immobilised water, and the experiment may be halted. Weight and S_{11} measurement were then correlated to determine the relationship between weight loss of the meat and change in EM signature from the sensor. Temperature was measured to ensure stability within the refrigerated environment during the experimental work; a temperature of 5 °C was maintained, ± 2 °C (measurement error in a standard fridge).

5.4.3. Real-world Experimental Results

Figure 5.31 shows the S_{11} measurements that were taken every hour (i.e. 24 times per day) over a period of 5 days. Measurements of the weight loss of the sample also were taken at

the same time during the experiment. The measurements from 12-hour intervals over 5-day period are presented in the Figure 5.31.

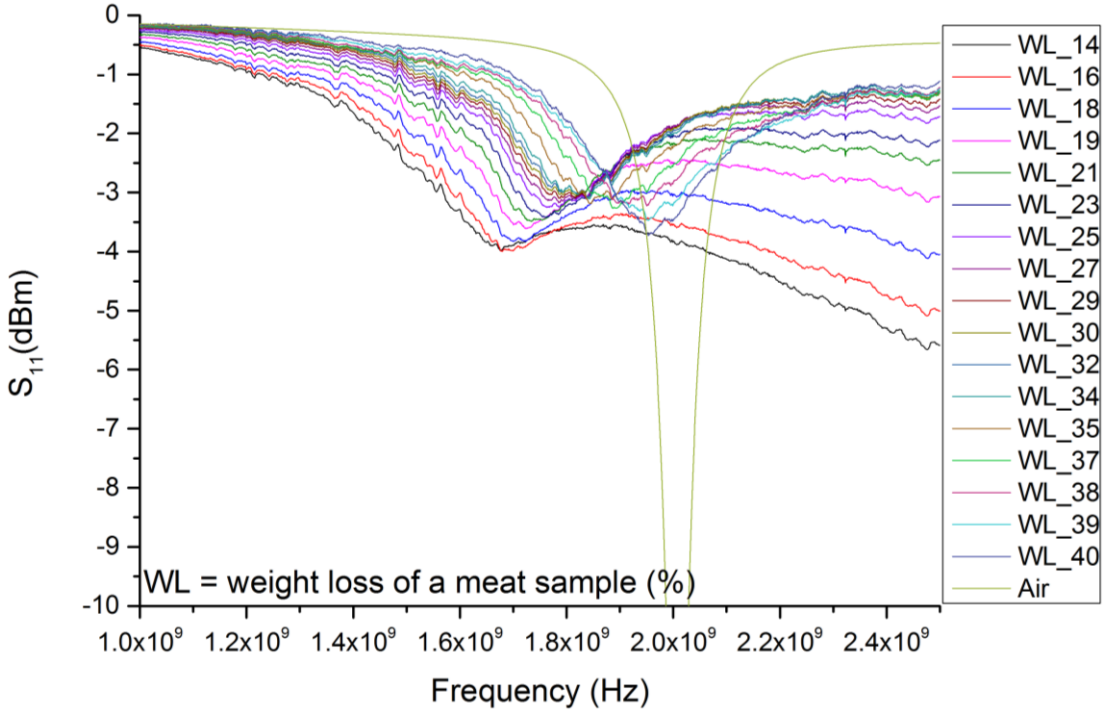

Figure 5.31. Readings from the electromagnetic wave sensor; measurements were taken once per hour in the frequency range 1-6 GHz; for clarity data from 1-2.5 GHz is presented, with measurements from 5 hour intervals over a 4 day period.

It can be seen in Figure 5.31 that there is a noticeable change in EM signature, namely decrease of the resonance frequency and increase of the bandwidth of the sensor. The change is thought to be caused by the decreasing amount of water in the meat sample, which would have a significant impact on its dielectric properties. This means that theoretical simulation for the microwave absorption using the sensor agrees well with the experimental results.

The change, which occurs, is present quite broadly within the measured spectra, particularly due to the broadband nature of the sensor used. The largest change in sensor output is experienced at approximately 3 GHz, although the smaller changes that occur in the 1-2 GHz region are highly repeatable.

Figure 5.32 illustrates a linear correlation between weight loss of the meat sample and (a) the resonance frequency increase, with $R^2 = 0.98$ and (b) S_{11} increase at 2 GHz, with $R^2 =$

0.99. This means that the sample weight loss in the experimental environment can typically be represented by a linear model.

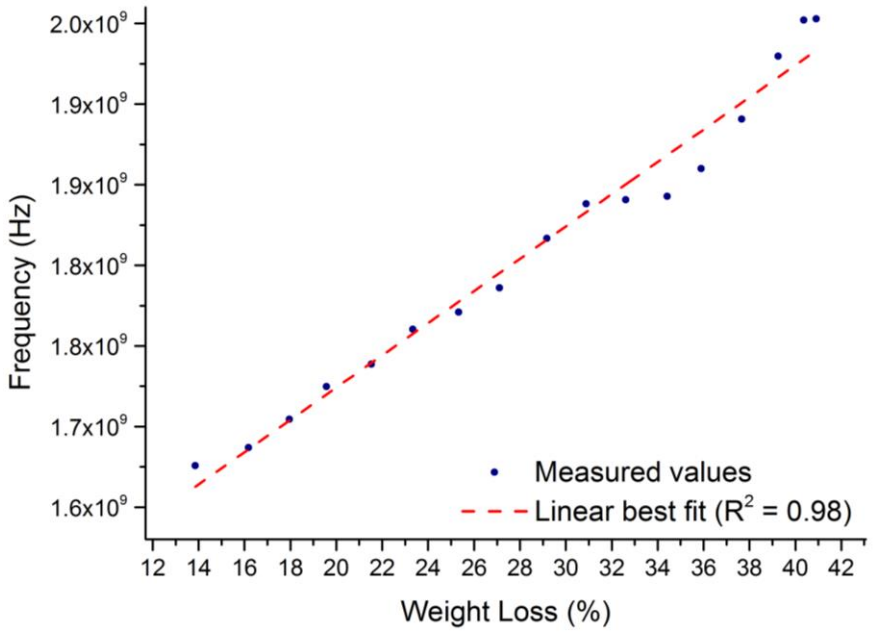

(a)

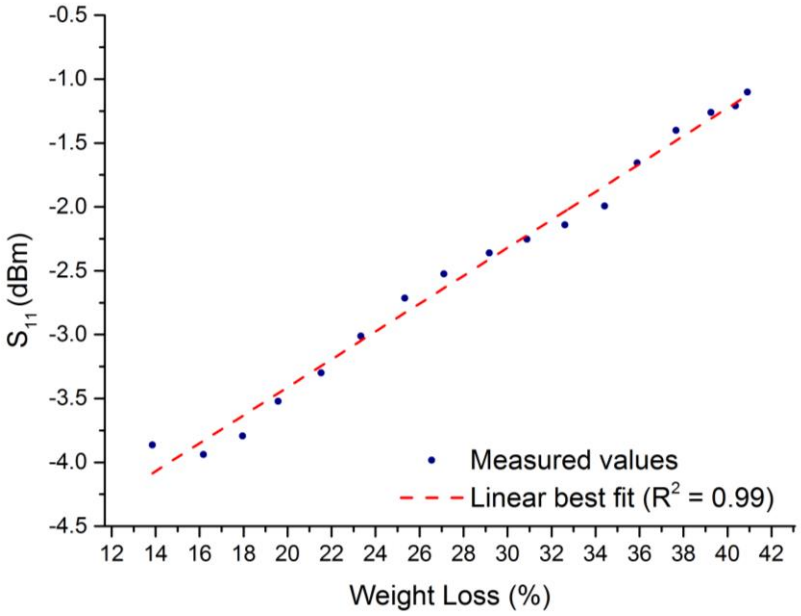

(b)

Figure 5.32. Linear correlation between weight loss and (a) frequency shift and (b) amplitude shift at 2 GHz

5.5. Summary

In this study, five electromagnetic wave sensors were modelled using High Frequency Structural Simulation software (HFSS) and then constructed. The first sensor designed for this investigation was a rectangular patch type sensor (Sensor version 1) that resonates at 2 GHz with a transmission line feeding technique. Then, the dimensions of the sensor were reduced by increasing the resonant frequency from 2GHz to 2.45GHz and changing the feeding method from transmission line to coaxial probe fed technique. These amendments led to the development of sensor version 2. The next enhancement of the sensor was a modification of its shape (i.e. from rectangular to circular type sensor) as the corners of a rectangular structure became an issue when meat samples started shrinking after a certain time. However, the resonant frequency (2.45GHz) and the feeding technique (coaxial probe fed) of the sensor (version 3) was left the same. The size of the sensor version 3 was reduced owing to requirements for smaller meat products, which led to the development of sensors version 3.1 and 3.2. To validate the theoretical models a preliminary experimental work was conducted using sensor version 1. The real-world experimental results demonstrated a good agreement with the simulation results that are presented in sections 5.4.1 and 5.4.3, respectively.

Chapter 6 Continuous Monitoring of Drying Process

In this chapter, the use of sensors version 1, 2 and 3 to monitor the meat curing process will be demonstrated. Results obtained from all three sensors will be processed, plotted and analysed to develop a prediction model for monitoring of the meat curing process using a microwave sensor system.

6.1. Sensor Version 1

6.1.1. Real-world Experimental Results

This section provides the results from the experimental work undertaken with sensor version 1 to monitor the meat curing process. Figure 6.1 shows the S_{11} measurements, which were taken once per hour (i.e. 24 times a day) during one week. Measurements of the weight loss of the sample also were taken at the same time during the week. It can be seen in Figure 6.1, that there is a noticeable change in EM signature. The change is thought to be caused by the decreasing amount of water in the meat sample. The sample was not touched or moved during the experimental work, and all other conditions, such as temperature and light remained nominally the same during the test. Additionally, there is a decrease of the resonance frequency and change in an attenuation of the signal similar to the results obtained from the HFSS simulation (see Figure 5.5). When a meat sample is placed on the sensor, an increasing storage of electric field energy can be observed which leads to a decreasing resonance frequency. The permittivity, which gets excited by the storage of energy, significantly changes in relation to the water content. In addition, the wet material absorbs energy of the resonator, which results in an increasing width of the resonance waves. While the meat sample starts to lose the moisture content, the resonance frequency increases and the amplitude decreases simultaneously.

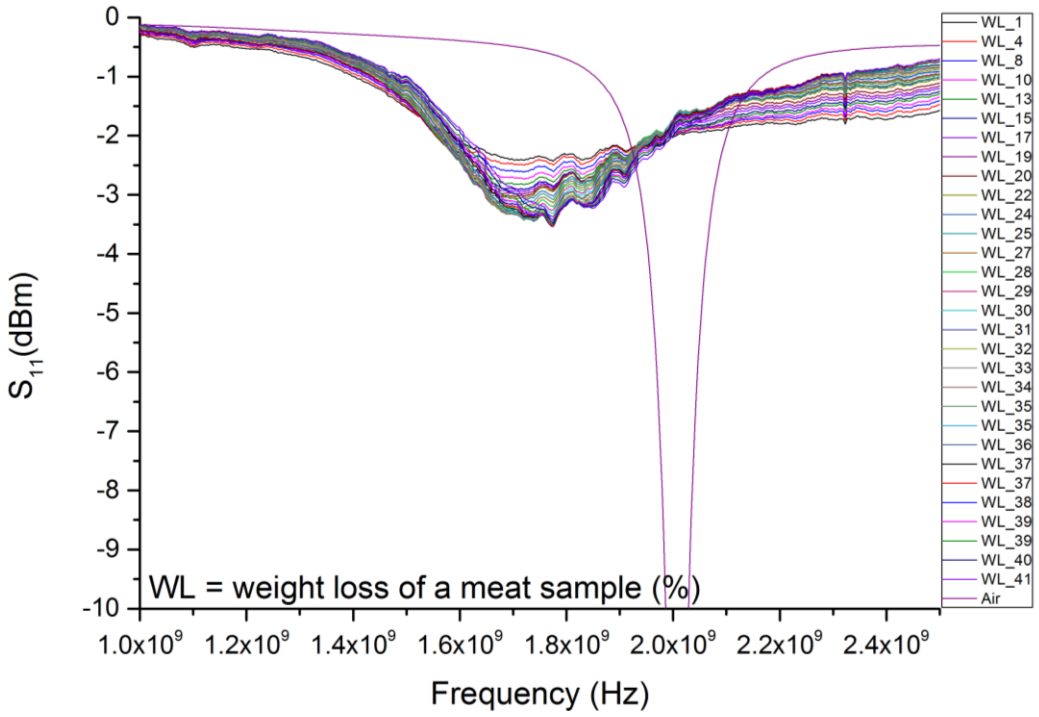

Figure 6.1. Readings from the electromagnetic wave sensor; measurements were taken once per hour in the frequency range 1-6 GHz, but for clarity data measurements from 5 hour intervals and from 1-2.5 GHz are presented.

Figure 6.2 (a) demonstrates the linear correlation between weight loss and resonance frequency shift, with $R^2 = 0.85$. The added salt increased the conductivity of the meat sample, which led to the decrease of the penetration capability of the sensor. Consequently, the sensitivity of the measurements were reduced. Figure 6.2 (b) presents linear correlation (R^2) between weight loss and S_{11} change across the full frequency spectrum, i.e. from 1 GHz to 6 GHz frequency range. The strongest linear correlation was determined between S_{11} change at 4.5 GHz and weight loss, with $R^2 = 0.99$ (see Figure 6.3).

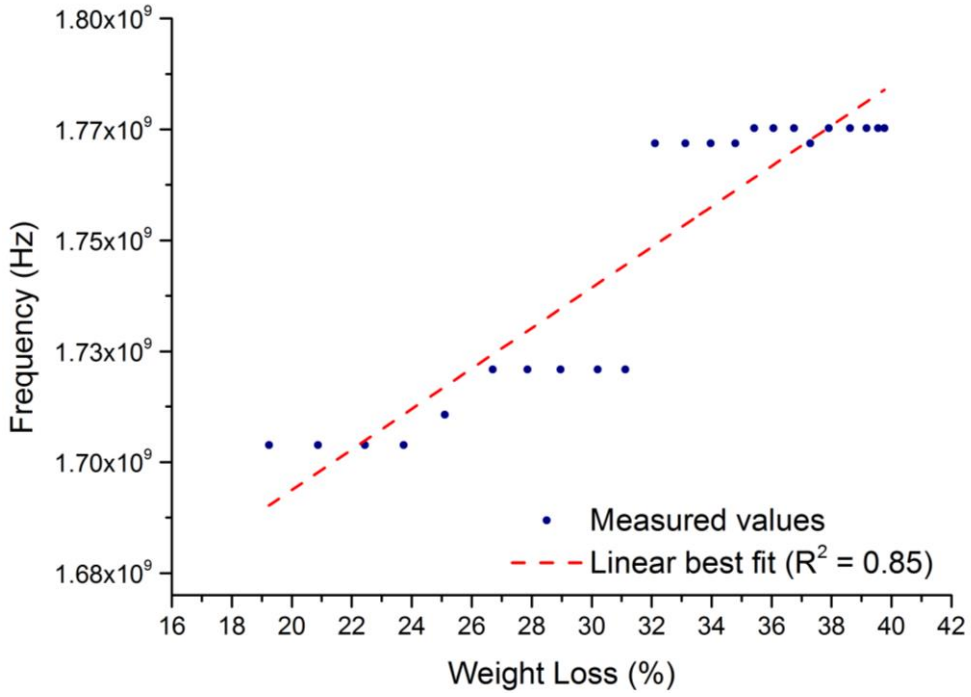

(a)

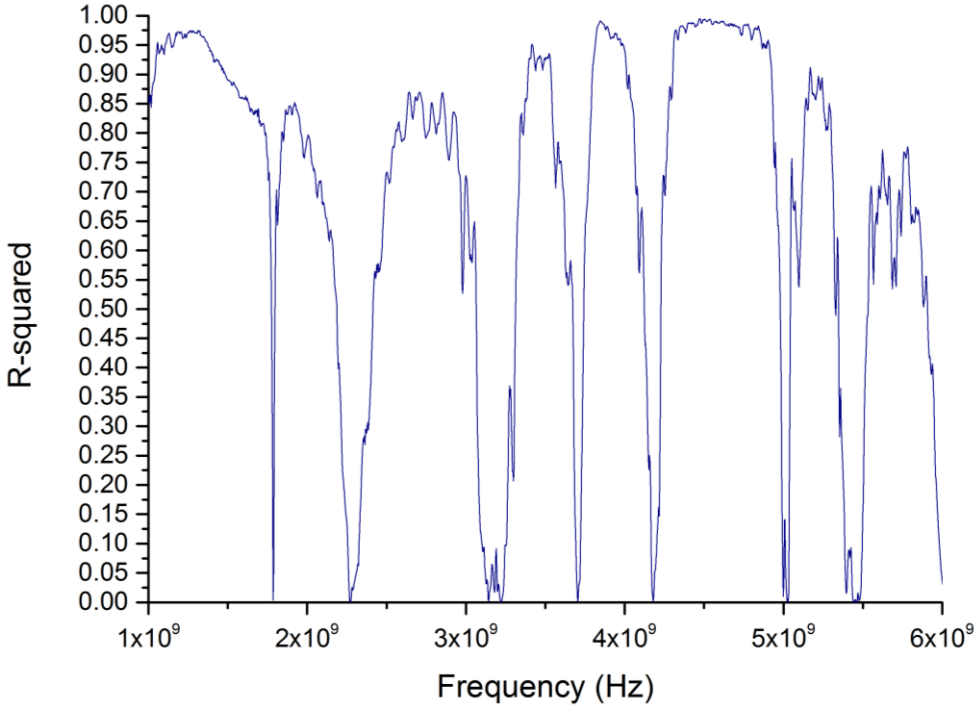

(b)

Figure 6.2. Correlation of weight loss and (a) resonance frequency, with $R^2 = 0.85$ and (b) R^2 between weight loss and S_{11} change across the full frequency spectrum (sensor version 1).

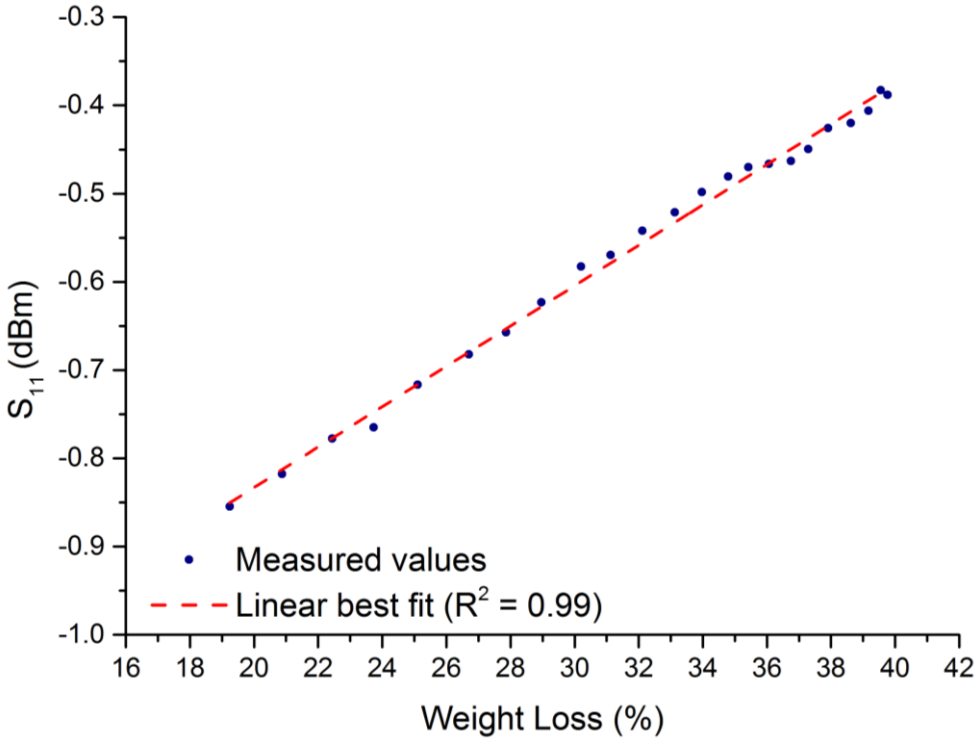

Figure 6.3. Linear fit between weight loss and S_{11} change at 4.5 GHz, with $R^2 = 0.99$.

To visualise graphically the performance of the PLSR models, the measured values obtained from the laboratory measurements and its predicted values resulting from 4-5 GHz frequency range, are plotted and displayed in Figure 6.4. The PLSR model exhibited a great capability to predict weight loss with $R^2_{prediction} = 0.99$ and with Root Mean Square Error of Prediction (RMSEP) = 0.41.

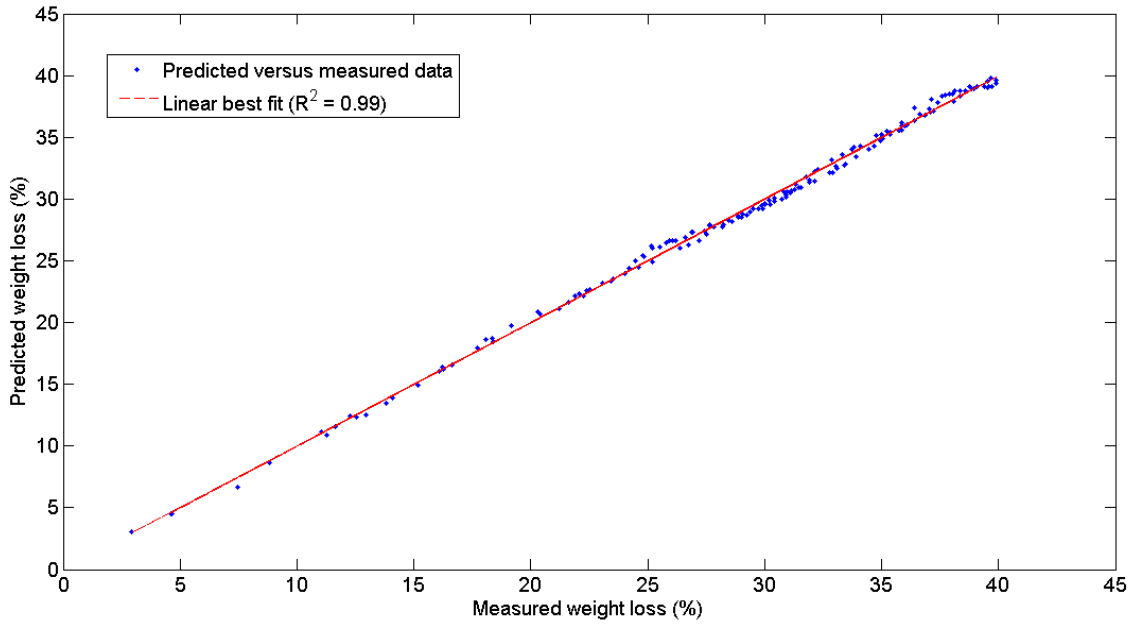

Figure 6.4. Measured and predicted weight loss from sensor version 1.

6.1.2. Discussion

The sensor showed high potential to be used for on-line monitoring of the meat curing process. However, the microstrip line feeding technique became an issue during replications of the experimental work due to the influence of the line on the signal. The sample had to be positioned exactly on the patch area of the sensor and avoid the direct contact of the meat sample with the microstrip line. Additionally, the technique increased the size of the sensor, which became a problem when the meat started shrinking while curing. The shrinkage led to an appearance of air gaps between the flat surface of the sensor and the deformed surface of the meat sample that is thought to be causing faulty measurements as part of the microwave radiation can reflect back or escape before reaching the surface of the sample. Figure 6.5 illustrates the usual deformation of the (a) meat sample during the test and (b) cured meat sample.

(a) (b)

Figure 6.5. Deformed shape of the meat samples due to curing process. This figure presents (a) a meat sample under the test and (b) a meat sample at the end of the curing process.

Two modifications to the sensor will be applied to solve the issue, namely increasing the resonance frequency from 2 GHz to 2.45 GHz and changing the microstrip feeding line technique to the coaxial probe feeding method. These amendments will reduce the size of the sensor.

6.2. Sensor Version 2

6.2.1. Real-world Experimental Results

In this section, the results from the experimental work carried out using sensor version 2 to monitor the meat curing process will be presented. Figure 6.6 shows the S_{11} measurements, which were taken once per hour (i.e. 24 times a day) during one week. Measurements of the weight loss of the sample also were taken at the same time during the week. It can be seen in Figure 6.6, that there is a noticeable change in EM signature. The change is thought to be caused by the decreasing amount of water in the meat sample. Additionally, there is a decrease of the resonance frequency and reflected power (i.e. S_{11}).

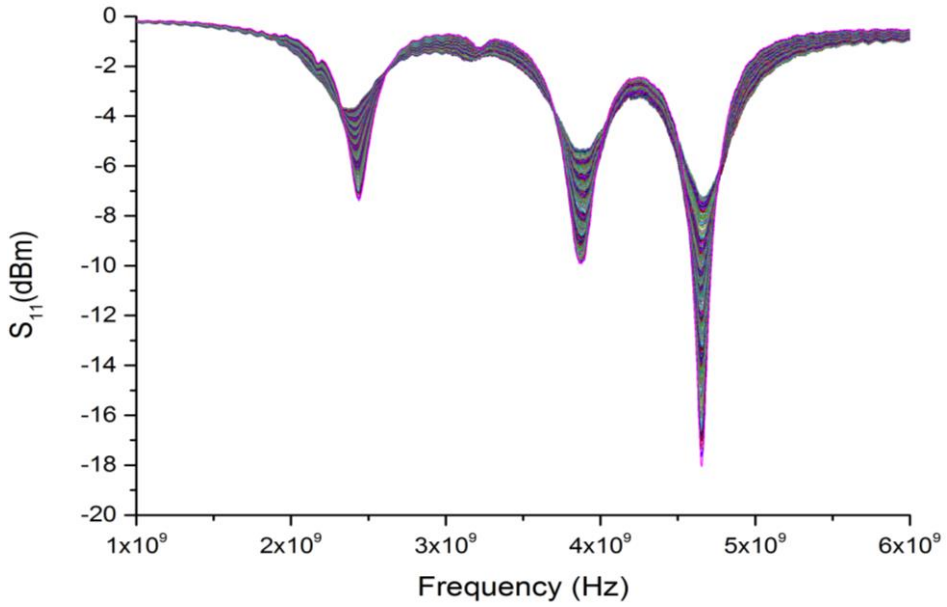

Figure 6.6. Readings from the electromagnetic wave sensor; measurements were taken once per hour in the 1-6 GHz frequency range.

Figure 6.7 demonstrates the linear correlation between weight loss and resonance frequency shift, with $R^2 = 0.79$. A linear correlation (R^2 value) between weight loss and S_{11} change across the full frequency spectrum (1-6 GHz) is shown in Figure 6.8. The strongest linear correlation was determined between weight loss and S_{11} change at 5 GHz, with $R^2 = 0.99$ (see Figure 6.9).

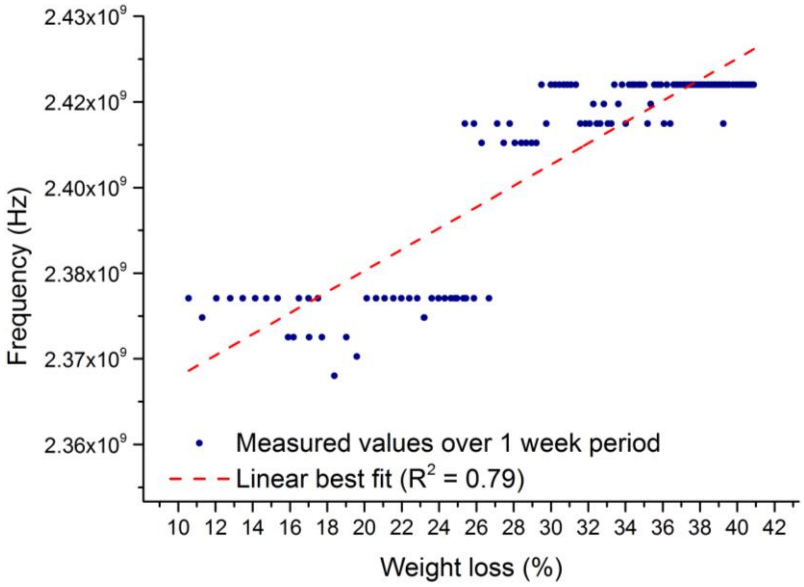

Figure 6.7. Correlation of weight loss and resonance frequency, with $R^2 = 0.79$.

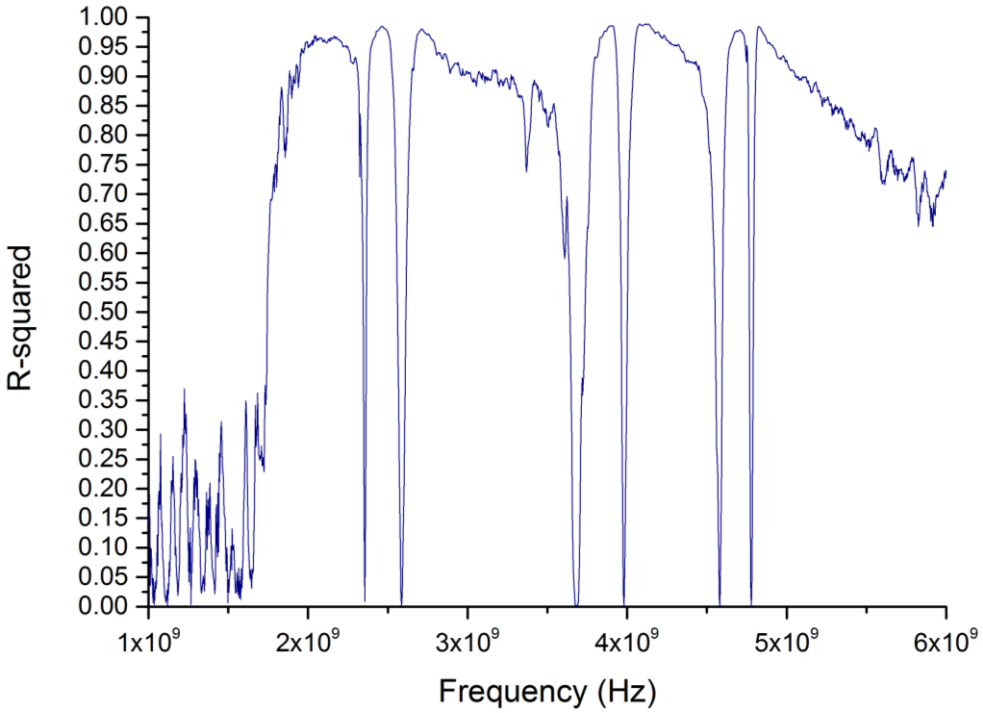

Figure 6.8. Linear correlation between weight loss and S_{11} change across the full frequency spectrum (sensor version 2).

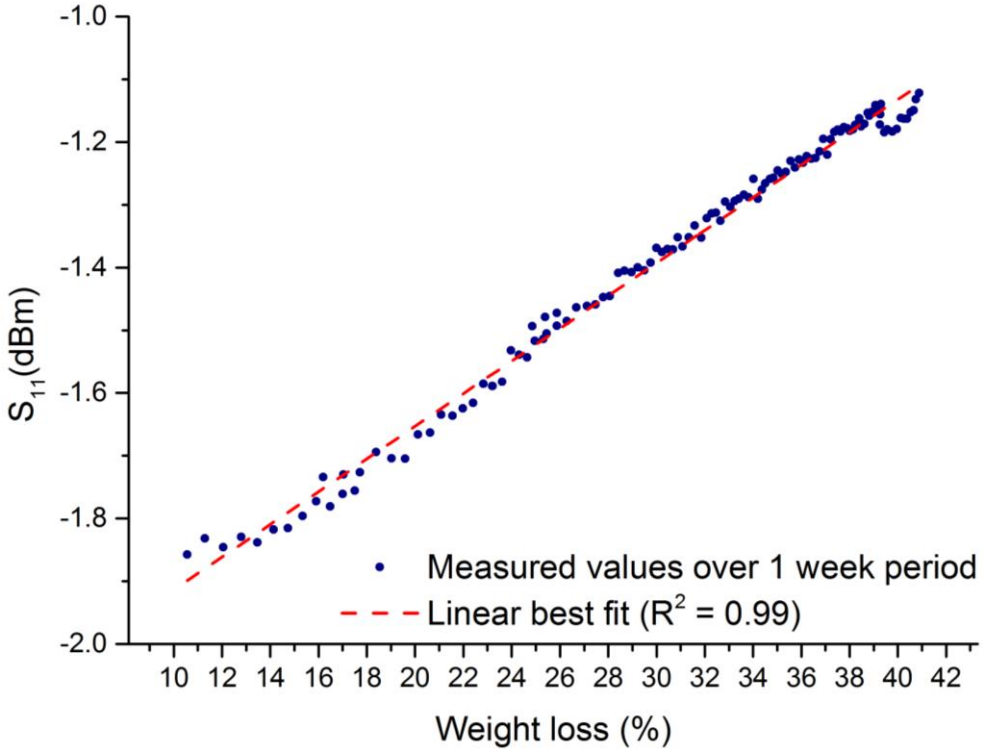

Figure 6.9. Correlation of weight loss and S_{11} at 5 GHz, with $R^2 = 0.99$.

The frequency range between 4.5-5.5GHz was selected as an optimal frequency range for development of a prediction model. Figure 6.10 demonstrates the PLSR model that exhibits a great capability to predict weight loss with $R^2_{prediction}$ = 0.99 and with Root Mean Square Error of Prediction (RMSEP) = 0.24.

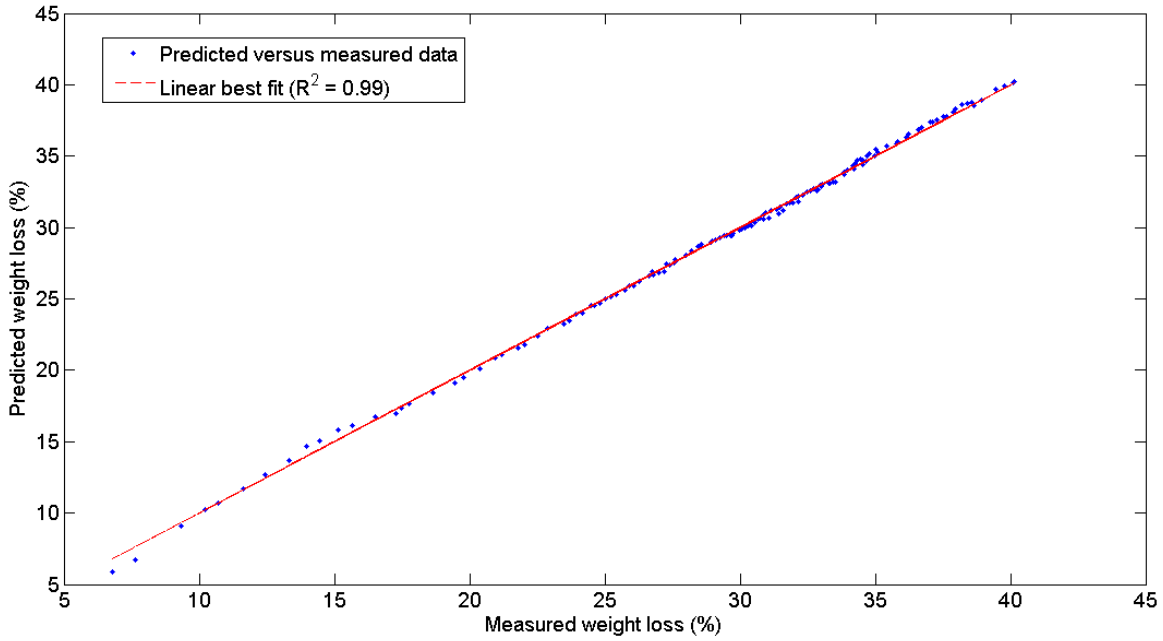

Figure 6.10. Measured and predicted weight loss from sensor version 2 using PLSR prediction model.

6.2.2. Discussion

Although the size of the sensor was reduced, the shape of the rectangular sensor was still a problem due to the uneven surface of the cured meat. Mainly, the corners of the sensor caused the difficulties. Thus, the alternative option to resolve the issue was modelling a circular type sensor. The shape of the sensor is not the only difference between these two types of sensors. The rectangular type sensor has linear polarisation whereas the circular sensor has circular polarisation that were described in section 2.5. There is one more type of polarisation called elliptical polarisation. However, this would not be the best choice as the design of the sensor is larger than the design of the circular sensor. Therefore, it was decided to model circular type sensor that resonates at 2.45 GHz frequency (ISM band).

6.3. Sensor Version 3

6.3.1. Real-world Experimental Results

In this section, the results from the experimental work carried out using sensor version 3 to monitor the meat curing process will be presented. Figure 6.11 (a) shows the S_{11} measurements that were taken once per hour (i.e. 24 times a day) during one week. Measurements of the weight loss of the sample also were taken at the same time during the week. Figure 6.11 (b) presents measurements from 5-hour intervals and from the 2-3 GHz frequency range for clarity data. It can be seen in the Figure 6.11, that there is a noticeable change in EM signature. The change is thought to be caused by the decreasing amount of water in the meat sample. There is a strong absorbing peak at 2.1 GHz and it achieves a maximum return loss of -1.5 dB (29.21%) when the moisture loss of the sample is 10%. The absorbing peak position moves to higher frequencies with decreasing weight of the sample and achieves 2.3 GHz with a return loss of -4.5 dB (64.52%) when the weight loss reaches 40%.

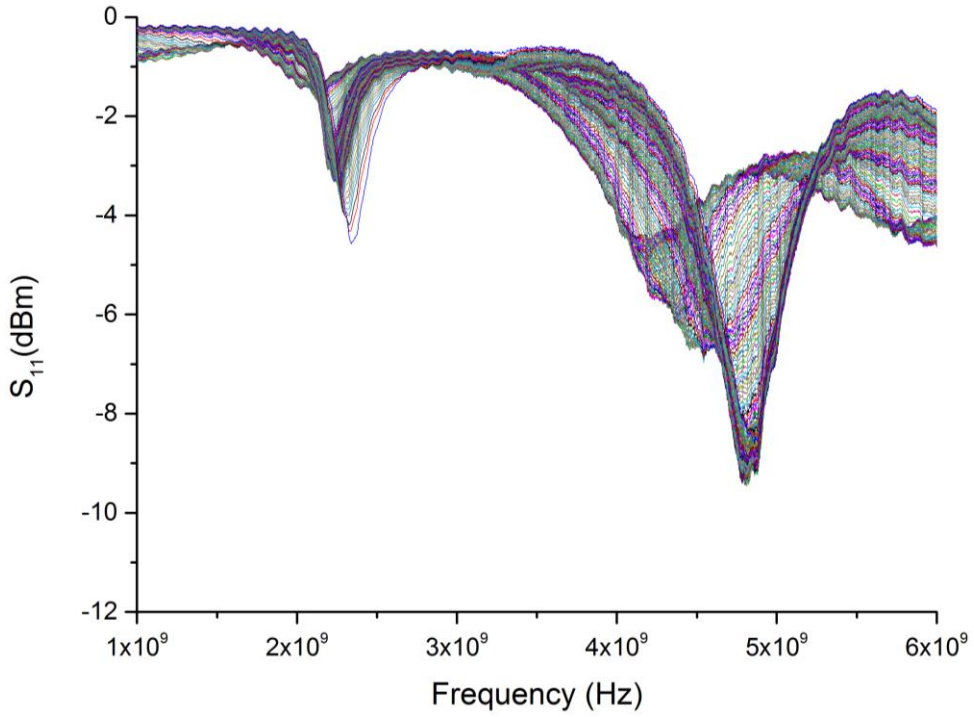

(a)

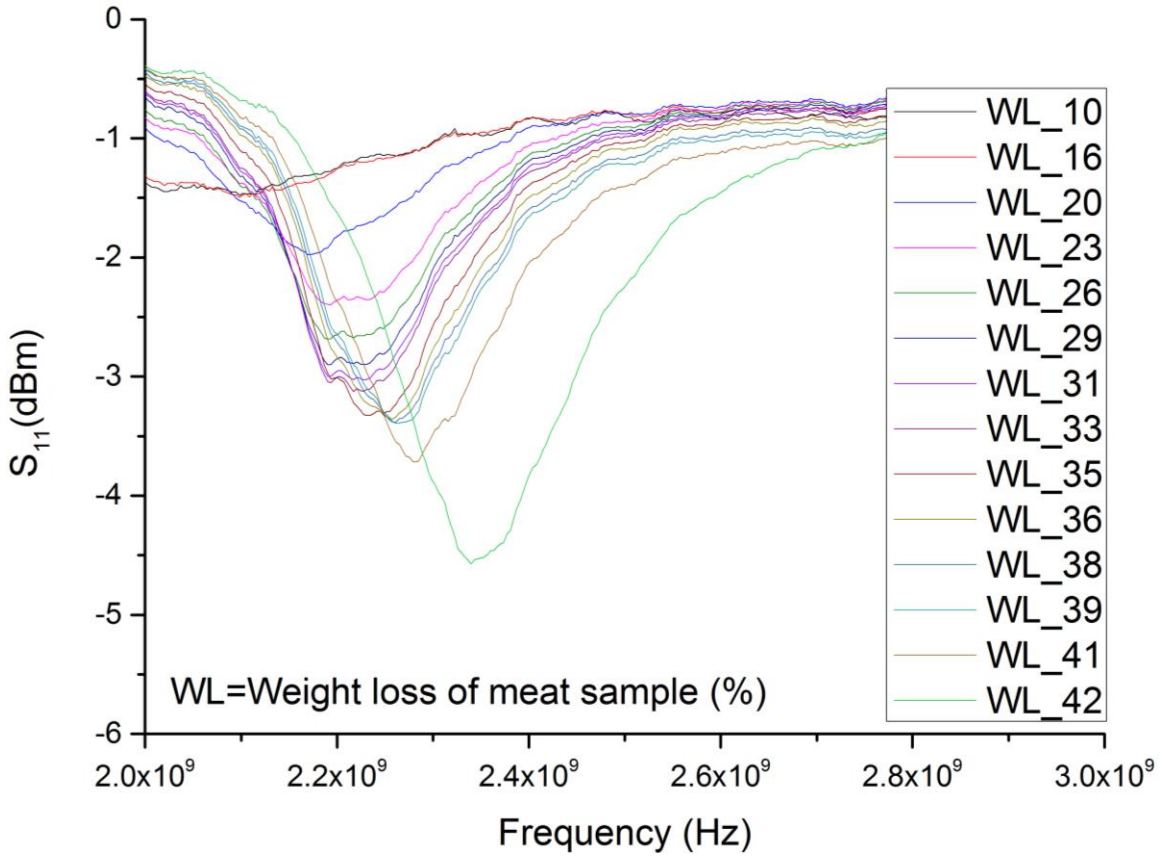

(b)

Figure 6.11. Readings from the electromagnetic wave sensor; measurements were taken (a) once per hour in the frequency range 1-6 GHz and (b) but for clarity data measurements from 5 hour intervals and from 2-3 GHz are presented.

Figure 6.12 demonstrates the linear correlation between weight loss and resonance frequency shift, with R^2 = 0.94. This means that theoretical simulation (see Figure 5.10) for the microwave absorption using the sensor agrees well with the experimental results. A linear correlation (R^2 value) between weight loss and S_{11} change across the full frequency spectrum (1-6 GHz) is shown in Figure 6.13. The strongest linear correlation was determined between weight loss and S_{11} increase at 5.5 GHz, with R^2 = 0.97 (see Figure 6.14).

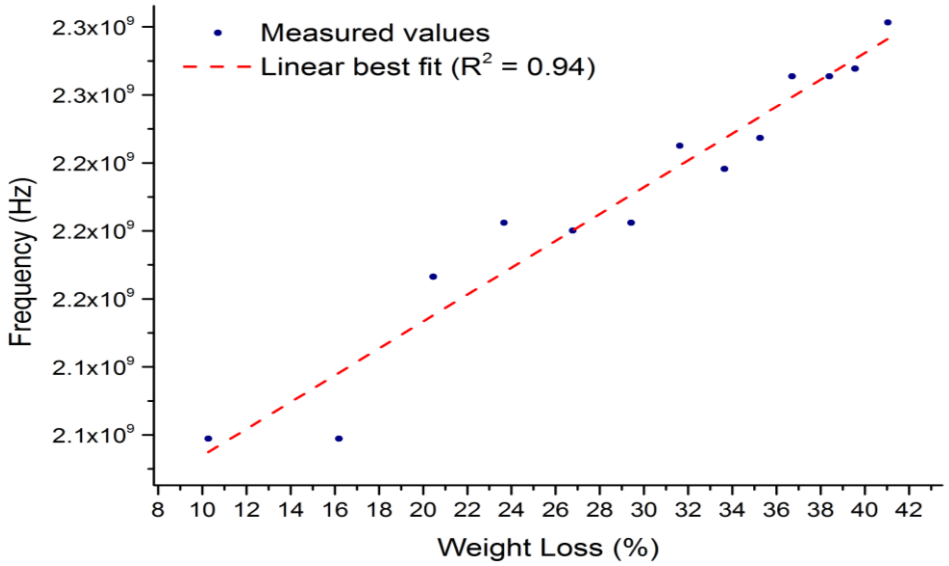

Figure 6.12. Correlation of weight loss and resonance frequency, with R^2 = 0.94.

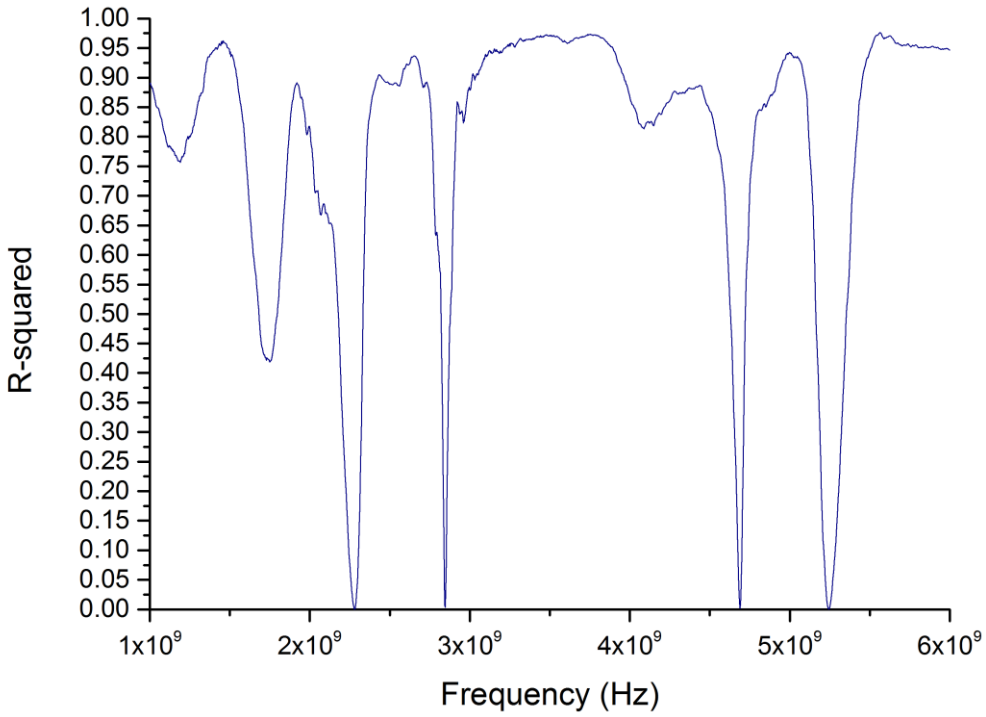

Figure 6.13. Linear correlation between weight loss and S_{11} change across the full frequency spectrum (sensor version 3).

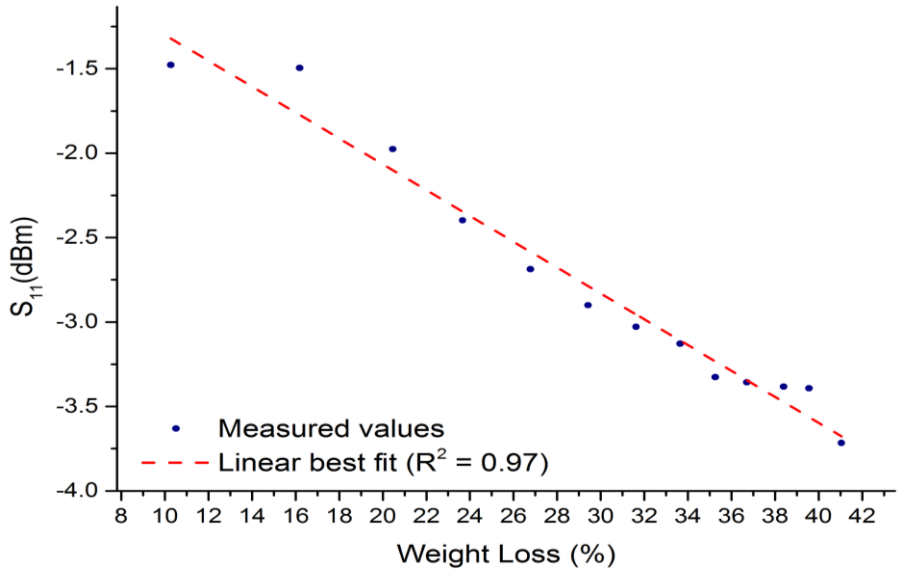

Figure 6.14. Correlation of weight loss and S_{11} at 5.5 GHz, with $R^2 = 0.97$.

To visualise graphically the performance of the PLSR models, the measured values obtained from the laboratory measurements and their predicted values resulting from 5-6 GHz frequency range, are plotted and displayed in Figure 6.15, respectively. The PLSR model exhibited a great capability to predict weight loss with $R^2_{prediction} = 0.99$ and Root Mean Square Error of Prediction (RMSEP) = 0.57 for sensor version 3.

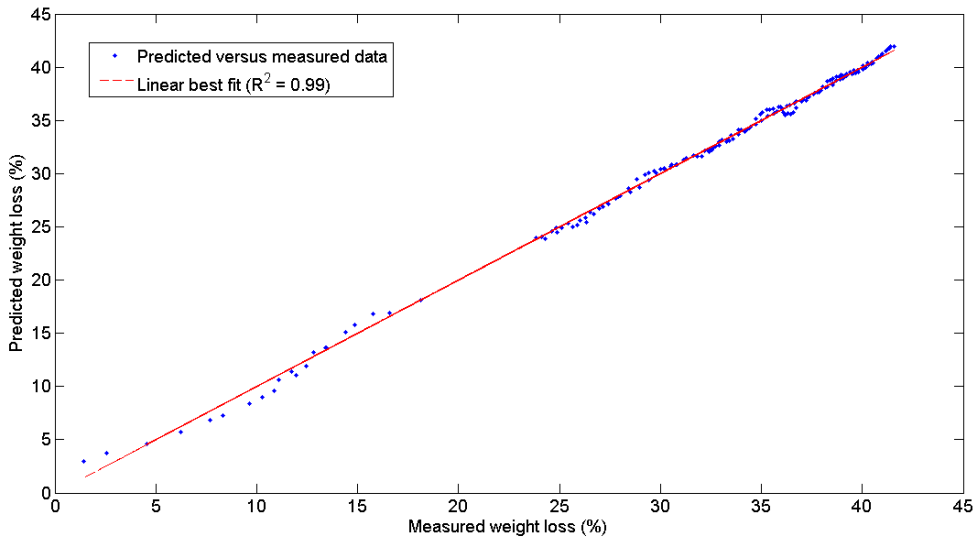

Figure 6.15. Measured and predicted weight loss from sensor version 3 using PLSR prediction model.

6.3.2. Discussion

The circular shape of the sensor solved the issues that occurred with rectangular type sensors, namely preventing full contact of the patch area of the sensor. Moreover, the sensor demonstrated good agreement with the theoretical model illustrating a good linear relationship (R^2 = 0.94) between resonance frequency shift and moisture loss of the meat sample. Better linear correlation (R^2 = 0.97) was determined between attenuation decrease at 5.5 GHz and the weight loss.

6.4. Summary

In this section, the following two points will be discussed: comparison between the results that were obtained using all three sensors and issues with the sensors and method for real-time monitoring of the meat curing process.

6.4.1. Summary of the Results

The first experimental work was undertaken by using sensor version 1. The sensor demonstrated a significant potential in monitoring the meat curing process. Although the sensor did not meet the expectations of a strong linear correlation at 2 GHz, it did show a significant relationship at higher frequencies. The results acquired from the sensor, specifically an amplitude shift of the EM signal at 4.5 GHz correlated with weight loss of the meat sample showing a linear relationship with R^2 = 0.99. The EM spectrum obtained over a one week period during the drying process of the meat sample was used to create a predictive model for on-line monitoring of the process. The PLSR prediction technique was used to analyse and develop the model. A range between 4 GHz and 5 GHz frequency was selected as 4.5 GHz showed the highest linear correlation between the change in attenuation and weight loss of the meat sample. The PLSR model exhibited a great capability to predict weight loss ($R^2_{prediction}$ = 0.99 and RMSEP = 0.41) for sensor version 1.

The sensor version 2 also showed a strong linear relationship between the reflected signal and weight loss of the meat sample with R^2 = 0.98. However, the correlation occurred at 5

GHz rather than at 4.5 GHz as it did with version 1. PLSR analysis was also applied to the data to create a predictive model. The model showed a great potential in predicting weight loss of the meat sample, with $R^2_{prediction}$ = 0.99 and RMSEP = 0.24.

The sensor version 3 illustrated better response during the monitoring of meat drying process than version 1 and version 2. First of all, the sensor demonstrated a strong agreement with the results obtained from the HFSS simulation. Particularly, a linear correlation between decrease of resonance frequency at 2.45 GHz and weight loss of the meat sample over one week period. The PLS prediction model was developed that showed a great predictive capability of the sensor with $R^2_{prediction}$ = 0.99 and RMSEP = 0.57.

6.4.2. Issues with Continuous Monitoring

The sensors version 1 and version 2 were tinned to eliminate issues with corrosion, which could cause damage to both the sample and the sensor [see Figure 6.16 (a)]. However, the corners of the sensor and the "weight" placed on top of the sensor oxidised [see Figure 6.16 (b)] during the experimental work, (the corrosion appeared at the end of the experiment, i.e. after 6-7 days). However, the meat samples were not visibly damaged. Then, a conformal polypropylene based spray coating was applied to the sensor version 3 (both radiating and ground planes). In this case, the sensor showed signs of corrosion, which also stained the meat sample, as can be seen in Figure 6.17 (a) and Figure 6.17 (b), respectively. The coating prevented the corrosion of the sensor head and meat samples at earlier stages (first 3-4 days) of the curing; however, then the coating came off/dissolved owing to the interaction with chloride ions.

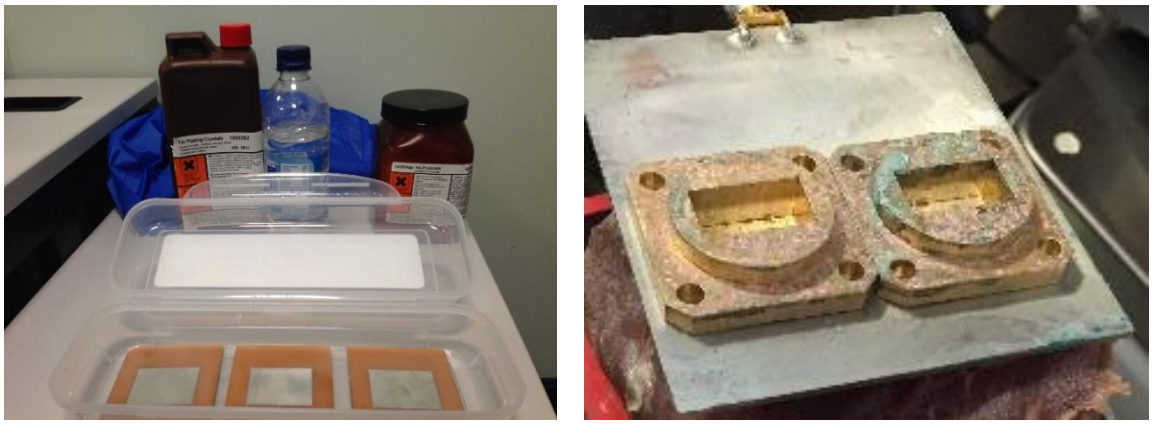

(a) (b)

Figure 6.16. (a) Tinning 2 GHz rectangular patch sensors and (b) oxidized corners of the sensor and "weights" at end of the experiment.

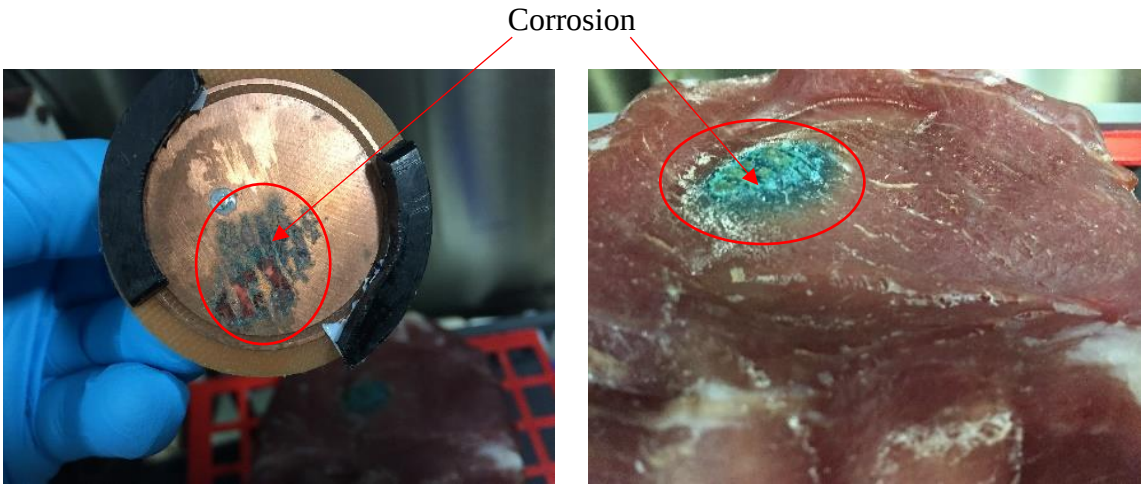

(a) (b)

Figure 6.17. (a) Conformal polypropylene based spray coated sensor version 3 and (b) oxidized meat sample at end of the experiment.

Besides the issues with the corrosion, another problem was identified with this technique. Figure 6.18 demonstrates the uncured spots left on the meat samples after 7 days of continuous monitoring of the meat drying process. This is a big problem as the purpose of the curing process is to develop a crust on the external surface/layer of meat products to reduce the a_w value. In addition, a staining has its own issues (aesthetics, contamination) but mitigation of the curing process will make the products affected unsafe. Therefore, this method of sensing would affect the safety of the product as it would not meet the HACCP

requirements. Based on the issues it was decided to conduct discrete measurements and stop the continuous measurements.

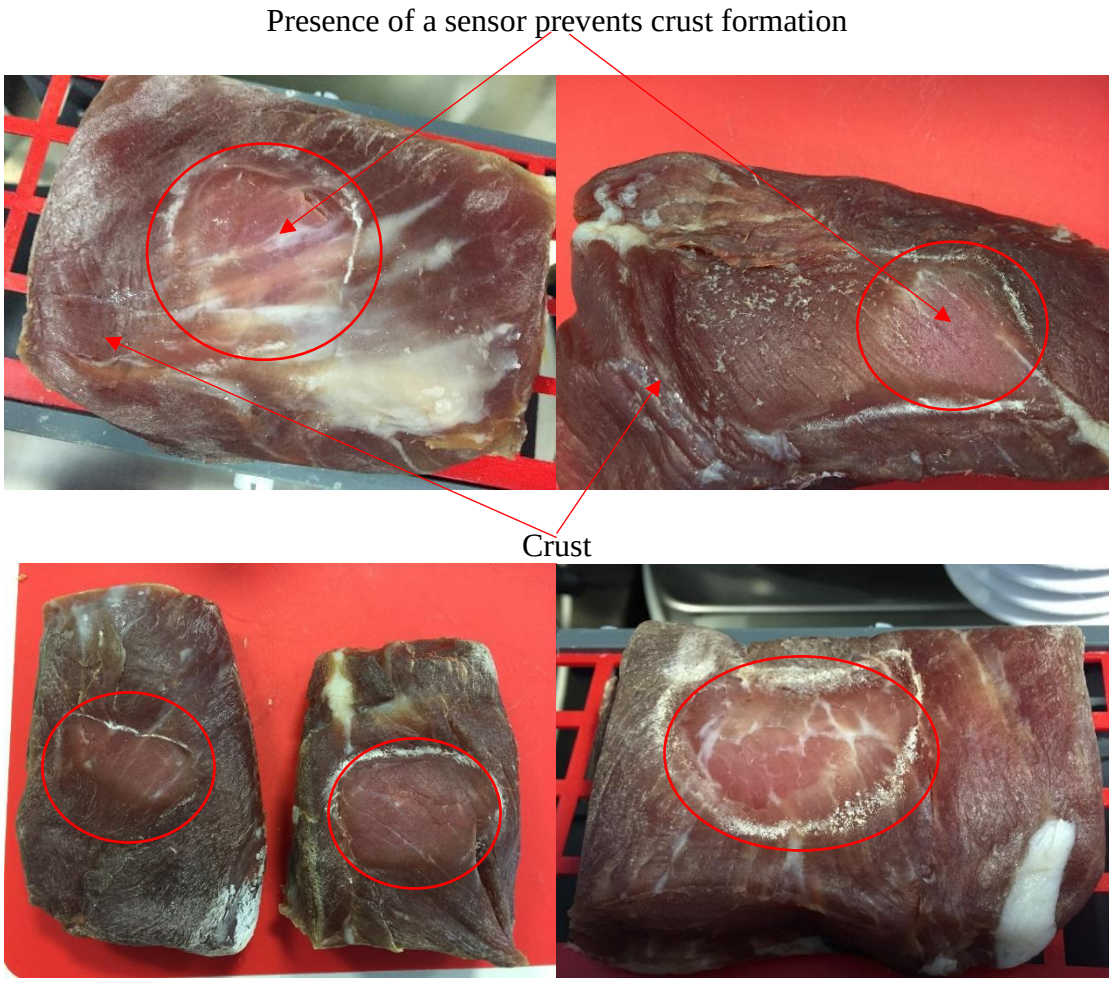

Figure 6.18. Uncured spots (red circles) on meat samples that were caused by the presence of a sensor.

Chapter 7 Discrete Monitoring for Prediction of Water Activity in Cured Meat

This chapter provides the real-world experimental results obtained using sensors version 3, 3.1 and 3.2. In addition, the chapter presents results gathered using a hand-held prototype based on sensor version 3. The prototype is tested in the LJMU laboratory as well as in the Animalia Meat and Poultry Research Centre, Norway. Moreover, the prediction models for determination of water activity in the meat samples based on the data from the sensors version 3, 3.1, 3.2 and hand-held prototype are provided in this chapter.

7.1. Sensor Version 3

7.1.1. Real-world Experimental Results

The measured values revealed that there were wide variations in water activity (a_w) for the examined meat samples that ranged from 0.722 to 0.975. A wide range of variability in the reference values is important to generate stable calibration models to be used later in the prediction.

The measurements were taken for a period of 7 months and the total of 83 meat samples were cured to investigate the capability of the microwave sensors to determine a_w in the meat samples. The frequency range of 1-13 GHz with 4000 sweep points were configured in this experiment.

It can be seen in the Figure 7.1, that there is a noticeable change in EM signature. The change is caused by the decrease of the relative permittivity of the meat samples owing to the moisture loss while curing. These changes leads to the reduction of water activity in the samples. Two changes occurred in the sensor's response (see Figure 7.1), namely a decrease of the resonance frequency and reflected power (i.e. S_{11}). The lower water content in the sample, the less power is lost/absorbed, which enables the sensor to track the changes.

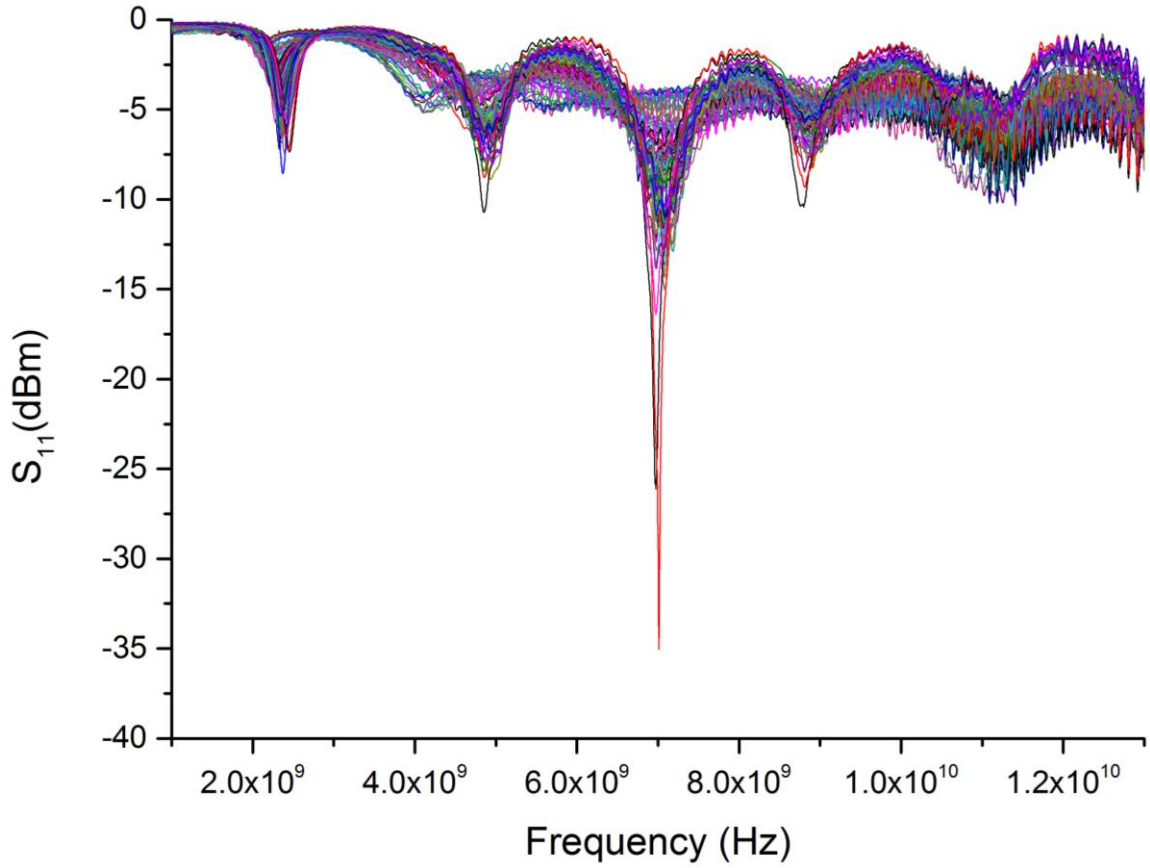

Figure 7.1. Readings from the electromagnetic wave sensor; measurements were taken from 83 cured meat samples over a period of 7 months in the frequency range 1-13 GHz.

The comparison of water activity measurements obtained is shown in Figure 7.2 and demonstrates a reasonable linear relationship with the change of resonance frequency (R^2 = 0.72). In addition, the second change (S_{11}) of the sensor's response was examined across the full frequency range (1-13 GHz) using the LabVIEW program (see Figure 4.10). The R^2 values between water activity and S_{11} across the full frequency range are shown in Figure 7.3. The results demonstrated that the strongest linear correlation (R^2 = 0.81) is between water activity and S_{11} change at 7 GHz (see Figure 7.4).

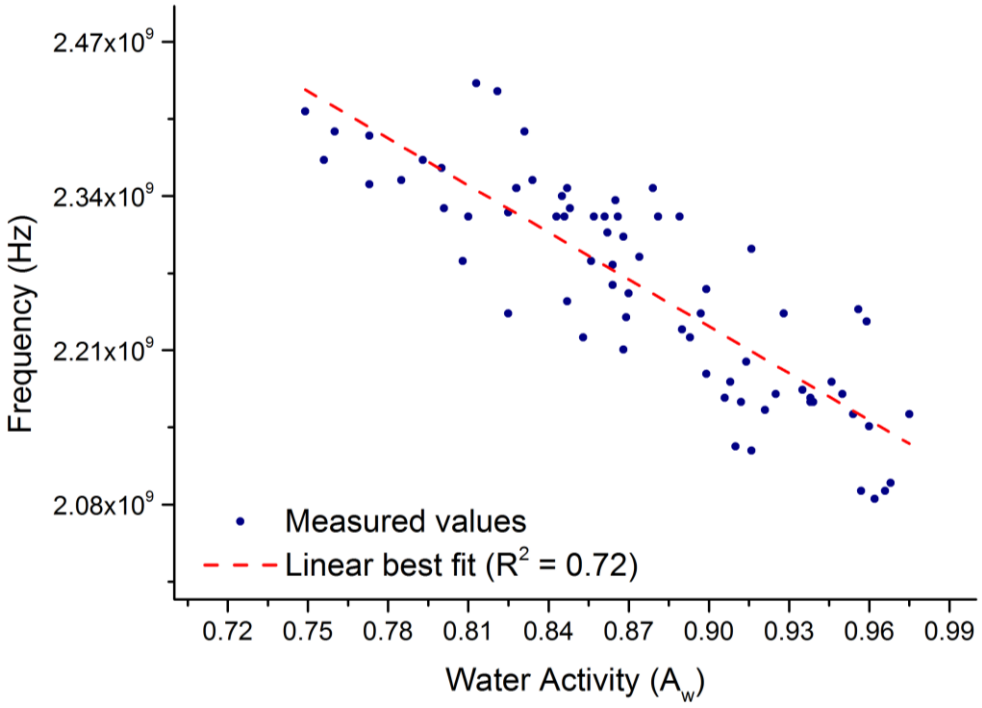

Figure 7.2. Correlation of a_w and resonance frequency, with $R^2 = 0.72$.

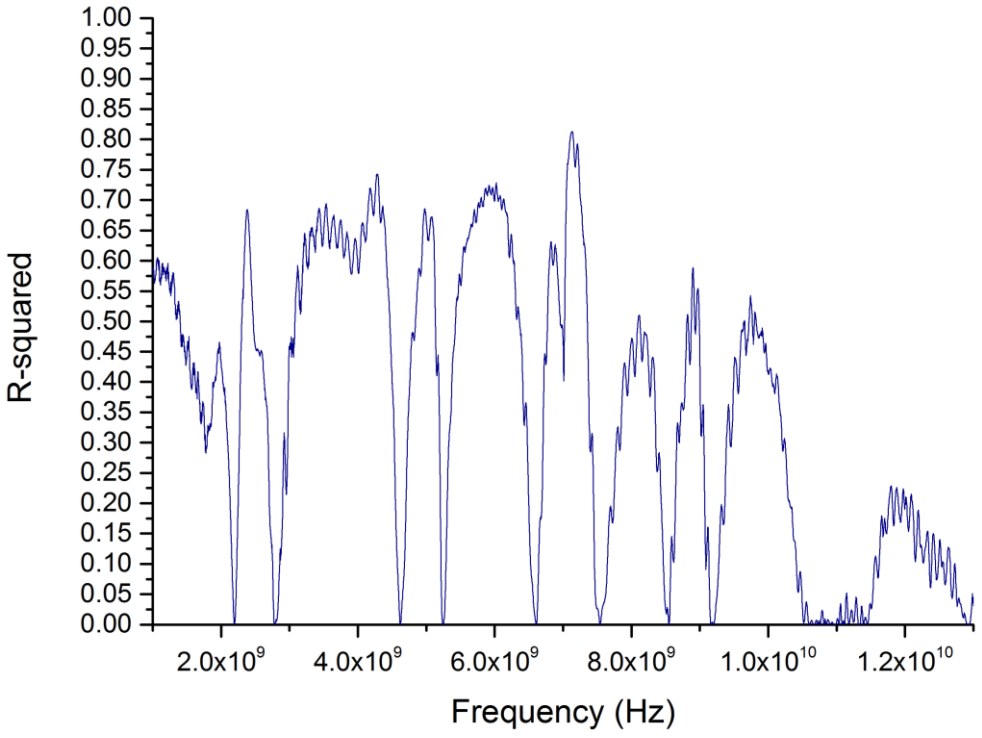

Figure 7.3. Linear correlation between water activity and S_{11} change across the full frequency spectrum (sensor version 3).

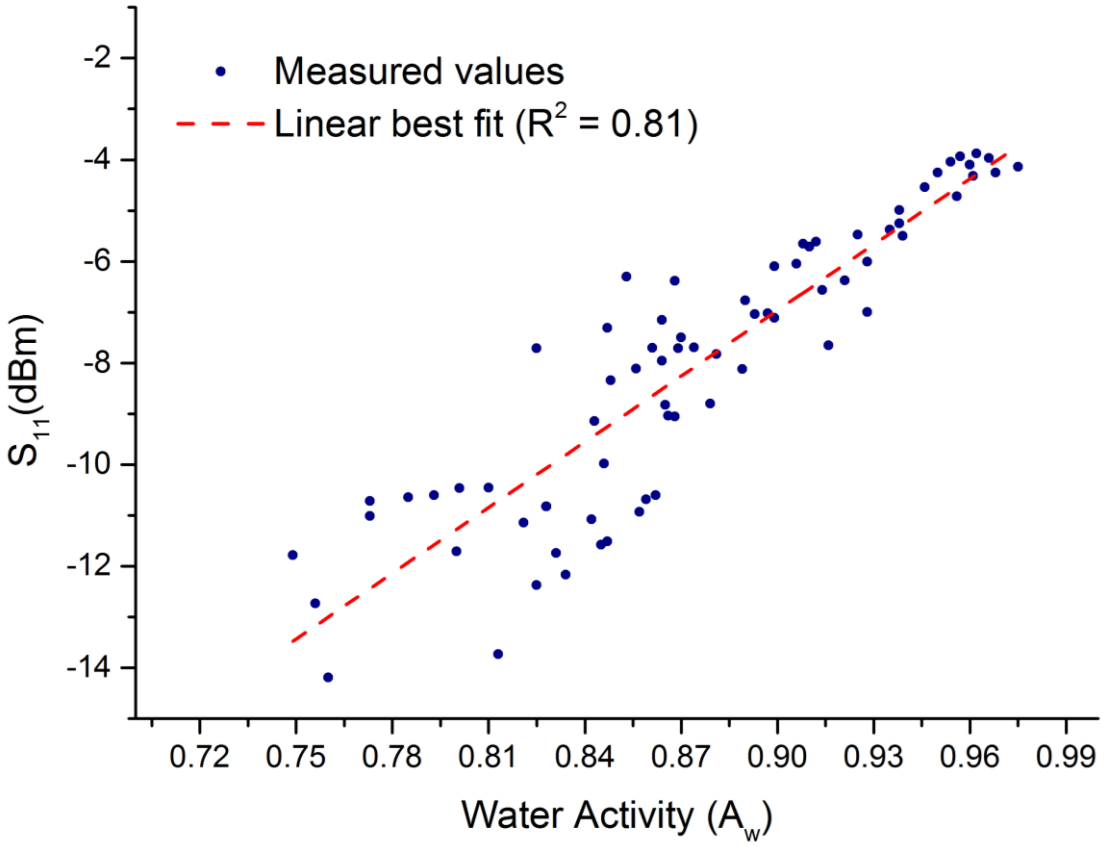

Figure 7.4. Correlation of a_w and S_{11} change at 7 GHz, with R^2 = 0.81.

7.1.2. Discussion

The sensor demonstrated a potential in determining a_w of cured meat samples at 7 GHz with R^2 = 0.81. As the measurements were taken discretely, the oxidation did not occur either on the sensor or on the meat sample. However, to avoid the corrosion or damage of the sensor and the meat products it is essential to cover the sensor. Therefore, the next section will provide the results obtained using the prototyped sensor (i.e. the sensor was embedded inside a handheld prototype).

7.2. Hand-held Prototype and Industrial Testing

The design of the hand-held prototype is shown in Figure 7.5. The sensor head is detachable from sensor body so it can be modified to suit preference and to avoid the modification of the sensor body. This particular sensor design enables a simple replacement of the sensor head, if the sensor head is improved or damaged. The sensor is embedded with plastic material to prevent metal-to-food contact.

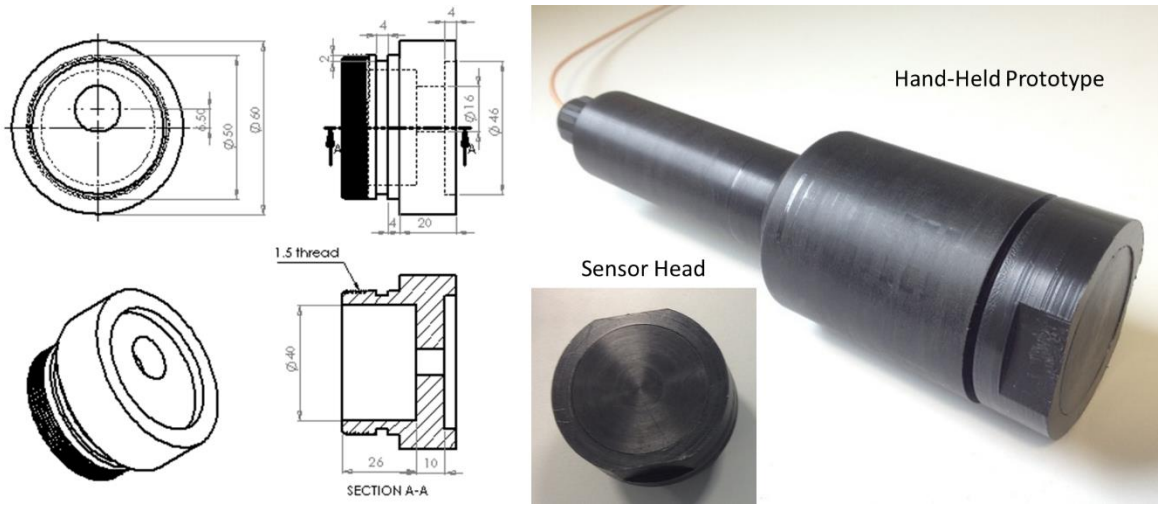

Figure 7.5. Design of the Hand-Held Prototype.

This section provides results from two sets of experimental work using a hand-held prototype shown in Figure 7.6 (b). The first experimental setup is presented in Figure 7.6 (a) that comprises the prototype on the meat sample (pork loins) measuring the reflected power. The sensor is connected to a laptop via VNA for data acquisition using the utilised LabVIEW program for discrete measurements. The second experiment was undertaken following the same experimental setup (see Figure 7.7), i.e. taking discrete measurements of reflected power using the hand-held prototype. However, the experiment was carried out in the Animalia Meat and Poultry Research Centre, Norway on dry-cured lamb.

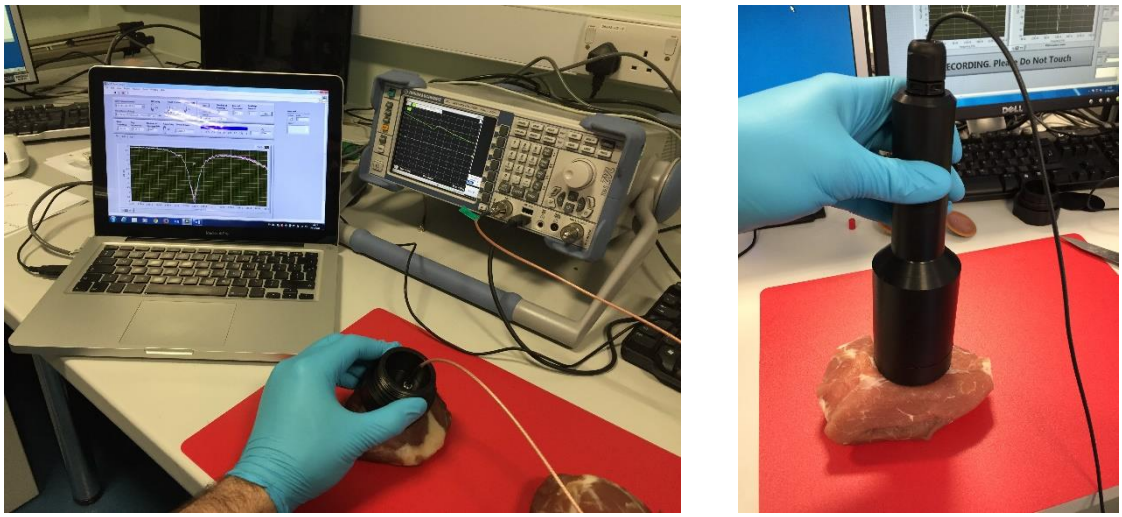

(a) (b)

Figure 7.6. (a) Experimental setup with head of a hand-held prototype (b) hand-held prototype.

Figure 7.7. Experimental work conducted in Norwegian pilot plant owned by Animalia, using hand-held prototype to measure dry cured lamb test products.

7.2.1. Real-world Experimental Results

Figure 7.8 shows the S_{11} measurements of sample of pork chump end. There is a noticeable change in EM signature in the full measured spectrum (1-13 GHz). However, the strongest absorption is at 7 GHz frequency region and higher. The 2.4 GHz and 5 GHz frequencies also demonstrated a reasonable correlation against a_w.

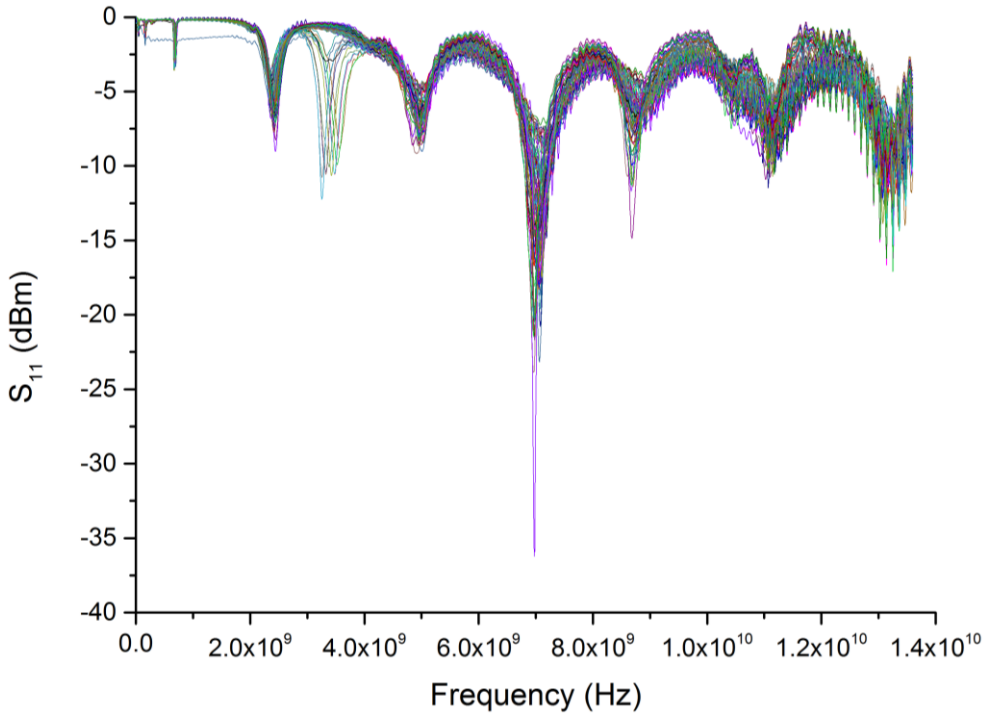

Figure 7.8. Readings from the hand-held prototype; measurements were taken from 83 cured meat samples over a period of 7 months in the frequency range 1-13 GHz.

The results obtained using the prototype demonstrated a stronger linear relationship between the changes in EM spectrum and a_w than the measurements taken with the direct contact of the sensor [see Figure 4.9 (b)] with the meat samples. The frequency shift of the resonance frequency at 2.45 GHz and a_w illustrated a reasonable linear agreement [$R^2 = 0.75$, see Figure 7.9 (a)]. The same linear relationship [$R^2 = 0.75$, see Figure 7.9 (b)] was determined between a_w and S_{11} change at the resonance frequency. However, the amplitude shift across the full frequency range was also investigated to determine a_w. The R^2 values between the amplitude

shift across the full spectrum and a_w is presented in Figure 7.10. A stronger correlation coefficient was shown by S_{11} change at 5 GHz and a_w, with $R^2 = 0.86$ [see Figure 7.11 (a)]. Though, the highest degree of correlation was determined between the amplitude shift at 7 GHz and a_w, with $R^2 = 0.91$ [see Figure 7.11 (b)].

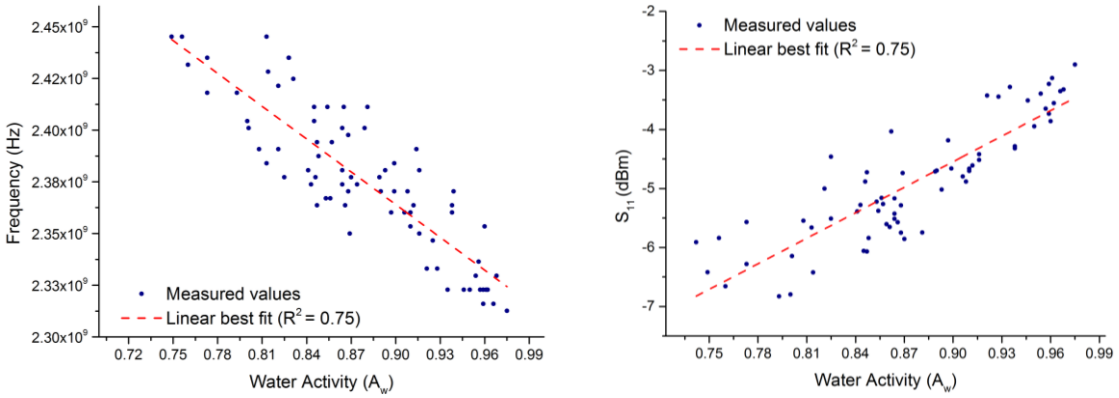

(a) (b)

Figure 7.9. Correlation of water activity and (a) resonance frequency, with $R^2 = 0.75$ and (b) S_{11} at 2.37 GHz, with $R^2 = 0.75$.

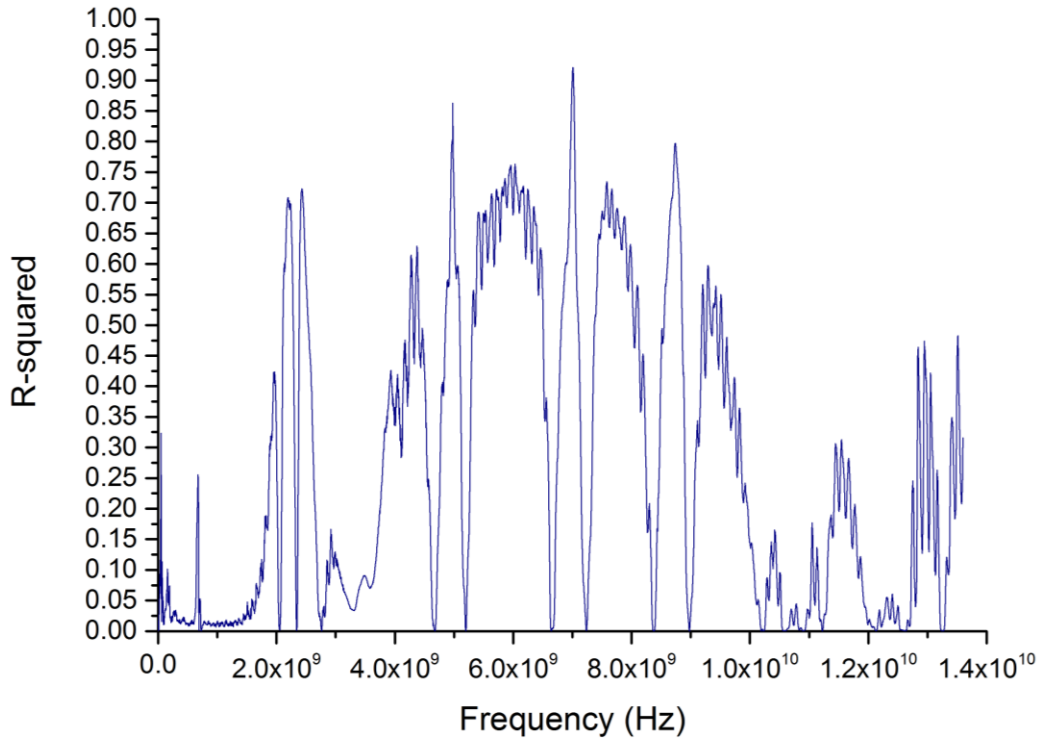

Figure 7.10. Linear correlation between water activity and S_{11} change across the full frequency spectrum (hand-held prototype).

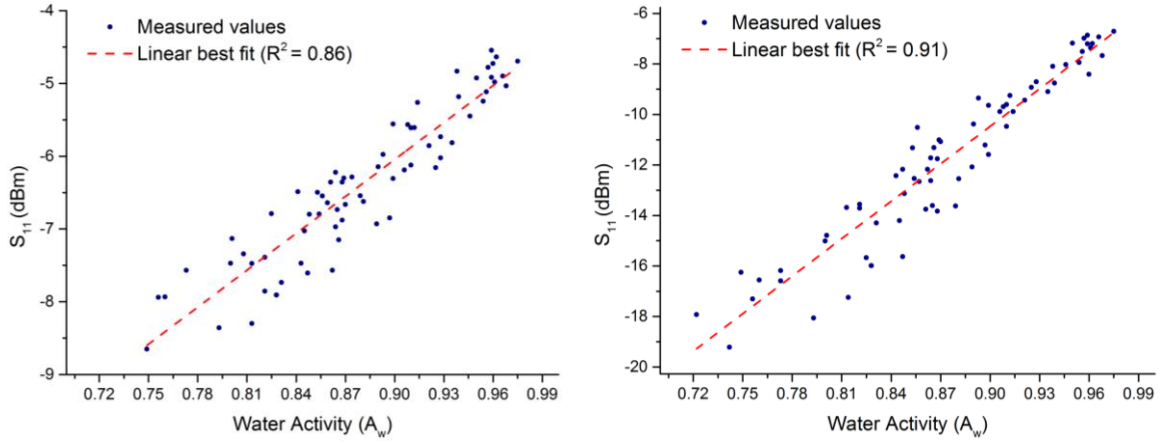

(a) (b)

Figure 7.11. Correlation of a_w and (a) S_{11} at 5 GHz, with R^2 = 0.86 and (b) S_{11} at 7 GHz, with R^2 = 0.91.

The frequency range with the highest absolute values of weighted regression coefficients are selected as the optimal frequency range for hand-held prototype to predict a_w, i.e. 6.5-7.5 GHz frequency range. This optimal frequency range provided potential indication of changes in chemical components, namely, water content, which can account for quality change of parameters such as a_w of the meat samples during dry-curing process.

To visualise graphically the performance of the PLSR prediction models, the measured values obtained from the laboratory measurements and its predicted values resulting from 6.5-7.5 GHz frequency range, are plotted and displayed in Figure 7.12. The PLSR model exhibited a good capability to predict a_w, with $R^2_{prediction}$ = 0.91 and Root Mean Square Error of Prediction (RMSEP) = 0.0173. The MATLAB code and explanation of the code is provided in Appendix B.

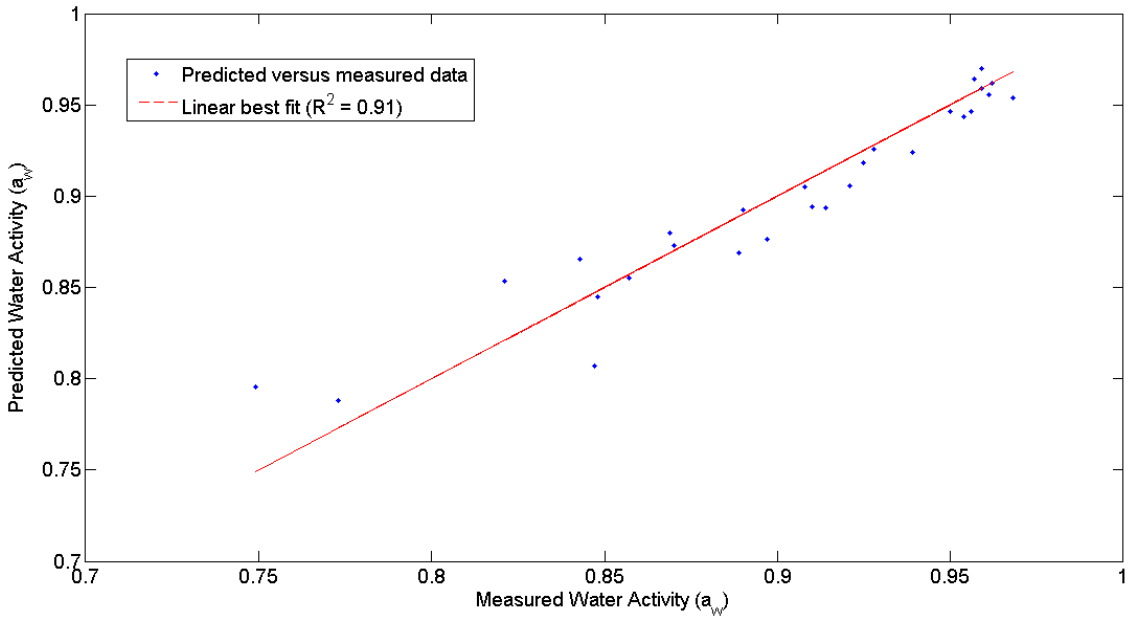

Figure 7.12. Measured and predicted a_w data (LJMU data only) from hand-held prototype using PLSR prediction model (see Appendix B for more details on this prediction model).

7.2.2. Results based on Animalia data

As the strongest linear relationship was determined between a_w and amplitude shift at 7 GHz, data from Animalia at that frequency was added to the existing data cluster, i.e. to the data shown in Figure 7.11 (b). Although, the measurements were taken from different animal products (pork and lamb), no impact was made on correlation ($R^2 = 0.91$) as it is shown in Figure 7.13. Blue colour data (dots) represents measurements taken in LJMU laboratory and the red colour data (dots) represents measurements taken in Animalia. This means that the sensors system is capable of predicting a_w in various cured meat products, namely cured pork and lamb products without any data offset or complex calibration/manipulation.

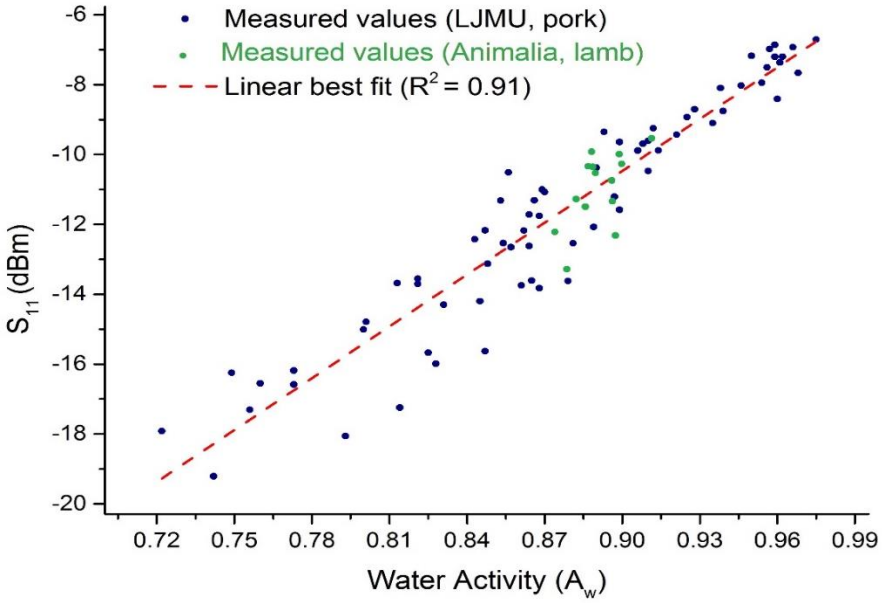

Figure 7.13. Animalia data fitted into LJMU data cluster.

The prediction model developed based on the LJMU laboratory data (see Figure 7.12) was applied on Animalia data, which is presented in Figure 7.14. The model also demonstrated a good capability of predicting a_w in cured lamb with $R^2_{prediction}$ = 0.91 and RMSEP = 0.176.

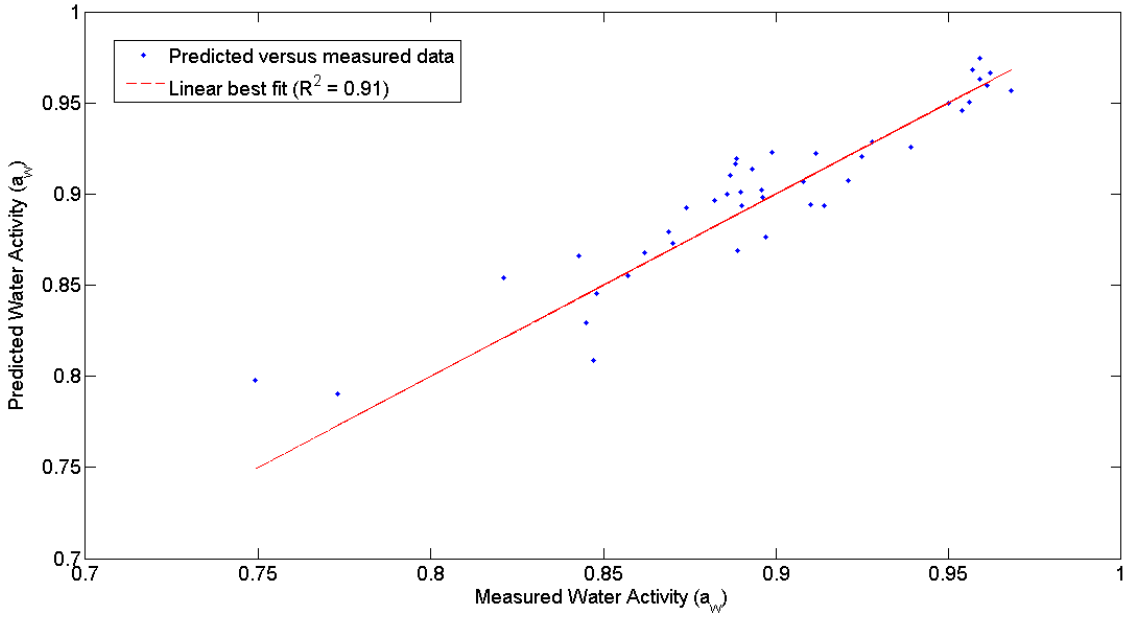

Figure 7.14. Measured and predicted a_w data (LJMU and Animalia data) from hand-held prototype using PLSR prediction model.

7.2.3. Discussion

The hand-held prototype demonstrated stronger linear relationships between a_w and S_{11} changes at 5 GHz and 7 GHz frequencies with R^2 = 0.86 and R^2 = 0.91, respectively. However, 2.4 GHz also illustrated good linear agreement with a_w, with R^2 = 0.75. In addition, the sensor was tested in the Animalia Meat and Poultry Research Centre, Norway. The measurements were taken from dry-cured lamb and the results demonstrated the data fits very well into the existing dataset, i.e. the measurements taken from pork loins in the LJMU laboratory. This shows a capability of this sensor system to be used on different types of cured meat products without any requirements of data offsets or calibration.

On the other hand, the sensor head of the prototype can cause an issue with the smaller meat samples (see Figure 7.15). Therefore, the size reduction of the sensor was undertaken and two sets of sensors were modelled, constructed and tested (see section 7.3 for the results).

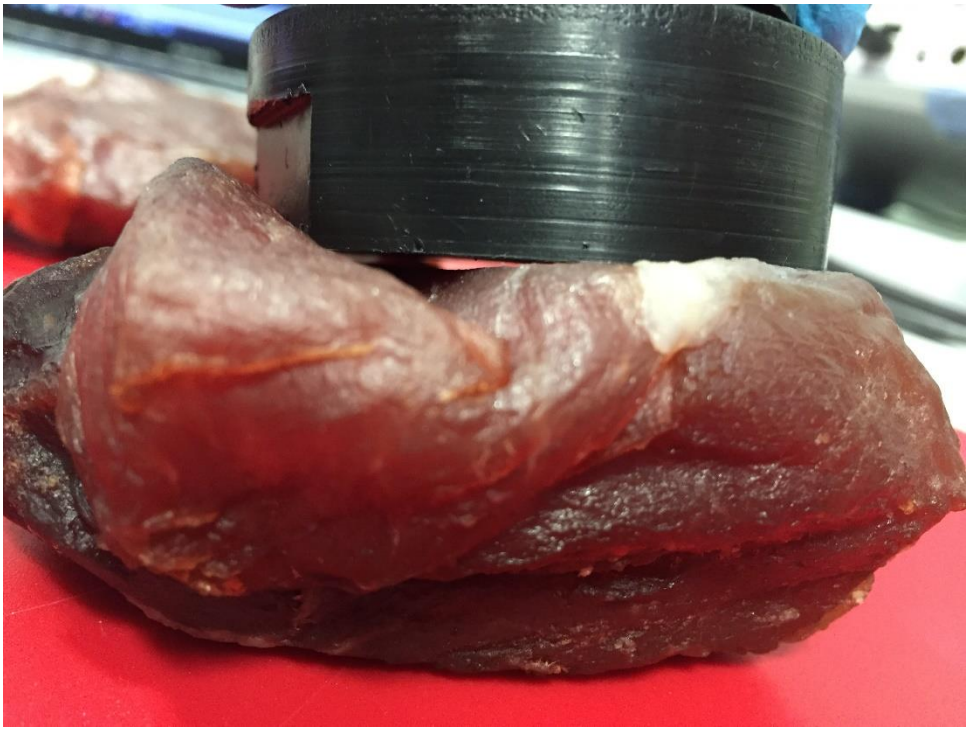

Figure 7.15. Measuring a meat sample with prototyped sensor.

7.3. Sensors version 3.1 and version 3.2

In this section, the results from the experimental work undertaken using sensors version 3.1 and 3.2 will be provided. In addition, the prediction model based on the obtained data from sensors version 3.1 and 3.2 will be demonstrated in this section.

7.3.1. Real-world Experimental Results

Figure 7.16 and Figure 7.17 show the S_{11} measurements, which were taken over a period of 5 weeks from the sensors version 3.1 and 3.2, respectively. In total, 37 meat samples were cured and measured with both sensors. The measurements were repeated 5 times during this experimental work.

It can be seen in the Figure 7.16 and Figure 7.17, that there is a noticeable change in EM signature. The change is thought to be caused by the decreasing amount of water in the meat sample, which reduces a_w. Both figures show a decrease of the resonance frequency and change of attenuation of the signal. There is a bigger shift of the second resonance frequency in both figures and smaller increase of first resonance frequency with decreasing a_w.

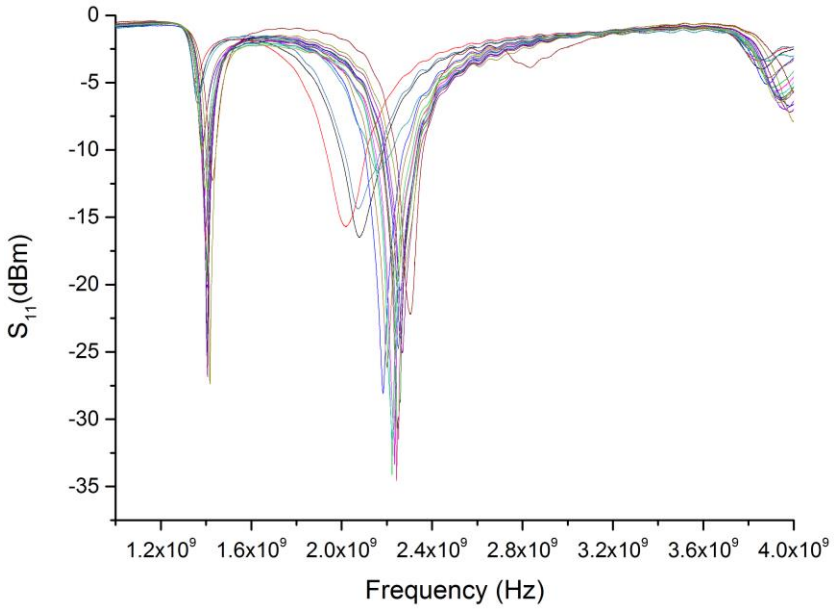

Figure 7.16. Readings from the sensor version 3.1; measurements were taken on 37 dry-cured meat samples.

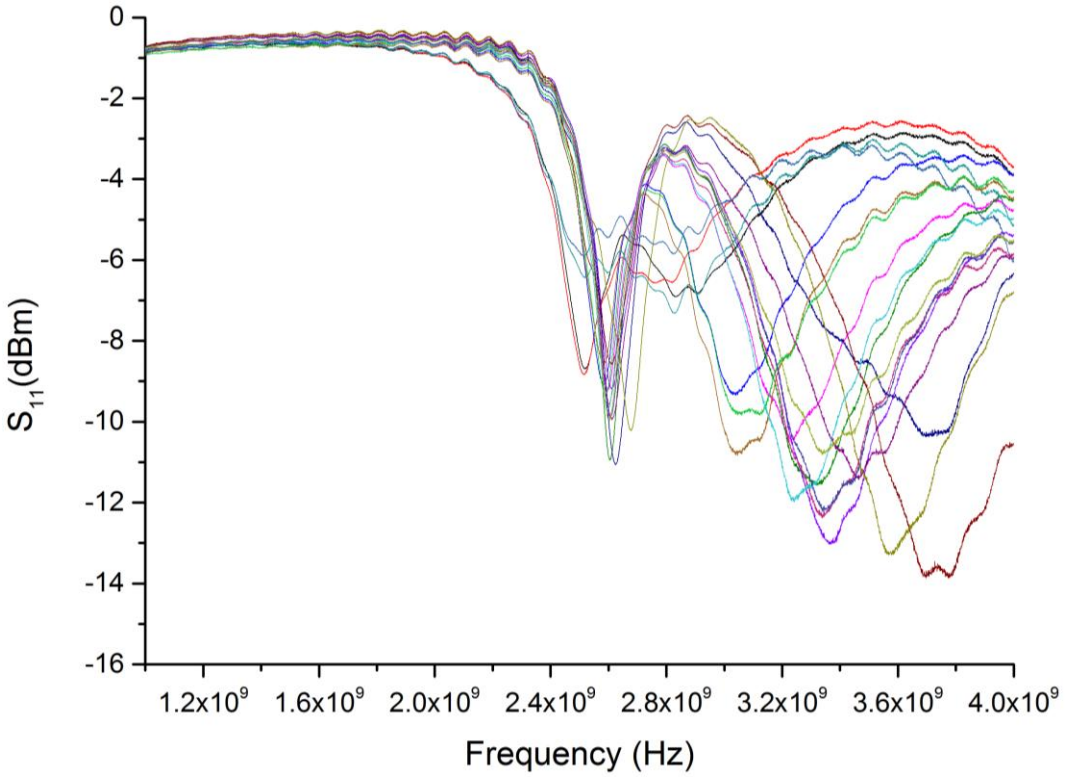

Figure 7.17. Readings from the sensor version 3.2; measurements were taken on 37 dry-cured meat samples.

The second resonance frequency of both sensors demonstrated a strong linear relationship with the decrease of a_w, with $R^2 = 0.77$ [see Figure 7.18 (a)] and $R^2 = 0.80$ [see Figure 7.18 (b)] for version 3.1 and version 3.2, respectively.

The attenuation change of the reflected microwave signal across the full frequency range was also investigated to determine a_w. The R^2 values between the attenuation change of the reflected power (i.e. S_{11}) across the full spectrum and a_w is presented in Figure 7.19 (a) and Figure 7.19 (b) for sensors version 3.1 and 3.2, respectively. The strongest linear relationship ($R^2 = 0.80$) between water activity and S_{11} change was determined at 3.8 GHz for sensor version 3.1 [see Figure 7.20 (a)]. The response from the sensor version 3.2 demonstrated similar linear coefficient ($R^2 = 0.80$) between water activity and S_{11}, however at 3.8 GHz.

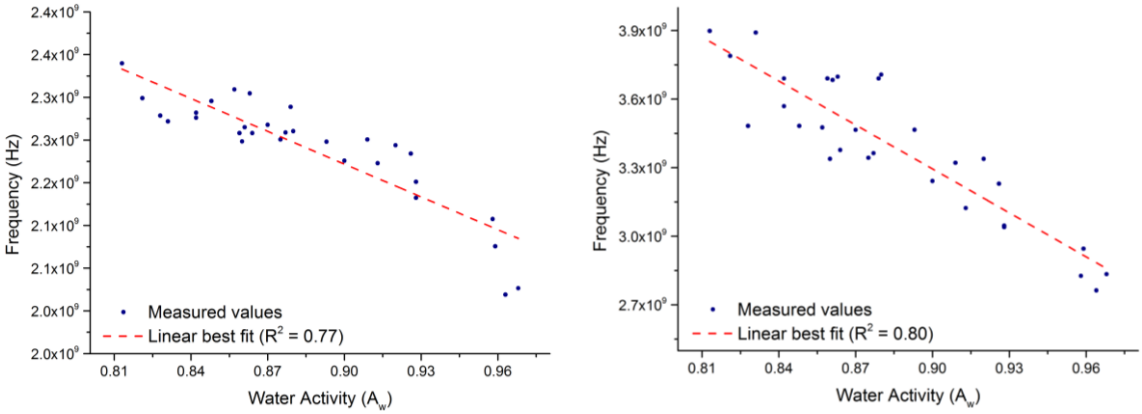

Figure 7.18. Correlation of a_w and resonance frequency, with $R^2 = 0.77$ and with $R^2 = 0.80$ from the results obtained using (a) version 3.1 and (b) version 3.2, respectively.

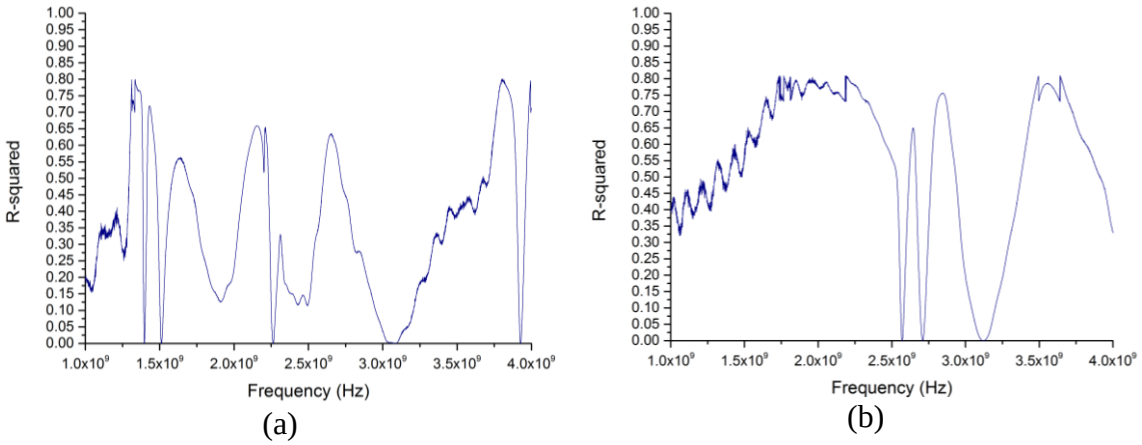

Figure 7.19. Linear correlation between water activity and S_{11} change across the full frequency spectrum from the sensors (a) version 3.1 and (b) version 3.2.

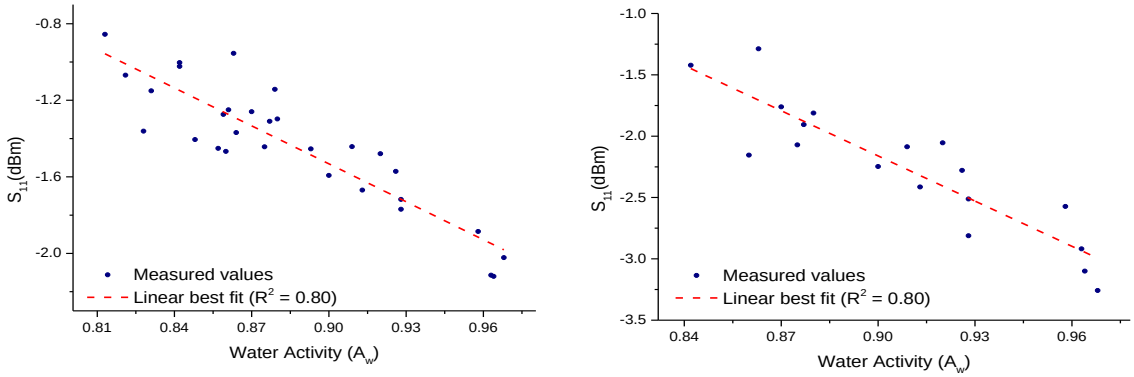

Figure 7.20. Correlation of a_w and (a) S_{11} at 3.8 GHz, with $R^2 = 0.80$ for sensor version 3.1 and (b) S_{11} at 3.6 GHz, with $R^2 = 0.80$ for sensor version 3.2.

The measurements from sensors version 3.1 and version 3.2 were analysed using full spectrum, i.e. the 1-4 GHz frequency range. The PLSR technique was applied on the data; two prediction models were created. The sensors demonstrated lower capability to predict a_w compared to hand-held prototype, with $R^2_{prediction}$ = 0.64 and RMSEP = 0.0468 for version 3.1 and $R^2_{prediction}$ = 0.79 RMSEP = 0.0296 for version 3.2. The predicted and measured data is illustrated in Figure 7.21 (a) and Figure 7.21 (b) for sensors version 3.1 and version 3.2, respectively.

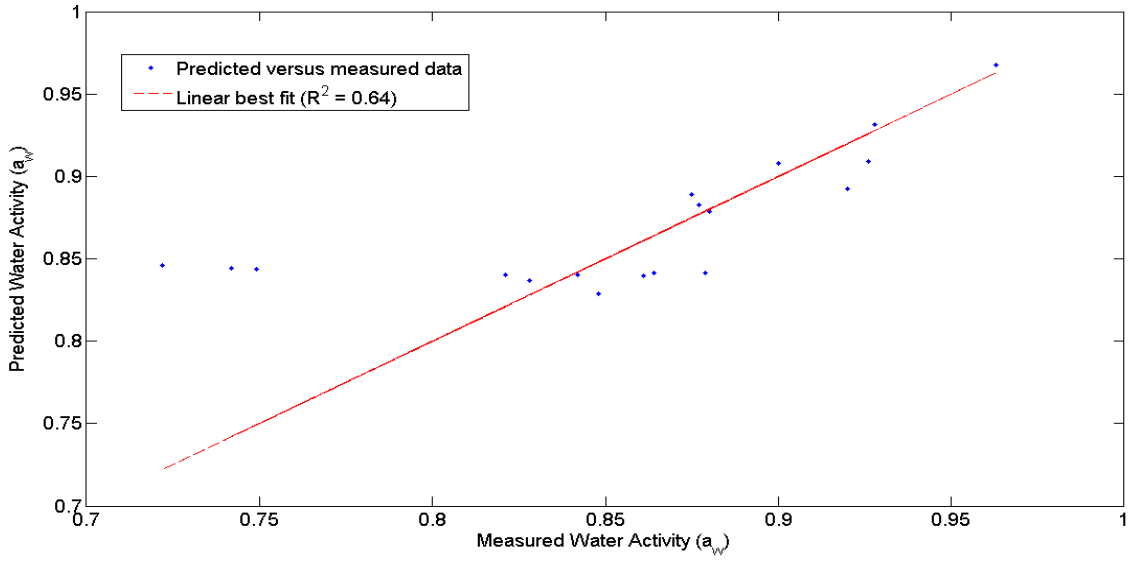

(a)

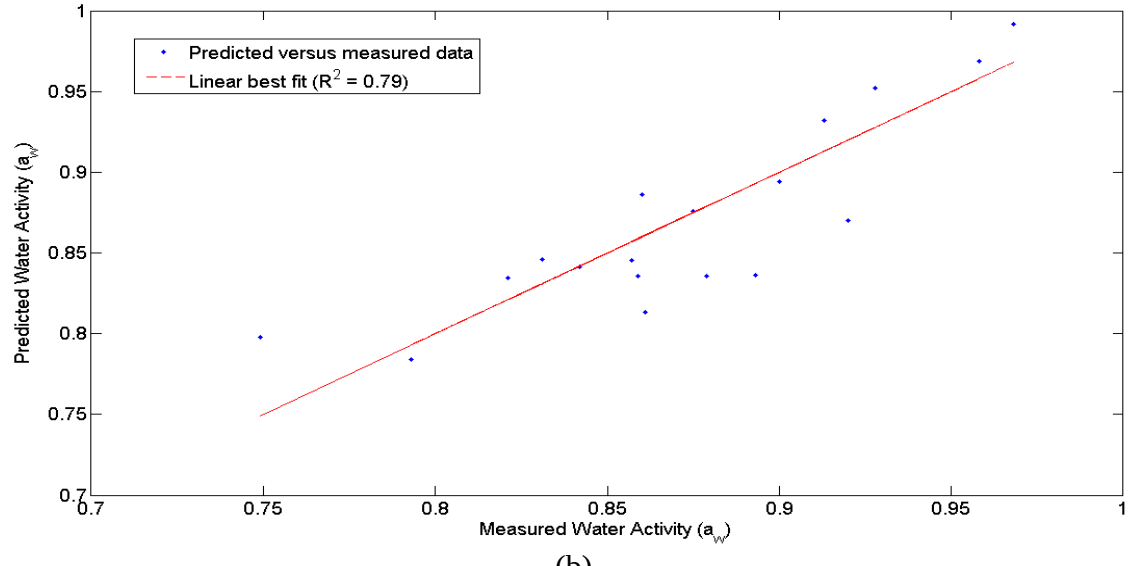

(b)

Figure 7.21. Measured and predicted a_w data from sensors (a) version 3.1 and (b) version 3.2 using PLSR prediction model.

7.3.2. Discussion

The size reduced circular patch sensors demonstrated a good linear relationship between a_w and decrease of resonance frequencies of both sensors. The results illustrated a linear correlation ($R^2 = 0.80$) at 3.8 GHz and 3.6 GHz for the sensors version 3.1 and version 3.2, respectively. However, the hand-held prototype showed a stronger linear relationship between a_w and S_{11} change at 7 GHz, with $R^2 = 0.91$. Further work could be done by applying other methods/techniques (mentioned in sub-section 3.3.2.2) to enhance the size of the sensor. In addition, various substrates could be investigated (mentioned in sub-section 3.3.4).

7.4. Summary

In this chapter, the results and prediction models for a_w determination in cured meat samples using a set of microwave sensors, namely sensors version 3, version 3.1, version 3.2 and also hand-held prototype were provided. The sensor version 3 demonstrated a good linear correlation between a_w and change in reflected power at 7 GHz frequencies, with $R^2 = 0.81$. Then, the sensor was embedded into hand-held prototype and tested on the cured meat samples. The prototype illustrated a stronger linear relationship ($R^2 = 0.91$) between a_w and change in reflected power at 7 GHz frequencies. To measure smaller meat samples the size of the sensor was reduced using complementary split ring resonator technique and two sets of sensors (i.e. sensors version 3.1 and version 3.2) were selected from various designs based on the simulation results. The sensors then were tested and an experimental work was conducted to determine a_w in cured meat samples. The results demonstrated a good linear correlation ($R^2 = 0.80$) between a_w and S_{11} change at 3.8 GHz and 3.6 GHz for sensors version 3.1 and version 3.2, respectively.

Finally, PLSR technique was applied on data obtained from the hand-held prototype, sensors version 3.1 and version 3.2 to create a prediction model. The prototype exhibited a good capability to predict a_w in cured pork loin and also in cured lamb using the same prediction model, with $R^2_{prediction} = 0.91$ and RMSEP = 0.0173 on pork loin and $R^2_{prediction} = 0.91$ and RMSEP = 0.0176 on pork loin and lamb combined. However, sensors version 3.1 and version 3.2 did not demonstrate as good a performance as the prototype (i.e. the higher error

of the smaller sensors makes the larger hand-held prototype favourable, currently). The comparison among these three sensors is presented in Table 7.1.

Table 7.1. Comparison of prediction models between hand-held prototype, sensor version 3.1 and sensor version 3.2.

Sensor	Data	Time (sec)	Training set	Testing set	R^2_p	RMSEP	Repeatability
Hand-held prototype	LJMU	<5	40	38	0.91	0.0173	5
	LJMU + Animalia	<5	40	38+14	0.91	0.0176	5
Sensor Version 3.1	LJMU	<5	20	17	0.64	0.0468	5
Sensor Version 3.2	LJMU	<5	20	17	0.79	0.0296	5

Chapter 8 Conclusion and Future Work

8.1. Conclusion

Water activity is the most important measurement in cured meat as it is the only moisture related measurement, which is accepted by HACCP control point. It is particularly important in determination of the shelf life of the product since it influences different chemical reactions in the product as well as the survival and the resistance of microorganisms. This makes a_w essential in the production of cured meat, as it becomes an indicator of when the curing process is completed, and the product ready for sale. This is important for safety reasons, but also for energy optimisation since curing requires high temperature and humidity. Currently commercially available a_w meters provide high accuracy. However, existing a_w measurement techniques are destructive, which limits their constant use by the industry. This encouraged researchers to investigate use of novel sensing technologies to develop non-destructive methods to predict a_w in meat and meat products. Promising results were achieved by using x-ray systems (namely Computed Tomography Scans), NIR and HSI. However, they had limitations such as high cost, large dimensions and they are not commercially available for the meat industry.

Use of microwave resonance sensors in meat drying processes, was successfully investigated and established. The literature review showed that out of all investigated microwave sensor structures microstrip met the required design criteria, namely size flexibility, cost and reproducibility. Therefore, this sensor structure was selected for further investigation. Various microstrip patch type sensors were modelled, constructed and tested.

Prior to the construction of the sensors, a HFSS (High Frequency Structural Simulation) model of the sensors and theoretical model of a meat sample was created and simulated. The simulation results demonstrated a strong linear relationship between the sensor response and theoretical model. Particularly, a linear correlation between the resonant frequency shift of the sensor and decrease of a dielectric constant of the theoretical model of the meat sample. Based on the simulation results, a sensor was constructed and tested in the laboratory.

The first experimental work was undertaken by using rectangular planar type sensor that resonates at 2 GHz frequency (version 1). The sensor demonstrated a significant potential in

monitoring the meat curing process, which is a current method of tracking curing in the meat industry. Although the sensor did not agree with HFSS simulation results, i.e. did not demonstrate a strong linear correlation between the resonant frequency shift and the weight loss, it did show a significant relationship at higher frequencies. The results acquired from the sensor, specifically an amplitude shift of the EM signal at 4.5 GHz frequency correlated with weight loss of the meat sample, showing a linear relationship with $R^2 = 0.99$.

However, the transmission line feeding technique caused two issues: with the positioning of the sensor and the size. The patch area of the sensor had to be placed at the exact position on a meat sample, in order to obtain a repeatable measurement owing to a location of the feeding line. The size of the sensor caused an issue after a few days of curing due to the shrinkage process of a meat sample, which led to an air gaps between the sample and the sensor. Therefore, a new rectangular type sensor was modelled with coaxial probe fed technique and resonating at 2.45 GHz frequency (version 2). These two amendments reduced the size of the sensor and issues with the positioning of the sensor.

The new sensor showed a strong linear relationship between the reflected signal and weight loss of the meat sample, with $R^2 = 0.98$. However, the correlation occurred at 5 GHz rather than at 4.5 GHz as it did with 2 GHz sensor. Nevertheless, the reduction of the sensor did not solve the issue with the air gaps as the corners of the rectangular shaped sensor barred the full contact between the patch area of the sensor and the surface of the meat sample. Thus, a circular shaped patch sensor was designed and constructed using coaxial feeding technique with dimensions to resonate at 2.4 GHz (version 3). The sensor illustrated better response during the monitoring of the meat drying process than sensors version 1 and version 2. It demonstrated a strong agreement with the results obtained from the HFSS simulation. Particularly, a linear correlation between a decrease of the resonant frequency (2.4 GHz) of the sensor and the weight loss of the meat sample. Additionally, the sensor illustrated a strong linear relationship between amplitude increase at 5.5 GHz and weight loss, with $R^2 = 0.99$.

The data obtained from the sensors version 1, 2 and 3 were used to develop a predictive model for weight loss determination of meat samples. The Partial Least Squares Regression (PLSR) prediction technique was used to analyse and develop the model. Frequency ranges

between 4 - 5 GHz, 4.5 - 5.5 GHz and 5 – 6 GHz were selected to develop the predictive model for sensors version 1, version 2 and version 3, respectively. All three models exhibited a great capability to predict weight loss with $R^2_p = 0.99$.

Although, the microwave sensors demonstrated great results in determining the weight loss of meat samples, two issues were identified with the method during the experimental work. Firstly, a corrosion of the sensors and meat samples occurred in the middle of the curing process (after 3-4 days), even though two different methods were applied to protect the sensors, namely tinning and coating. The coating dissolved and came off, which is thought to be caused due to a continuous contact of the sensor with a sample (the sample was rubbed with salt, which could be the reason) for a period of 3-4 days. The second issue with the method was leaving uncured spots on the samples, where the sensors were located/attached for measurements. Therefore, this method of sensing would affect the safety of the product, as it would not meet the HACCP requirements. Based on the issues it was decided to conduct discrete measurements and stop the continuous monitoring.

The size became an issue during the continuous measurements, thus the size reduction techniques were investigated and two sets of sensors were produced based on the sensor version 3. The sensors (version 3 and two sets of size reduced sensors version 3.1 and version 3.2) were used for the determination of a_w in cured meat samples, which is an indicator of the safety of a product. The results demonstrated a good linear correlation (R^2) of 0.77, 0.77 and 0.80 between a_w and the resonant frequency of the sensors version 3, version 3.1 and version 3.2, respectively.

Then, the Partial Least Square Regression (PLSR) analysis was applied to develop a_w prediction model on data obtained using sensors version 3, 3.1 and version 3.2. The PLSR model for the sensors exhibited a good capability to predict a_w, with $R^2_p = 0.81$ and RMSEP = 0.0294, $R^2_p = 0.64$ and RMSEP = 0.0468 and $R^2_p = 0.79$ and RMSEP = 0.0296, respectively.

The hand-held prototype was developed and tested in the LJMU laboratory as well as in the industrial environment (in a Norwegian pilot plant owned by Animalia). The experimental results obtained in the laboratory demonstrated a good linear agreement between the prototype's response and water activity, with $R^2 = 0.91$. The strongest linear correlation was

identified at the amplitude decrease of the electromagnetic signal at 7GHz. The PLSR technique was used to create a prediction model for this data to predict a_w in cured meat samples. The model exhibited a good capability to determine the a_w value in the samples with $R^2_p = 0.91$ and RMSEP = 0.0173. The next stage of the investigation was testing the prototype in the industrial environment. The results illustrated a good agreement with the laboratory results, with $R^2 = 0.91$. Then, the prediction model was applied to the cured meat products, which also demonstrated a good capability to predict a_w, with $R^2_p = 0.91$ and RMSEP = 0.0176. This shows that the microwave sensor has stronger linear correlation with the commercially available devices than Computed Tomography ($R^2 = 0.832$) and Near Infrared ($R^2 = 0.618$). While the correlation is similar to Hyperspectral Imaging ($R^2 = 0.906$), the fact that the RF approach is completely portable and non-destructive make this a more desirable approach for the meat industry.

The aim of this research was to develop a rapid non-destructive method to predict water activity in cured meat using microwave spectroscopy, which was established by meeting the set objectives. The contribution to knowledge is the experimental demonstration of the microwave sensors at low GHz frequencies, namely below 7GHz frequency to monitor and determine the parameters of meat and meat products, i.e. weight loss and a_w prediction, which unlocks the potential of low-cost, rapid and non-destructive applications for the meat industry.

The sensing system will enable the manufacturers of cured meat products to adapt and change their recipes in line with healthy eating guidance, such as that offered by the World Health Organisation (WHO) and the European Food Information Council (EUFIC). For example, the use of frequent or continuous aw prediction will enable manufacturers to monitor the effect of reducing the salt levels in their products and work toward launching low-salt derivatives. It will go further than other enterprises in this field, since the developed method of aw prediction enables simple through life product monitoring. This will clearly have a huge positive impact on social health since reducing salt intake will reduce risk of high blood pressure, heart disease and strokes for European Union (EU) citizens, as most countries are above the 6g per day salt intake targets. Thus, the impact of this will be felt at national and European levels through reduced mortality and healthcare costs.

Additionally, the novel system will provide an opportunity to improve the quality and consistency of products, as the manufacturers will be able to control every single product, which is not possible with the existing methods. Currently, manufacturers rely on an experienced worker with the right instinct, who estimates the water activity by simply squeezing the product. Therefore, the system will improve the efficiency by enabling even non-experienced workers to accurately measure water activity and control the curing process by using the implemented prediction model/algorithm. Finally, the system will provide enhanced knowledge of water activity that will decrease the timing of the drying process. This will reduce expenses on energy-consuming dryers and improve the productivity.

8.2. Future Work

Future work in developing this technique could consider a number of directions, which include:

- The application of the prototype sensor to a range of different meat products, such as beef, lamb, chicken and fish, as well as wider food products including breads and other baked goods.
- Enhancement of the sensor so that it may accommodate different shapes of food, and those with rough or uneven surface texture, as well as a broad range of water activity values (i.e. beyond the range of relevance to cured meat products where the focus of this work lay).
- Increase sensitivity of the sensor through design of devices specifically for 5.8 GHz (ISM band) or 7 GHz, which should also assist in enabling the device to be smaller than that currently produced.
- Development of the prototype so that it no longer relies upon a VNA system for operation, but rather houses the necessary electronics in an “all-in-one” hand held unit.
- Commercialisation of the sensor for wider use in the food industry, for safety analysis, quality improvement and recipe development.

It is notable that the current idea is the subject of a patent pending application in both the UK (application number 1515498.2) and Internationally (PCT/GB2016/052642), and

significant interest in the concept has been generated in Norway, Spain and Italy who are all key players in the production of high-value cured meat products. With this backing, and the evidence of effectiveness presented in this thesis, there is a strong potential for a commercially viable and successful tool, which is currently unavailable to industry.

Reference

Abdou, A. A., Shaw, A., Mason, A., Al-Shamma'a, A., Cullen, J., Wylie, S. and Diallo, M. (2013) 'A matched Bow-tie antenna at 433MHz for use in underwater wireless sensor networks', *Journal of Physics: Conference Series*, 450, pp. 1–8. doi: 10.1088/1742-6596/450/1/012048.

Abdullah, B. M., Cullen, J. D., Korostynska, O., Mason, A. and Al-Shamma'a, A. I. (2014) 'Assessing Water-Holding Capacity (WHC) of Meat Using Microwave Spectroscopy', *Sensing Technology: Current Status and Future Trends I*, 7, pp. 117–140. doi: 10.1007/978-3-319-02318-2_7.

ActionSalt (2016) *NICE Public Health Guidance: Prevention of Cardiovascular Disease*. Available at: http://www.actiononsalt.org.uk/salthealth/Recommendations on salt/42503.html (Accessed: 22 April 2016).

Adous, M., Quéffélec, P. and Laguerre, L. (2006) 'Coaxial/cylindrical transition line for broadband permittivity measurement of civil engineering materials', *Measurement Science and Technology*. IOP Publishing, 17(8), pp. 2241–2246. doi: 10.1088/0957-0233/17/8/026.

Al-Muhtaseb, A. H., McMinn, W. A. M. and Magee, T. R. A. (2002) 'Moisture Sorption Isotherm Characteristics of Food Products: A Review', *Food and Bioproducts Processing*, 80(2), pp. 118–128. doi: 10.1205/09603080252938753.

Al-Sajee, A. A. D. and Hamad, K. A. (2011) 'Improving bandwidth rectangular patch antenna using different thickness of dielectric substrate', *Journal of Engineering and Applied Sciences*, 6(4), pp. 16–21.

Alsager, A. F. (2011) 'Design and Analysis of Microstrip Patch Antenna Arrays', (1), pp. 1–80.

ANSYS (2016) *High Frequency Electromagnetic Field Simulation, ANSYS HFSS*. Available at: http://www.ansys.com/Products/Electronics/ANSYS-HFSS (Accessed: 16 June 2016).

Antenna Standards Committee (1983) *IEEE Standard Definitions of Terms for Antennas*. New York: IEEE. doi: 10.1109/IEEESTD.1983.82386.

AQUALAB (2016) *AquaLab PAWKIT*. Available at: http://www.aqualab.com/ (Accessed: 22 April 2016).

Austin, J., Rodriguez, S., Sung, P.-F. and Harris, M. (2013) 'Utilizing microwaves for the determination of moisture content independent of density', *Powder Technology*, 236, pp. 17–23. doi: 10.1016/j.powtec.2012.06.039.

Balanis, C. (2008) *Modern Antenna Handbook*. Second. Canada: John Wiley & Sons, Inc. doi: 10.1002/9780470294154.

Balanis, C. . (2005) *Antenna Theory Analysis and Design*. Third. New Jersey: John Wiley & Sons, Inc.

Berglund, N. (2015) *Norway set to export its cured mutton*. Available at: http://www.newsinenglish.no/2015/06/22/norway-to-export-its-cured-mutton/ (Accessed: 22 April 2016).

Bjarnadottir, S. G., Lunde, K., Alvseike, O., Mason, A. and Al-Shamma'a, A. I. (2014) 'Assessing Water Activity in Dry-Cured Ham using Microwave Spectroscopy', in *Proceedings of the 8th International Conference on Sensing Technology*. Liverpool, pp. 543–546.

Bjarnadottir, S. G., Lunde, K., Alvseike, O., Mason, A. and Al-Shamma'a, A. I. (2015) 'Assessing Quality Parameters in Dry-Cured Ham Using Microwave Spectroscopy', *Meat Science, In-Press*.

Bjarnadottir, S. G., Lunde, K., Alvseike, O., Mason, A. and Al-Shamma'a, A. I. (2015) 'Assessing quality parameters in dry-cured ham using microwave spectroscopy.', *Meat science*, 108, pp. 109–114. doi: 10.1016/j.meatsci.2015.06.004.

Buschmüller, C., Wiedey, W., Döscher, C., Dressler, J. and Breitkreutz, J. (2008) 'In-line monitoring of granule moisture in fluidized-bed dryers using microwave resonance technology.', *European journal of pharmaceutics and biopharmaceutics*, 69(1), pp. 380–7. doi: 10.1016/j.ejpb.2007.09.014.

CadSoft US (2016) *What is EAGLE, CadSoft Computer US*. Available at: Easy Applicable

Graphical Layout Editor (Accessed: 13 June 2016).

Canadian Cancer Society (2016) *Cured, smoked and salt-preserved foods*. Available at: http://www.cancer.ca/en/cancer-information/cancer-101/what-is-a-risk-factor/diet/cured-smoked-and-salt-preserved-foods/?region=on (Accessed: 29 June 2016).

Carter, B. and Fontana, A. J. (2008) 'Water Activity: The Key to Pet Food Quality and Safety', *Decagon Devices*, pp. 0–3.

Clerjon, S. and Damez, J. L. (2009) 'Microwave sensing for an objective evaluation of meat ageing', *Journal of Food Engineering*. Elsevier Ltd, 94(3–4), pp. 379–389. doi: 10.1016/j.jfoodeng.2009.04.004.

Clerjon, S., Daudin, J.-D. and Damez, J.-L. (2003) 'Water activity and dielectric properties of gels in the frequency range 200 MHz–6 GHz', *Food Chemistry*, 82(1), pp. 87–97. doi: 10.1016/S0308-8146(02)00580-0.

Cole-Parmer (2016a) *Novasina LabMaster Advanced Water Activity Meter with Full Temperature Control*. Available at: http://www.coleparmer.co.uk/ (Accessed: 22 April 2016).

Cole-Parmer (2016b) *Novasina LabTouch Water Activity Instrument, with Semi-Temp Stabilized*. Available at: http://www.coleparmer.co.uk (Accessed: 22 April 2016).

Collell, C., Gou, P., Arnau, J. and Comaposada, J. (2011) 'Non-destructive estimation of moisture, water activity and NaCl at ham surface during resting and drying using NIR spectroscopy', *Food Chemistry*, 129(2), pp. 601–607. doi: 10.1016/j.foodchem.2011.04.073.

Cordis (2015) *Optimization Of The Salting Process For The Production Of Healthier And Higher Quality Dry-Cured Meat Products With Reduced And More Standardized Salt Content*. Available at: http://cordis.europa.eu (Accessed: 22 April 2016).

Corredor, C. C., Bu, D. and Both, D. (2011) 'Comparison of near infrared and microwave resonance sensors for at-line moisture determination in powders and tablets.', *Analytica chimica acta*, 696(1–2), pp. 84–93. doi: 10.1016/j.aca.2011.03.048.

Damez, J. L. and Clerjon, S. (2013) 'Quantifying and predicting meat and meat products quality attributes using electromagnetic waves: An overview', *Meat Science*. Elsevier Ltd, 95(4), pp. 879–896. doi: 10.1016/j.meatsci.2013.04.037.

Decagon Devices (2012) 'Fundamentals of Water Activity'. Washington: Devices, Decagon, pp. 1–12.

Decagon Devices (2015) 'Portable Water Activity Measurement System Operator's Manual'. Pullman: Decagon Devices, Inc., pp. 1–61.

Decagon Devices (2017) *AquaLab Series 4TE*.

Devine, C. and M. Dikeman (2004) *Encyclopedia of Meat Sciences, Three-Volume Set*. Edited by W. K. Jensen. Pennsylvania: Academic Press.

Edling, T. (2012) *Design of circular polarized dual band patch antenna*. Uppsala University.

Ehyaie, D. (2011) *Novel Approaches to the Design of Phased Array Antennas*.

EUFIC (2017) *Regulation and standards, European Food Information Council*. Available at: http://www.eufic.org/en/food-safety/category/regulation-and-standards (Accessed: 6 March 2017).

Fellows, P. J. (2000) *Water activity*. 2nd edn, *Food Processing Technology. Principles and Practice*. 2nd edn. Oxford: Woodhead Publishing Limited.

Ferlay, J., Autier, P., Boniol, M., Heanue, M., Colombet, M. and Boyle, P. (2007) 'Estimates of the cancer incidence and mortality in Europe in 2006', *Annals of Oncology*, 18(3), pp. 581–592. doi: 10.1093/annonc/mdl498.

Font, M., Fulladosa, E. and Garcia-Gil, N. (2013) *Computed Tomography Scan, International Reciprocal Trade Association*. Monells.

Font Furnols, M., Teran, M. F. and Gispert, M. (2009) 'Estimation of lean meat content in pig carcasses using X-ray Computed Tomography and PLS regression', *Chemometrics and Intelligent Laboratory Systems*, 98(1), pp. 31–37. doi: 10.1016/j.chemolab.2009.04.009.

Food and Drug Administration (2014) *Water Activity (aw) in Foods*. Silver Spring.

Food and Drug Administration (2015) *Inspection Technical Guides - Water Activity (aw) in Foods*. Available at: http://www.fda.gov/ICECI/Inspections/InspectionGuides/InspectionTechnicalGuides/ucm072916.htm (Accessed: 22 April 2016).

Frame, A. (2012) *Cured Meat Is In, But Is it Safe?, Food Safety News*. Available at: http://www.foodsafetynews.com/2012/09/cured-meat-is-in-but-is-it-safe/#.V1qlQrsrJdh (Accessed: 10 June 2016).

Fung, C. (2011) *Basic Antenna Theory and Application*. Worcester Polytechnic Institute.

Gallagher, J. (2013) *Processed meat 'early death' link, BBC News*. Available at: http://www.bbc.co.uk/news/health-21682779 (Accessed: 29 June 2016).

Garg, B., Verma, R. D. and Samadhiya, A. (2012) 'Design of Rectangular Microstrip Patch Antenna Incorporated with Innovative Metamaterial Structure for Dual band operation and Amelioration in Patch Antenna Parameters with Negative μ and ε', *International Journal of Engineering & Technology*, 1(3), pp. 205–216. doi: 10.14419/ijet.v1i3.124.

Garg, R. (2001) *Microstrip antenna design handbook*. First. Norwood: Artech House, Inc.

Garson, D. (2016) *Partial Least Squares: Regression and Structural Equation Models*. Carolina: Statistical Associates Publishing. doi: 10.18111/9789284418145.

Goh, J. H., Mason, A., Field, M., Browning, P. and Al-Shamma'a, A. (2013) 'Using a Microwave Sensor as an Online Indicator of Neurological Impairment during Surgical Procedures', *Key Engineering Materials*, 543, pp. 368–372.

Goh, J. H., Mason, A., Korostynska, O., Al-Shamma'a, A. I., Browning, P. and Field, M. (2013) 'Real-Time Monitoring of Bodily Fluids Using a Novel Electromagnetic Wave Sensor', *Journal of Public Health Frontier*, 2(4), pp. 201–206. doi: 10.5963/PHF0204004.

Goh, J. H., Shaw, A., Cullen, J. D., Al-shamma, A. I., Oliver, M., Vines, M., Brockhurst, M., Beatty, B., Solutions, U. and Road, W. S. (2011) 'Water Pipe Leak Detection Using

Electromagnetic Wave Sensor for the Water Industry', *Symposium on Computers & Informatics*, pp. 290–295.

Goy, B., Martin, P. and Leban, J.-M. (1992) 'The measurement of wood density by microwave sensor', *Holz als Roh- und Werkstoff*, 50(4), pp. 163–166. doi: 10.1007/BF02663259.

Gradinarsky, L., Brage, H., Lagerholm, B., Björn, I. N. and Folestad, S. (2006) 'In situ monitoring and control of moisture content in pharmaceutical powder processes using an open-ended coaxial probe', *Measurement Science and Technology*. IOP Publishing, 17(7), pp. 1847–1853. doi: 10.1088/0957-0233/17/7/024.

Green, R. L., Thurau, G., Pixley, N. C., Mateos, A., Reed, R. A. and Higgins, J. P. (2005) 'In-line monitoring of moisture content in fluid bed dryers using near-IR spectroscopy with consideration of sampling effects on method accuracy.', *Analytical chemistry*, 77(14), pp. 4515–22. doi: 10.1021/ac050272q.

Gustavo V. Barbosa-Cánovas, Anthony J. Fontana, J., Schmidt, S. J. and Labuza, T. P. (2007) *Water Activity in Foods: Fundamentals and applications*. First edit, *Electrochemical Methods, 2nd ed.* …. First edit. Oxford: Blackwell Publishing. doi: 10.1038/nprot.2009.120.Multi-stage.

Haseth, T. T., Hoy, M., Egelandsdal, B. and Sorheim, O. (2009) 'Nondestructive analysis of salt, water, and protein in dried salted cod using computed tomography.', *Journal of food science*, 74(3), pp. E147-53. doi: 10.1111/j.1750-3841.2009.01102.x.

Heller, K. J. (2001) 'Probiotic bacteria in fermented foods : product characteristics and', *The American Journal of Clinical Nutrition*, 73(2), pp. 374–379.

Hendriksen, M. A. H., van Raaij, J. M. A., Geleijnse, J. M., Breda, J. and Boshuizen, H. C. (2015) 'Health gain by salt reduction in europe: a modelling study.', *Public Library of Science*, 10(3), pp. 1–12. doi: 10.1371/journal.pone.0118873.

Ibarz, A. and Barbosa-Canovas, G. V (2014) *Introduction to Food Process Engineering*. Boca Raton: CRC Press.

James, J. R. and Hall, P. S. (1989) 'Handbook of microstrip antennas', *IEE Electromagnetic Waves Series*, 28.

Jang, H. a, Kim, D. O. and Kim, C. Y. (2012) 'Size Reduction of Patch Antenna Array Using CSRRs Loaded Ground Plane', *Electromagnetics Research Symposium (PIERS) Proceedings*, pp. 1487–1489.

Kolstad, K., Morkore, T. and Thomassen, M. S. (2008) 'Quantification of dry matter % and liquid leakage in Atlantic cod (Gadus morhua) using computerised X-ray tomography (CT)', *Aquaculture*, 275(1–4), pp. 209–216. doi: 10.1016/j.aquaculture.2007.12.011.

Korostynska, O., Mason, A. and Al-Shamma'a, A. (2014) 'Microwave sensors for the non-invasive monitoring of industrial and medical applications', *Sensor Review*, 34, pp. 182–191. doi: 10.1108/SR-11-2012-725.

Korostynska, O., Mason, A., Ortoneda-Pedrola, M. and Al-Shamma'a, A. (2014) 'Electromagnetic wave sensing of NO3 and COD concentrations for real-time environmental and industrial monitoring', *Sensors and Actuators B: Chemical*, 198, pp. 49–54. doi: 10.1016/j.snb.2014.03.030.

Korostynska, O., Ortoneda-Pedrola, M., Mason, A. and Al-Shamma'a, a I. (2014) 'Flexible electromagnetic wave sensor operating at GHz frequencies for instantaneous concentration measurements of NaCl, KCl, MnCl 2 and CuCl solutions', *Measurement Science and Technology*, 25(6), p. 65105. doi: 10.1088/0957-0233/25/6/065105.

Kot, P., Ali, A. S., Shaw, A., Riley, M. and Alias, A. (2016) 'The application of electromagnetic waves in monitoring water infiltration on concrete flat roof: The case of Malaysia', *Construction and Building Materials*. Elsevier Ltd, 122, pp. 435–445. doi: 10.1016/j.conbuildmat.2016.06.092.

Labcell Ltd (2016a) *Aqualab Pawkit*, *Labcell Water Activity Instruments*. Available at: http://www.labcell.com/ (Accessed: 22 April 2016).

Labcell Ltd (2016b) *Aqualab Pre Water Activity Meter*, *Labcell Water Activity Instruments*. Available at: http://www.labcell.com/food-pharmaceuticals/water-activity/water-

activity/aqualab-pre (Accessed: 22 April 2016).

Lawson, B. (2005) *Electromagnetic Radiation and Radio Waves, Woodbank Communications Ltd*. Available at: http://www.mpoweruk.com/ (Accessed: 22 April 2016).

Lee, S., Woo, J., Ryu, M. and Shin, H. (2003) 'Corrugated circular micro-strip patch antennas for miniaturization', *Electronics Letters*, 38(6), pp. 262–263.

Lee, Y., Tse, S., Hao, Y. and Parini, C. G. (2007) 'A compact microstrip antenna with improved bandwidth using complementary split-ring resonator (CSRR) loading', *IEEE Antennas and Propagation Society International Symposium*, pp. 5431–5434.

Li, H., Xu, Q. and Liang, Y. (2014) 'libPLS: An Integrated Library for Partial Least Squares Regression and Discriminant Analysis', *PeerJ PrePrints 2 (source codes available at www.libpls.net)*, pp. 1–4.

Liu, D., Qu, J., Sun, D.-W., Pu, H. and Zeng, X.-A. (2013) 'Non-destructive prediction of salt contents and water activity of porcine meat slices by hyperspectral imaging in a salting process', *Innovative Food Science & Emerging Technologies*, 20, pp. 316–323. doi: 10.1016/j.ifset.2013.09.002.

Lizhi, H., Toyoda, K. and Ihara, I. (2008) 'Dielectric properties of edible oils and fatty acids as a function of frequency, temperature, moisture and composition', *Journal of Food Engineering*, 88(2), pp. 151–158. doi: 10.1016/j.jfoodeng.2007.12.035.

López-Malo, A. and Alzamora, S. M. (2015) 'Water Activity and Microorganism Control: Past and Future', in Gutiérrez-López, G. F., Alamilla-Beltrán, L., del Pilar Buera, M., Welti-Chanes, J., Parada-Arias, E., and Barbosa-Cánovas, G. V. (eds) *Water Stress in Biological, Chemical, Pharmaceutical and Food Systems*. New York, NY: Springer New York (Food Engineering Series), pp. 245–262. doi: 10.1007/978-1-4939-2578-0.

Manolakis, D. and Shaw, G. (2002) 'Detection Algorithms Hyperspectral Imaging Applications', *IEEE Signal Processing Magazine*, pp. 1–15.

Marriott, N. G., Graham, P. P. and Extension, V. C. (2000) 'Some Solutions to Difficulties of Home-curing Pork', *Food Science and Technology*. Virginia Cooperative Extension, p. 6.

Mason, A., Abdullah, B., Muradov, M., Korostynska, O., Al-Shamma'a, A., Bjarnadottir, S. G., Lunde, K. and Alvseike, O. (2016) 'Theoretical Basis and Application for Measuring Pork Loin Drip Loss Using Microwave Spectroscopy.', *Sensors*, 16(2), pp. 1–13. doi: 10.3390/s16020182.

Mason, A., Korostynska, O., Ortoneda-Pedrola, M., Shaw, A. and Al-Shamma'a, A. (2013) 'A resonant co-planar sensor at microwave frequencies for biomedical applications', *Sensors and Actuators A: Physical*, 202, pp. 170–175. doi: 10.1016/j.sna.2013.04.015.

Mathlouthi, M. (2001) 'Water content, water activity, water structure and the stability of foodstuffs', *Food Control*, 12(7), pp. 409–417. doi: 10.1016/S0956-7135(01)00032-9.

Meats and Sausages (2016) *Meat Curing Methods*. Available at: http://www.meatsandsausages.com/sausage-making/curing/methods (Accessed: 6 March 2017).

Mess-Elektronik (2016) *Passive Magnetic TX Loop Antenna*. Schönau.

National Cancer Institute (2016) *Computed Tomography (CT) Scans and Cancer*. Available at: http://www.cancer.gov/about-cancer/diagnosis-staging/ct-scans-fact-sheet (Accessed: 22 April 2016).

Nielsen, M. S., Lauridsen, T., Christensen, L. B. and Feidenhans'l, R. (2013) 'X-ray dark-field imaging for detection of foreign bodies in food', *Food Control*. Elsevier Ltd, 30(2), pp. 531–535. doi: 10.1016/j.foodcont.2012.08.007.

Nitikanikks, N. (2017) *Microstrip Patch Antenna - Introduction, Emaze*. Available at: https://www.emaze.com/@AFZTIZZI/Presentation-Name (Accessed: 7 March 2017).

Novasina (2016) 'Water Activity Measurement Instruments', *General Catalogue AW*. Lachen, Switzerland: Novasina AG, pp. 7–10.

Ogherohwo, E. P. and Barnabas, B. (2015) 'Design , Construction and Performance Analysis of Helical Antenna Operating at 5.8ghz', *International Journal of Advanced Research in Physical Science*, 2(11), pp. 29–38.

Pardo, E., Marín, S., Sanchis, V. and Ramos, A. J. (2004) 'Prediction of fungal growth and ochratoxin A production by Aspergillus ochraceus on irradiated barley grain as influenced by temperature and water activity.', *International journal of food microbiology*, 95(1), pp. 79–88. doi: 10.1016/j.ijfoodmicro.2004.02.003.

Pendry, J. B., Holden, A. J., Robbins, D. J. and Stewart, W. J. (1999) 'Magnetism from conductors and enhanced nonlinear phenomena', *IEEE Transactions on Microwave Theory and Tech- niques*, 47, pp. 1–21.

Prediktor (2016) *Spektron*. Available at: http://www.prediktor.no/ (Accessed: 22 April 2016).

Prolongo (2016) *Prolongo*. Available at: http://www.prolongo.com/?lang=en (Accessed: 17 June 2016).

Ray, F. (2010) *Meat Curing, Oklahoma State University*. Stillwater: Oklahoma Cooperative Extension Service. Available at: http://pods.dasnr.okstate.edu/docushare/dsweb/Get/Document-2055/ANSI-3994web.pdf (Accessed: 22 April 2016).

Reich, G. (2005) 'Near-infrared spectroscopy and imaging: Basic principles and pharmaceutical applications', *Advanced Drug Delivery Reviews*, 57(8), pp. 1109–1143. doi: 10.1016/j.addr.2005.01.020.

Reid, D. (2001) 'Factors to Consider When Estimating Water Vapor Pressure', in *Current Protocols in Food Analytical Chemistry*. California: John Wiley & Sons, Inc.

Rentfrow, G., Chaplin, R. and Suman, S. P. (2012) *Technology of dry-cured ham production: Science enhancing art*. Lexington.

Resano, H., Pérez-cueto, F. J. A., Sanjuán, A. I., Barcellos, M. D. De, Grunert, K. G. and Verbeke, W. (2011) 'Consumer satisfaction with dry-cured ham in five European countries', *Meat Science*. The American Meat Science Association, 87(4), pp. 336–343. doi: 10.1016/j.meatsci.2010.11.008.

Romas (2016) *Meats, Roma's Italian Specialty Market*. Available at:

http://www.romasitalianspecialties.com/meats/ (Accessed: 19 December 2016).

Rosso, L. and Robinson, T. P. (2001) 'A cardinal model to describe the effect of water activity on the growth of moulds', *International Journal of Food Microbiology*, 63(3), pp. 265–273. doi: 10.1016/S0168-1605(00)00469-4.

Rotronic (2012) 'HygroPalm HP23-A / HP23-AW-A Hand-Held Indicator User Guide'. Bassersdorf: Rotronic AG, pp. 1–51.

Rotronic Instruments Ltd (2016) *HygroLab C1*. Available at: http://www.rotronic.co.uk/humidity-measurement-feuchtemessung-temperaturmessung/water-activity-wasseraktivitaet/hygrolab-c1.html (Accessed: 22 April 2016).

Sablani, S. S., Rahman, M. S. and Labuza, T. P. (2001) 'Measurement of Water Activity Using Isopiestic Method', in *Current Protocols in Food Analytical Chemistry*. John Wiley & Sons, Inc.

Santos-Garcés, E., Gou, P., Garcia-Gil, N., Arnau, J. and Fulladosa, E. (2010) 'Non-destructive analysis of aw, salt and water in dry-cured hams during drying process by means of computed tomography', *Journal of Food Engineering*, 101(2), pp. 187–192. doi: 10.1016/j.jfoodeng.2010.06.027.

Seeram, E. (2009) *Computed Tomography: Physical Principles, Clinical Applications, and Quality Control*. third. Philadelphia, PA.: W.B. Saunders Co.

Segtnan, V. H., Høy, M., Sørheim, O., Kohler, A., Lundby, F., Wold, J. P. and Ofstad, R. (2009) 'Noncontact salt and fat distributional analysis in salted and smoked salmon fillets using X-ray computed tomography and NIR interactance imaging.', *Journal of agricultural and food chemistry*, 57(5), pp. 1705–10. doi: 10.1021/jf802080s.

Seo, J. and Woo, J. (2004) 'Miniaturization of microstrip antenna using iries', *Electronics Letters*, 40, pp. 718–719.

Sharawi, M. S., Khan, M. U. and Mittra, R. (2015) 'Microstrip patch antenna miniaturisation techniques: a review', *IET Microwaves, Antennas & Propagation*, 9, pp. 913–922. doi:

10.1049/iet-map.2014.0602.

Sharma, G. P. and Prasad, S. (2002) 'Dielectric properties of garlic (Allium sativum L.) at 2450 MHz as function of temperature and moisture content', *Journal of Food Engineering*, 52(4), pp. 343–348. doi: 10.1016/S0260-8774(01)00125-X.

Sipahioglu, O. and Barringer, S. A. (2003) 'Dielectric Properties of Vegetables and Fruits as a Function of Temperature, Ash, and Moisture Content', *Journal of Food Science*, 68(1), pp. 234–239. doi: 10.1111/j.1365-2621.2003.tb14145.x.

Stutzman, W. L. and Thiele, G. A. (2013) *Antenna Theory and Design*.

Swiss Meat (2014) *Production of Meat Specialties*. Available at: http://www.schweizerfleisch.ch/en/swiss-meat/handling/production-of-meat-specialties/ (Accessed: 22 April 2016).

Tan, Z. M. and Mcdonald, K. T. (2012) *Babinet's Principle for Electromagnetic Fields*. Princeton.

Tomra (2016) *QVision*. Available at: https://www.tomra.com/en/ (Accessed: 22 April 2016).

US Public Health Service (2013) *Food Code, Drugs*. Alexandria. doi: 10.1016/j.parint.2011.08.011.

Venkatesh, M. S. and Raghavan, G. S. V (2004) 'An overview of microwave processing and dielectric properties of agri-food materials', *Biosystems Engineering*, 88(1), pp. 1–18. doi: 10.1016/j.biosystemseng.2004.01.007.

Verbeke, W. (2011) 'Consumer attitudes and communication challenges for agro-food technologies', *Agro Food Industry HI-TECH*, pp. 34–36.

Verbeke, W., Van Wezemael, L., de Barcellos, M. D., Kügler, J. O., Hocquette, J.-F., Ueland, Ø. and Grunert, K. G. (2006) 'Future trends and consumer lifestyles with regard to meat consumption.', *Meat science*, 74(1), pp. 149–60. doi: 10.1016/j.meatsci.2006.04.016.

Verbeke, W., Van Wezemael, L., de Barcellos, M. D., Kügler, J. O., Hocquette, J.-F., Ueland, Ø. and Grunert, K. G. (2010) 'European beef consumers' interest in a beef eating-

quality guarantee Insights from a qualitative study in four EU countries.', *Appetite*, 54(2), pp. 289–96. doi: 10.1016/j.appet.2009.11.013.

Vestergaard, C., Erbou, S. G., Thauland, T., Adler-Nissen, J. and Berg, P. (2005) 'Salt distribution in dry-cured ham measured by computed tomography and image analysis.', *Meat science*, 69(1), pp. 9–15. doi: 10.1016/j.meatsci.2004.06.002.

Vestergaard, C., Risum, J. and Adler-Nissen, J. (2004) 'Quantification of salt concentrations in cured pork by computed tomography', *Meat Science*, 68(1), pp. 107–113. doi: 10.1016/j.meatsci.2004.02.011.

Vesterlund, S., Salminen, K. and Salminen, S. (2012) 'Water activity in dry foods containing live probiotic bacteria should be carefully considered: A case study with Lactobacillus rhamnosus GG in flaxseed', *International Journal of Food Microbiology*, 157(2), pp. 319–321. doi: 10.1016/j.ijfoodmicro.2012.05.016.

Waterhouse, R. (1995) 'Small microstrip patch antenna', *Electronics Letters*, 31, pp. 604–605.

Wong, K. L. and Wu, J. Y. (1997) 'Single-feed small circularly polarized square microstrip antenna', *Electronics Letters*, 33, pp. 1833–1834.

World Health Organization (2004) 'Global strategy on diet , physical activity and health Report by the Secretariat', (April), pp. 1–22.

Wright, M. (2011) *Meat Curing Safety*, *Mattikaarts*. Available at: http://mattikaarts.com/blog/meat-curing-safety/ (Accessed: 8 June 2016).

Zhao, X., Lee, Y. and J. Choi (2011) 'Design of compact patch antenna using split-ring resonator embedded substrate', *Microwave and Optical Technology Letters*, 53(12), pp. 2789–2790.

Appendix A

The Sixth Automation and Analytical Management Group (AAMG) Conference, the Royal Society of Chemistry, Burlington House, Piccadilly, London, UK, 18/06/2014.

A novel non-invasive and real-time electromagnetic wave sensor for the meat industry.

Magomed Muradov, Alex Mason*, Muhammad Ateeq, Jeff Cullen and Ahmed Al-Shamma'a

BEST Research Institute
School of the Built Environment
Liverpool John Moores University
Liverpool, L3 3AF, UK.

Abstract: Accurate real-time monitoring and analysis of meat quality is a significant problem in the meat industry. Changes in the meat properties, such as water loss, dryness, ageing and curing, are have direct impact on meat quality which makes them relevant parameters for the industry to quantify during processing. This work presents development of a novel electromagnetic wave sensor operating at microwave frequencies for real-time analysis of meat samples. The sensor structure radiates low power electromagnetic waves which interact with the samples, altering the nature of this radiation depending on the aforementioned parameters. This phenomenon has been characterised by correlation of laboratory based tests conducted alongside studies using the developed sensor. These results are presented here, and demonstrate the viability of using electromagnetic wave based sensor for real-time non-invasive measurement of meat in the food industry.

Keywords: microwave sensors; non-invasive monitoring; real-time meat analysis; food industry.

The Eighth International Conference on Sensing Technology (ICST 2014), Liverpool John Moores University, Liverpool, UK, 2-4 September 2014

Real-time monitoring of meat drying process using microwave spectroscopy.

Magomed Muradov*, Jeff D. Cullen, Badr Abdullah, Muhammad Ateeq, Alex Mason, Andy Shaw and Ahmed I. Al-Shamma'a.

School of Built Environment
Liverpool John Moores University
Liverpool, UK
*M.Muradov@2009.ljmu.ac.uk.

Abstract. The objective of this investigation is to monitor the meat drying process and try to analyse the changes of the electromagnetic (EM) signature from a patch antenna during the process. The antenna has been modelled using High Frequency Structure Simulation Software (HFSS) and then constructed. The experimental work carried out by placing a meat sample on a scale inside the fridge and recording reflection coefficient (S11) and weight measurements 24 times (every hour) a day during one month at the frequency range of 1GHz-6GHz. Then, the change in EM signature and weight loss is correlated and analysed. The results demonstrate a relationship between the reflection coefficient and weight loss of the meat sample. The weight of the sample drops down dramatically first week and then keeps steadily decreasing. Likewise, an amplitude shift is greater at the beginning of the drying process and then the shift stabilises.

Keywords-component; **dry-curing; microwave sensor; non-invasive sensor; real-time meat analysis.**

Chapter: Next Generation Sensors and Systems. Volume 16 of the series Smart Sensors, Measurement and Instrumentation pp 221-233. Date: 29 July 2015.

Real-Time Monitoring of Meat Drying Process Using Electromagnetic Wave Sensors.

Magomed Muradov, Jeff Cullen, Alex Mason.

Abstract: There are currently limited options for the meat producers for monitoring the water content of their products as they are processed or cured. Most existing methodologies are destructive, or require the use of probes which touch or penetrate the meat and lead to issues of contamination and damage. Thus, the aim of this investigation is to use an electromagnetic (EM) wave sensor to monitor the meat drying process and determine its suitability as a non-destructive and non-contact technique. The sensor has been modelled using High Frequency Structure Simulation Software (HFSS) and then constructed. Experimental work was conducted involving measurement of meat weight and EM signature (namely the S_{11} parameter in the frequency range 1–6 GHz) over a period of approximately 1 week, with measurements recorded every hour. The change in EM signature and weight loss has been analysed and correlations drawn from the resultant data. The results demonstrate a strong relationship between the S_{11} measurement and weight loss of the meat sample (R^2 = 0.8973), and it is proposed that this could be used as the basis for future industrial application for measuring meat products during drying processes, such as those used in curing.

Keywords: **Dry-curing Electromagnetic wave Non-invasive Sensor Real-time meat analysis.**

Institute of Food Science and Technology Young Scientist Competition 2015, Manchester Metropolitan University, Manchester, UK, 29/04/2015.

Real-time Monitoring of Meat Drying Process using Microwave Spectroscopy.

Magomed Muradov* and Alex Mason.

School of Built Environment
Liverpool John Moores University
Liverpool, UK
M.Muradov@2009.ljmu.ac.uk*

Abstract. The aim of this investigation is to monitor the meat drying process and analyse the change in electromagnetic (EM) signature from a suitable sensor during the process. The sensor has been modelled using High Frequency Structure Simulation Software (HFSS) and then constructed. Experimental work was conducted, involving measurement of meat weight and EM signature (namely the S11 parameter in the frequency range 1-6 GHz) over a period of one week (it takes approx. 1 week to lose 40% of weight, at which point the measuring is stopped), with measurements recorded every hour. The change in EM signature and weight loss has been analysed and correlations drawn from the resultant data. The results demonstrate a strong relationship between the S11 measurement and weight loss of the meat sample, and it is proposed that this could be used as the basis for future industrial application for measuring meat products during drying processes, such as those used in curing.

The Ninth International Conference on Sensing Technology (ICST 2015), Massey University, Auckland, New Zealand, 8-10 December 2015.

Online non-destructive monitoring of meat drying using microwave spectroscopy.

Magomed Muradov*, Jeff D. Cullen, Andy Shaw, Olga Korostynska, Alex Mason and Ahmed I. Al-Shamma'a.

School of Built Environment
Liverpool John Moores University
Liverpool, UK
M.Muradov@2009.ljmu.ac.uk*

Stefania G Bjarnadottir and Ole Alvseike

Dept. Quality and Processing
ANIMALIA, Norwegian Meat and Poultry Research Centre
Lørenveien 38, PB 396 Økern, 0513 Oslo

Abstract. The aim of this investigation is to monitor the meat drying process and analyse the change in electromagnetic (EM) signature from a bespoke sensor during the process. The sensor has been modelled using High Frequency Structure Simulation Software (HFSS) and then constructed and tested. Experimental work was conducted, involving measurement of meat weight and EM signature (namely the reflected signal in the 1-6GHz frequency range) over a period of one week (it takes approx. 1 week to lose 40% of weight and then the measuring is stopped as the general weight loss of dry-cured meat is 30-35 % in the final product), with measurements recorded once per hour. The change in EM signature and weight loss has been analysed and correlations drawn from the resultant data. The results demonstrate a strong relationship between the reflection coefficient and weight loss of the meat sample, and it is proposed that this could be used as the basis for future industrial application for measuring the quality of meat products during drying processes, such as those used in curing.

Keywords-component; dry-curing; microwave sensor; non-invasive sensor; real-time meat analysis.

Received: 16 November 2015 / Revised: 21 January 2016 / Accepted: 25 January 2016 / Published: 2 February 2016. *Sensors* 16, no. 2: 182.

Theoretical Basis and Application for Measuring Pork Loin Drip Loss Using Microwave Spectroscopy.

Alex Mason [1],* , Badr Abdullah [1], Magomed Muradov [1], Olga Korostynska [1], Ahmed Al-Shamma'a [1], Stefania Gudrun Bjarnadottir [2], Kathrine Lunde [2] and Ole Alvseike [2]

[1] Faculty of Engineering and Technology, Liverpool John Moores University, Henry Cotton Building, 15-21 Webster Street, Liverpool L3 2ET, UK

[2] ANIMALIA, Norwegian Meat and Poultry Research Centre, Lørenveien 38, Postboks 396 Økern, Oslo 0513, Norway

Abstract. During cutting and processing of meat, the loss of water is critical in determining both product quality and value. From the point of slaughter until packaging, water is lost due to the hanging, movement, handling, and cutting of the carcass, with every 1% of lost water having the potential to cost a large meat processing plant somewhere in the region of €50,000 per day. Currently the options for monitoring the loss of water from meat, or determining its drip loss, are limited to destructive tests which take 24–72 h to complete. This paper presents results from work which has led to the development of a novel microwave cavity sensor capable of providing an indication of drip loss within 6 min, while demonstrating good correlation with the well-known EZ-Driploss method (R2 = 0.896).

Keywords: drip loss; microwave; sensor; water holding capacity; pork loin; meat processing

European Microwave Week 2016, Excel London Exhibition and Convention Centre, London, UK, 3 - 7 October 2016

Microwave Spectroscopy: Novel Cost-Effective Approach to Measure Drip Loss in Pork Loin.

Alex Mason*, Badr Abdullah, Magomed Muradov, Olga Korostynska, Ahmed Al-Shamma'a

Faculty of Engineering and Technology
Liverpool John Moores University
Liverpool, United Kingdom
a.mason1@ljmu.ac.uk

Stefania Gudrun Bjarnadottir, Kathrine Lunde and Ole Alvseike

ANIMALIA Norwegian Meat and Poultry Research Centre Oslo, Norway
ole.alvseike@animalia.no

Abstract — Each stage of meat cutting and processing, from the moment of slaughter until packaging, results in the loss of water, the amount of which is critical in determining both meat product quality and value. Every 1% of lost water potentially costs a large meat processing plant in the region of €50,000 per day. Current standard practice of monitoring the loss of water from meat, or determining its drip loss, employs a destructive laboratory based test which takes 24-72 hours to complete. This paper reports on feasibility studies of using microwave spectroscopy as a cost-effective approach to measure pork loin drip loss. Notably, the developed novel microwave cavity sensor is capable of providing an indication of drip loss within 6 minutes, while demonstrating good correlation with the industry standard EZ-Dripless method ($R^2 = 0.896$).

Keywords— drip loss; microwave spectroscopy; water holding capacity; pork loin; meat processing.

Appendix B

To build a calibration model that can predict water activity given its spectrum and evaluate its performance, the first step partitioning the data into a calibration/training set and a test set. The state-of-the-art Kennard-Stone (KS) is used for data partition:

```
Rank=ks(X); %+++ Data partition using Kennard-Stone algorithm
Xcal=X(Rank(1:40),:);
ycal=y(Rank(1:40),:);
Xtest=X(Rank(41:78),:);
ytest=y(Rank(41:78),:);
```

As a result, there is a calibration/training set and a test set, which contain 40 and 38 samples, respectively. The number of optimal latent variables (LV) needs to be determined before building a PLSR model. There are various ways for this task. Here 10-fold cross validation is used to give a reasonable choice (with the maximal number of nLV limited to 15):

```
CV=plscv(Xcal,ycal,15,10);  %by default, 'center' is used for data
pretreatment inside plscv.m.
plot(CV.RMSECV,'bo-','linewidth',2);
xlabel('number of latent variables');
ylabel('RMSECV');
set(gcf,'color','w');
```

Running the above codes, RMSECV (Root Mean Squared Error of Cross Validation) against number of LVs will be produced. The detailed output from cross validation can be obtained by simply typing "CV" in the command window.

```
CV =

        method: 'center'
         Ypred: [40x15 double]
     predError: [40x15 double]
       RMSECV: [1x15 double]
```

```
            Q2: [1x15 double]
      RMSECV_min: 0.0210
         Q2_max: 0.8776
          optLV: 4
```

So, using 4 components to build a PLS model may be a reasonable choice, where optLV is the suggested optimal number of latent variables for PLS modelling determined by the lowest RMSECV and Q2_max is the corresponding Q2.

The PLSR prediction model can be built by simply running:

```
PLS=pls(Xcal,ycal,4,'center');  %+++ Build a PLS model with 4 components, pretreat method is 'center'.
```

A structural data with a number of useful components, namely (X_scores), loadings (X_loadings), weight (W), W*(Wstar), regression coefficients (regcoef_pretreat) for pretreated data (X_pretreat, y_pretreat), regression coefficients(regcoef_original) for original input data (Xcal, ycal), R^2, fitting error (RMSEF), variable importance in projection (VIP), SR(selectivity ratio) can be obtained by typing “PLS” in the command window:

```
>> PLS
PLS
                  method: 'center'
            X_pretreat: [40x300 double]
            y_pretreat: [40x1 double]
       regcoef_pretreat: [300x1 double]
    regcoef_original_all: [301x4 double]
       regcoef_original: [301x1 double]
             X_scores: [40x4 double]
            X_loadings: [300x4 double]
                 VIP: [1x300 double]
                   W: [300x4 double]
               Wstar: [300x4 double]
               y_fit: [40x1 double]
```

```
        fitError: [40x1 double]
        tpscores: [40x1 double]
     tploadings: [300x1 double]
             SR: [1x300 double]
            SST: 0.1439
            SSR: 0.1316
            SSE: 0.0123
          RMSEF: 0.0173
             R2: 0.9145
```

The test set generated above can be used to evaluate the built PLS model using the following commands:

```
[ypred,RMSEP]=plsval(PLS,Xtest,ytest); %+++ make predictions on
test set
figure;
plot(ytest,ypred,'.',ytest,ytest,'r-');
xlabel('experimental');
ylabel('predicted');
set(gcf,'color','w');
```